`

MYOCARDIAL ENERGETIC ALTERATIONS IN POST MYOCARDIAL INFARCTION LEFT VENTRICULAR REMODELING, HIBERNATING MYOCARDIUM AND PACING INDUCED CONGESTIVE HEART FAILURE AND AMELIORATION WITH STEM CELL TRANSPLANTATION

A DISSERTATION
SUBMITTED TO THE FACULTY OF THE GRADUATE SCHOOL
OF THE UNIVERSITY OF MINNESOTA
BY

MOHAMMAD NURULQADR JAMEEL

IN PARTIAL FULFILLMENT OF THE REQUIREMENTS
FOR THE DEGREE OF
DOCTOR OF PHILOSOPHY

Advisor: Jianyi Zhang MD., Ph.D.

August 2011

Acknowledgements

I would like to sincerely thank and acknowledge Dr. Jianyi Zhang, my advisor, for his guidance, help and his expertise in this field, Dr. Stephen Katz for his support, directions and guidance throughout my research, Dr. Bitterman for his words of encouragement and expert feedback and Dr. Bache for serving like a true role model and mentor.

I would also like to thank all the members of Dr. Zhang's lab especially Xiaohong Wang, Qinglu Li, Abdul Mansoor, Cory Swingen and my colleague Qiang Xiong for all their help during my research.

This work was supported by U.S. Public Health Service Grants HL50470, HL61353, HL 67828, HL 95077. M.N.J was supported by AHA Greater Midwest Predoctoral Award # 0810015Z.

Dedication

This dissertation is dedicated to my wife, Alya Jawaid, whose love, support and patience has accompanied me along the way through this process and to my parents, Dr. Muhammad Jameel and Kauser Jameel who taught me to pursue my dreams and to whom I owe full gratitude for my accomplishments.

TABLE OF CONTENTS

LIST OF TABLES

LIST OF FIGURES

CHAPTER 1. INTRODUCTION

This dissertation consists of eight chapters. Chapter 1 Introduction will delineate the goals of the research. Chapter 2 Background reviews the literature with respect to stem cell transplantation in ischemic heart disease and myocardial bioenergetics in animal models of heart disease. The specific projects are addressed in Chapter 3,4,5 and 6. Chapter 7 Conclusion summarizes the results of the thesis research.

The specific aims of the current thesis are as follows:

- To examine the safety and effects of stem cell transplantation through a transcoronary injection in a clinically relevant ischemia/reperfusion porcine model using a catheter based approach. The functional and bioenergetic effects of stem cell transplantation and the mechanisms underlying the beneficial effects will be examined short term at 4 weeks. (Chapter 3)
- To examine the long terms functional and bioenergetic effects of stem cell transplantation in a porcine model of post-infarction left ventricular remodeling. The engraftment of cells will be examined long term at 4 months. Differential expression of genes will be studied to explore mechanisms underlying the beneficial effects of stem cells. (Chapter 4)

- To create a model of chronic hibernating myocardium in mini-pigs and examine the long term myocardial bioenergetics in this model. (Chapter 5)
- To examine the effects of adenosine and K+ATP channel blockade on myocardial energetics in the failing heart. (Chapter 6)

CHAPTER 2. BACKGROUND

2.1. Stem cell transplantation in ischemic heart disease

Although coronary interventions and medical therapy improve post-infarction cardiac function in patients with coronary artery disease, approximately 45% progress to endstage heart failure [1]. Cardiac transplantation is the only definitive therapy for replacing the lost muscle, but it is limited by the inadequate supply of donor hearts. A potential therapy for limiting post-infarction left ventricular (LV) remodeling and the development of CHF is the replacement of infarcted myocardium with new myocardium generated from transplanted stem cells.

Recent studies have provided evidence to support the notion that cardiomyocyte regeneration may occur during physiological and pathological states in the adult heart; these data highlight the possibilities that myocardial regeneration may occur via cardiomyocyte proliferation or proliferation and differentiation of putative cardiac stem cells [2]. A number of cell types have been used for cardiac repair, including skeletal myoblasts, bone marrow derived cells, mesenchymal stem cells (MSCs), endothelial progenitor cells (EPCs), umbilical cord blood stem cells, cardiac stem cells (CSCs), and embryonic stem cells (ESCs).

The bone marrow (BM) contains many adult stem cells, which have been used to treat hematological disorders for decades. It has recently been shown that bone marrow derived stems can traverse cell lineage boundaries and upon appropriate stimulation transdifferentiate into hepatocytes, endothelial cells, skeletal muscle and neurons [3-5]. The ability of bone marrow derived cells to differentiate into cardiomyocytes is controversial. Bittner et al. were the first to suggest that cardiac muscle cells may be derived from BM cells [6]. Goodel et al. demonstrated that following transplantation of murine BM Side population (SP) cells (c-kit+, Sca-1+, CD34-/low), donor derived cells with cardiomyocyte morphology as well as smooth muscle and endothelial cells were found in the heart following left anterior descending (LAD) coronary artery ligation [7]. Orlic et al. [8] showed that transplantation of GFP-labeled $Lin^{-}c\text{-}kit^{+}$ cells [presumably containing both hematopoietic stem cells (HSC) and mesenchymal stem cells] into the ventricular wall after LAD coronary artery ligation resulted in improved function of the ventricle and they detected a large number of GFP^{+} cells that coexpressed myocardial proteins in the myocardium. In contrast to these findings, other laboratories using genetic mouse models to label cell populations (and their derivatives) showed that lineage negative, c-kit positive cells did not differentiate into cardiomyocytes [9-10]. However, more recently Anversa and colleagues have shown using similar genetic techniques, that c-kit+ bone marrow cells can engraft in the injured myocardium and differentiate into cells of the cardiogenic lineage, forming functionally competent cardiomyocytes and vascular structures [11].

In the late 1980s and in the 1990s, Caplan's laboratory identified a subset of cells within the bone marrow which gave rise to osteoblasts and adipocytes and termed them Mesenchymal Stem Cells (MSCs) [12]. MSCs are present in many different organs of the body including muscle, skin, adipose tissue and bone marrow. They can be isolated from the bone marrow by a simple process involving Ficoll centrifugation and adhering-cell culture in serum-containing medium. In the early studies, MSCs could be expanded for 4 to 20 population doublings only [13] with preservation of the karyotype, telomerase activity and telomere length [14-15]. Phenotypically, these cells are negative for CD31, CD34 and CD 45, unlike hematopoietic progenitors from bone marrow, and are positive for CD29, CD44, CD71, CD90, CD105, CD106, CD120a, CD124, SH2, SH3 and SH4 [16-18]. In the bone marrow, only 0.001-0.01% of the initial unfractionated bone marrow mononuclear cell (BMMNC) population consists of MSCs [13, 16]. However, in a number of rodent studies, the adherent fibroblastic cells obtained from the unfractionated mononuclear class of the bone marrow are termed mesenchymal stem cells [19-20].

MSCs have been reported to have the potential to differentiate into any tissue of mesenchymal origin [12]. MSCs derived from rodent marrow aspiration have been shown to differentiate into cardiomyocyte like cells in the presence of 5-azacytidine [21-22]. The morphology of the cells changes from spindle shaped to ball shaped and finally rod shaped form. Thereafter, these cells fuse together to form a syncitium which resembles a myotube [23]. These cells exhibit markers of

fetal cardiomyocytes [22]. Specific transcription factors of the myocyte and cardiac lineage including GATA4, Nkx2.5 and HAND 1/2 can be detected [21]. There are differences (as compared to native cardiomyocytes) in cardiomyocytes derived from MSCs. First, the ß-isoform of cardiac myosin heavy chain is more abundant than the α-isoform in these cells. Second, myosin light chain 2v is present. Third, MEF2A and MEF2D replace MEF2C isoforms from early to late passage. It is reported that these cells beat spontaneously and synchronously, which is most likely due to the formation of intercalated discs, as has been shown when they are co-cultured with neonatal myocytes [24]. They express competent α- and ß-adrenergic and muscarinic receptors as indicated by an increased rate of contraction in response to isoproterenol and a decreased rate of contraction induced by ß-adrenergic blockers [25]. Other studies suggest that bone marrow stem cells can not differentiate to the cardiac myocytes (29,30). Whether MSCs can differentiate into functional cells of 3 lineages requires further investigation.

MSCs have features that make them attractive candidates for cell transplantation. As they are easily accessible and expandable, MSCs could potentially become an “off the shelf’ allogeneic product, which would be more cost effective, easier to administer, allow a greater number of cells to be transplanted and permit transplantation at the time of urgent interventions to relieve ischemia and injury such as percutaneous or surgical revascularization procedures. Importantly, these cells appear to be hypoimmunogenic [26-28]. These cells lack MHC-II and B-7 costimulatory molecule expression and thus

limit T-cell responses [29-30]. They can also directly inhibit inflammatory responses via paracrine mechanisms including production of transforming growth factor beta1 and hepatocyte growth factor [31-32]. All the above properties make them attractive candidates for cell transplantation.

MSC transplantation was tested in a study in which isogenic adult rats were used as donors and recipients to simulate autologous transplantation clinically. MSC intracoronary delivery in these rat hearts following myocardial infarction showed mileu dependent differentiation of these cells; fibroblastic phenotype within the scar and cardiomyocyte phenotype outside the infarction area [33]. However, direct intramyocardial injection of autologous MSC into the scar resulted in the differentiation into cardiac like muscle cells within the scar tissue, increased angiogenesis and improved myocardial function [34]. The delivery of MSCs via direct left ventricular cavity infusion in a rat myocardial infarction model resulted in preferential migration and colonization of the cells in the ischemic myocardium at 1 week [35]. MSCs also resulted in increased vascularity and improved cardiac function 2 months following delivery in a canine model of chronic ischemic disease [36]. However, Kloner's laboratory using a rat model of postinfarction LV remodeling found that the beneficial effect on left ventricular function was short term and was absent after 6 months [37].

MSC transplantation has led to functional improvement in large animal models of myocardial infarction. Direct intramyocardial injection of 5-azacytadine treated

autologous MSCs was performed 4 weeks after MI in a swine model. These cells formed islands of cardiac like tissue, induced angiogenesis, prevented thinning and dilatation of the infarct region, and improved regional and global contractile function [38].

Bone Marrow Cells (BMCs) have also received intense interest for cell therapy use for patients with cardiovascular disease. The Transplantation of Progenitor Cells and Regeneration Enhancement in Acute Myocardial infarction (TOPCARE-AMI) trial revealed significant improvement in LV ejection fraction as well as significantly enhanced myocardial viability and regional wall motion in the infarct area following transplantation of BMMNCs or blood derived progenitor cells [39-40]. The Bone marrow transfer to enhance ST-elevation infarct regeneration (BOOST) study [41] also showed an increase in LV ejection fraction at 6 months with cell transplantation, but surprisingly there was no difference between the treated and placebo groups at 18 months. Reinfusion of Enriched Progenitor Cells and Infarct Remodeling in Acute Myocardial Infarction (REPAIR-AMI) trial [42] randomized 204 patients with acute MI to receive an intracoronary infusion of progenitor cells derived from bone marrow or placebo medium into the infarct artery 3 to 7 days after successful reperfusion therapy. The absolute increase in LVEF was significantly greater (2.5%) in the BMC group than in the placebo group at 4 months. However, other trials (ASTAMI- Autologous Stem Cell Transplantation in Acute Myocardial Infarction and STEMI- ST-elevation Acute Myocardial Infarction) [43],[44] have shown negative results with no

improvement in ejection fraction with cell transplantation Differences in cell preparation [45] and numbers have been proposed as possible causes for these conflicting results. Bone Marrow Cells have also been used in chronic heart failure setting; In the Transplantation of Progenitor Cells and Recovery of LV Function in Patients with Chronic Ischemic Heart Disease (TOPCARE-CHD) trial [46], 75 patients with stable ischemic heart disease who had had a myocardial infarction at least 3 months previously were assigned to receive either no cell infusion or infusion of circulating progenitor cells or BMC into the patent coronary artery supplying the most dyskinetic left ventricular area. The transplantation of BMC was associated with a moderate (2.9 percentage points), but significant improvement in left ventricular function 3 months post-transplantation.

MSC transplantation has been used in patients with acute myocardial infarction 18 days after primary percutaneous intervention and resulted in significant improvement in LVEF up to 6 months [47-48]. This was associated with a significant reduction in the size of the perfusion defect measured by positron emission tomography at 3 months [47-48]. More recently, it has been demonstrated in a randomized double blind placebo controlled trial that intravenous delivery of allogenic human MSCs leads to improved ventricular function after myocardial infarction [49]. The degree of response to IV therapy occurs early after MI and compared favorably with previous studies using intacoronary infusions of bone marrow [49].

Thus, it seems that a large amount of preclinical data supports the hypothesis that stem cell treatment has potential in improving left ventricular function post myocardial infarction, but the clinical data is not as convincing. The main theme of the current thesis is that the clinical data so far has raised many questions which require definitive answers. Specifically, it needs to be established whether stem cell transplantation leads to functional improvement if delivered intracoronary through a catheter versus an intramyocardial injection. Secondly, it has to be determined if stem cell treatment leads to long term functional and bioenergetic improvement. Moreover, stem cell engraftment and differentiation many months after transplantation needs to be investigated. Thirdly, paracrine mechanisms underlying the beneficial effects of stem cell transplantation need further exploration.

These questions can only be answered by performing experiments on large animal models of myocardial infarction. Our laboratory has a well established model of post infarction left ventricular remodeling. In this model, acute coronary occlusion is followed by remarkable remodeling of the non-infarcted myocardium with LV chamber dilation, reduced systolic performance, increased systolic and diastolic wall stresses and significant bioenergetics abnormalities. All of these alterations are correlated with the size of the initiating infarct. The severity of the abnormalities varies from compensated ventricular dysfunction to frank heart failure, which develops in 20-30% of animals. The feasibility of performing

detailed in vivo physiological and biochemical studies makes this an excellent model for detailed studies of hearts with post-infarction LV remodeling.

2.2. Myocardial Bioenergetics

Cardiac energy metabolism has three components. The first is substrate utilization which involves the cellular uptake of substrates (mainly fatty acids and glucose) and their breakdown by beta-oxidation and glycolysis resulting in the formation of acetyl coenzyme A (CoA), which is fed into the Krebs cycle and produces NADH and carbon dioxide (CO_2). The second component is oxidative phosphorylation which involves transfer of electrons from NADH to oxygen through the mitochondrial respiratory chain that creates a proton electrochemical gradient across the inner mitochondrial membrane subsequently driving the F1-F0 ATP synthase to produce ATP by phosphorylating ADP. The third component is ATP transfer and utilization that involves the creatine kinase shuttle. The principal method for studying in vivo myocardial energy metabolism is through NMR spectroscopy. Our laboratory has specialized in performing in vivo NMR spectroscopy in large animals to study abnormalities in high energy phosphate metabolism, oxidative phosphorylation, creatine kinase kinetics and flux, and substrate utilization.

Our laboratory has created a porcine model of postinfarction remodeling to study myocardial energetics [50]. Proximal circumflex artery was occluded in 18 young pigs and 12 went on to develop left ventricular remodeling (LVR) after about 50 days while 6 developed LVR and CHF within 20 days. The mean scar surface area expressed as a ratio of the total LV surface area was 0.16±0.02 and 0.31±0.03 in the LVR group and LVR+CHF group respectively. This resulted in ventricular hypertrophy in the LVR group as compared to control animals while the LVR+CHF group had the most hypertrophy (LV weight/Body weight was 3.03±0.12 vs. 3.65±0.25 vs. 4.99±0.42). The infarct caused a decrease in ejection fraction to about 35% and 27% in the LVR and LVR+CHF groups, respectively. LV end-systolic volume increased significantly in both groups of animals with remodeling and was significantly higher in LVR+CHF hearts than in LVR hearts. Both LV diastolic wall stresses and mean LV systolic wall stresses were significantly increased in hearts with LVR and were further increased in LVR+CHF hearts. The bioenergetic abnormalities were characterized by a lower ATP, CP, creatine and PCr/ATP ratio in the LVR hearts and the LVR+CHF hearts had an even lower PCr/ATP ratio. The myocardial calculated free ADP levels were significantly increased only in CHF hearts. The increase in myocardial free ADP was associated with reductions in mitochondrial F0F1-ATPase protein expression[51]. These HEP levels did not improve with increasing blood flow with adenosine although the subendocardial flow reserve was impaired in CHF animals. A subsequent study revealed that the CK-M and CK-mito protein levels were decreased in LVR animals while the CK-B levels were increased [52].

However, the total CK activity did not change significantly in the LVR group [52]. These changes may partially contribute to the altered HEP metabolism in hearts with postinfarction remodeling. Subsequently, it has been shown that the CK flux rates are decreased in hearts with postinfarction remodeling but this change does not seem to limit their response to dobutamine [53]. However, the animals that develop CHF have further decreased high energy phosphates and CK flux rate and these changes may contribute to their decreased response to dobutamine [53]. It is also known that the decrease of PCr/ATP in LVR animals during dobutamine infusion is not the result of insufficient myocardial oxygen availability [54]. Furthermore, in CHF hearts, the low basal PCr/ATP and the attenuated response to dobutamine occurred in the absence of myocardial hypoxia, indicating that the HEP and contractile abnormalities were not the result of insufficient oxygen availability [54]. There is also a loss of total adenine nucleotide pool in hearts with postinfarction remodeling as shown by accumulation of interstitial purine metabolites found in a rat model of postinfarction remodeling [55]. The alterations in myocardial HEP and mtATPase have been shown to be substantially more severe in the peri-infarct region than in the remote zone of hearts with compensated postinfarction LV remodeling [56]. These abnormalities mirror the contractile dysfunction of the border zone myocardium and may play a role in the eventual transition to heart failure. The bioenergetic and contractile abnormalities of the BZ, which are triggered by elevated regional wall stress, may extend laterally and eventually involve the

entire LV, thereby leading to global LV dysfunction and the development of CHF[57].

Substrate utilization in post-infarction LV hypertrophy also exhibits shifts in fatty acid and glucose metabolism. In a post-infarction rat model, glucose oxidation was increased by 84% while there was no change in palmitate oxidation 8 weeks after MI [58]. The pattern of gene expression regulating substrate utilization could change as LV remodeling progresses to heart failure, so the same group followed these animals for 20 weeks [59]. At 8 weeks, when left ventricular hypertrophy was present without signs of heart failure, myocardial mRNA expression of glucose transporters (GLUT-1 and GLUT-4) was not altered, whereas mRNA expression of medium-chain acyl-CoA dehydrogenase (MCAD) was significantly reduced in the peri-infarction region. In hearts exhibiting heart failure 20 weeks after infarct-induction there was a change of both mRNA and protein content of GLUT-1 and MCAD [59].

Congestive Heart Failure (CHF) is associated with a decrease in coronary blood flow (CBF) that is matched to a decrease in myocardial oxygen consumption (MVO_2) suggesting a down-regulation of energy utilization [60]. Our laboratory has previously shown that in normal animals ATP sensitive Potassium (K_{ATP}) channel blockade inhibits the decrease in myocardial energy demands in response to hypoperfusion [61]. K_{ATP} channel blockade with intracoronary glibenclamide resulted in a decrease in CBF and MVO_2 without a change in the

relationship between CBF and MVO_2 in CHF animals [62]. The effect of K_{ATP} channel blockade on myocardial energetic in CHF animals remains to be investigated.

In clinical practice, hibernating myocardium refers to areas of regional dysfunction, decreased blood flow and absence of scar in patients with coronary artery disease which are thought to recover after revascularization [63-65]. In animal models, chronic hibernating myocardium can be created by constriction of a proximal coronary artery that leads to progressive reduction in myocardial blood flow and regional dysfunction [66-76]. As opposed to acute ischemia and congestive heart failure, animals with chronic hibernation at short term follow-up had well preserved myocardial energetic despite a reduction in myocardial blood flow and regional function [75]. However, myocardial energetic have not been characterized in a long term follow-up of chronic hibernating myocardium.

CHAPTER 3. STEM CELLS FOR MYOCARDIAL REPAIR USING A TRANS-ARTERIAL CATHETER

Xiaohong Wang[*], Mohammad Nurulqadr Jameel[*], Qinglu Li, Abdul Mansoor, Xiong Qiang, Cory Swingen, Carmelo Panetta, Jianyi Zhang

[*], Authors contributed equally to this manuscript

Using a swine model of postinfarction LV remodeling, this study investigated marrow derived multi potent progenitor cell (MPC) transplantation into hearts with acute myocardial infarction (AMI) via a novel trans-arterial catheter. The left anterior descending artery was balloon occluded after percutaneous transluminal angiography to generate AMI (60 minute no-flow ischemia). The trans-arterial catheter was then placed in the same coronary artery and either 50 million MPCs (Cell, n=6) or saline (Control, n=6) were injected into the border zone myocardium (BZ). LV function was assessed by MRI at pre-AMI, week 1 and week 4 post AMI, whereas myocardial energy metabolism was assessed by ^{31}P-MR spectroscopy at week 4. One week after AMI, the ejection fraction (EF) was significantly reduced in both groups from a baseline of ~ 50% to 31.3±3.9 (Cell) and 33.3±3.1 (Control). However, at week 4, the Cell group had a significant recovery in EF. The functional improvements were accompanied by a significant improvement in myocardial bioenergetics. Histological data demonstrated a 0.55% cell engraftment rate 4 weeks after MPC transplantation. Only 2% of engrafted cells were co-staining positive for cardiogenic markers. Vascular density in the BZ was increased in the Cell group. Conditioned medium from cultured MPCs contained a high level of VEGF which was increased in response to hypoxia. MPCs cocultured with cardiomyocytes inhibited cardiomyocyte mitochondrial membrane potential change and cytochrome C release induced by TNFα. Thus, a paracrine effect may contribute significantly to the observed therapeutic effects of MPC transplantation.

INTRODUCTION

Stem cell transplantation has emerged as a novel therapeutic strategy for limiting post-infarction left ventricular (LV) remodeling and the consequent development of congestive heart failure (CHF) in both animal [77-80] and clinical [39, 41-42, 44, 46] studies. Using a swine model of post myocardial infarction (MI) LV remodeling, we recently reported that transplantation of bone marrow derived multipotent progenitor cells (MPCs) resulted in a significant improvement of cardiac function and correction of abnormal energy metabolism [77]. However, the mechanisms underlying these beneficial effects are not well defined. We and others have demonstrated a very low engraftment rate and even lower cardiomyocyte differentiation rate a few weeks after bone marrow stem cell transplantation [77, 81]. Therefore, the direct contribution of regenerated myocytes to the improved cardiac contractile function appears less likely. Dzau's group has shown a significant protection of stressed cardiomyocytes from apoptosis and consequent reduction in infarct size by injection of concentrated cell culture medium that was obtained from bone marrow derived mesenchymal stem cells (MSCs) with overexpression of Akt, or by injection of MSCs themselves into the myocardium at the time of acute myocardial infarction [81-83]. More recently they demonstrated that the frizzled related protein 2 (Sfrp2) is the key paracrine factor secreted by Akt-modified MSCs that mediates myocardial survival and repair [84]. Using a swine model of concentric left ventricular hypertrophy (LVH), we have demonstrated that transplantation of

vascular endothelial growth factor (VEGF) overexpressing MSCs (VEGF-MSCs) at the time of ascending aortic banding markedly attenuated the development of LVH and resulted in the preservation of LV contractile performance and bioenergetic characteristics [85], supporting the notion that the beneficial effects after bone marrow stem cell transplantation are mediated through a paracrine mechanism by secretion of trophic factors from stem cells that exert a protective effect.

Many different approaches have been used to deliver stem cells into the heart including direct intramyocardial, intravenous, intracoronary and retrograde coronary venous routes [86]. Intracoronary infusion of stem cells at the time of angiography seems the most practical approach clinically. However, its efficacy and safety remain an issue. Using a canine model, it was reported that coronary artery infusion of stem cells resulted in blockage of small vessels, which in turn caused discrete micro-myocardial necrosis [87]. The Micro-Syringe Infusion Catheter (From Mercator MedSystems, CA) used in the present study has the unique feature of a micro-needle that penetrates the coronary artery wall and allows the user to inject the stem cells directly into the myocardium.

The present study has a two-fold hypothesis. Firstly, we hypothesize that MPC delivery via the Micro-Syringe Infusion Catheter would be safe and effective in a clinically relevant porcine model of myocardial ischemia reperfusion. Secondly, we hypothesize that “a trophic effect” plays an important role in

mediating the myocardial structural changes that lead to the beneficial effects of cellular therapy. Namely, the engrafted cells release cytokines that result in enhanced angiogenesis, maintenance of mitochondrial integrity, and inhibition of apoptosis of ischemia threatened and overstretched myocytes in the border zone myocardium (BZ) adjacent to the myocardial infarct. These structural changes are accompanied by the improvement of BZ myocardial contractile performance, which in turn, results in ameliorating the LV wall stress and myocardial bioenergetics.

METHODS

All experiments were performed in accordance with the animal use guidelines of the University of Minnesota, and the experimental protocol was approved by the University of Minnesota Institutional Animal Care and Use Committee (IACUC). The investigation conformed to the *"Guide for the care and use of laboratory animals"* published by the National Institutes of Health (NIH publication No 85-23, revised 1985).

Cell Culture MPCs were provided by Athysis Inc., which were derived from one of the male swine multipotent adult progenitor cell (MAPC) lines generated at the University of Minnesota [88]. MPCs isolation, expansion and differentiation were performed as described previously [77].

Bone marrow derived Multipotent Progenitor Cells (MPCs) were provided from Athysis Inc. The MPCs were expanded from one of the established swMAPC (swine multipotent adult progenitor cell) lines generated in the laboratories of Drs. Verfaille and Zhang [88]. MPCs were transduced with a Lac-Z Retrovirus (RV) supernatant (Lac-Z RV supernatants were generated by co-transfection of pVSV-G retroviral vector (BD Biosciences) and pCL-MFG-LacZ RV packaging vector (Imgenex) using the calcium phosphate method (BD Bioscience, K2051-1) in GP-293 cell line (BD Bioscience). Following transduction with a Lac-Z retrovirus at Athersys Inc., re-evaluation of the cells indicated that the level of Oct3a was significantly lower than in the parent population, and that the cells expressed CD44 and MHC-class I. Cells were maintained for extensive population doublings (>100) following gene marking and large scale expansion (data not shown), and were cytogenetically normal. Cells were assayed for in vitro differentiation response by quantitative PCR, with induction of lineage specific markers compared to non differentiated controls. The robustness of differentiation to hepatocyte and neuroectoderm-like cells was reduced in Lac-Z transduced cells, which expressed low Oct3a transcript levels compared with the parent cells that expressed high levels of Oct3a. These MPCs have previously been shown to maintain multi-potent differentiation potentials [77].

The transduced swine cells were expanded using methods developed for clinical scale production of human Multistem^{TM}. The detailed cell culture methods have been previously described [77]. Briefly, cells were cultured in 60% DMEM-LG /

40% MCDB-201 supplemented with 1x ITS, 0.5x LA-BSA, 0.1mM L-ascorbic acid 2-phosphate, 100U penicillin and 1,000U streptomycin, 50 nM dexamethasone and 2% pre-screened FBS with 10 ng/ml each human PDGF-BB and human EGF and passaged every 2 to 3 days through removal of the growth media and addition of 5 ml 0.25% trypsin per T150 flask.

MPCs were harvested, centrifuged and resuspended at 10 million cells / 1 ml cryo preservation solution that consists of 70% growth media, 20% FBS, and 10% DMSO in 1 mL cryovials. Cells were frozen at ~1^{o}C per minute to –80^{o}C and transferred into liquid nitrogen for long-term storage until of implantation. To thaw MPCs prior to grafting, basal media (expansion media without PDGF-BB, EGF, FBS, and penicillin/streptomycin) was pre-warmed to 37^{o}C, and 9 ml of the warmed media was placed into a 15 ml conical centrifuge tube. Vials of frozen MPCs were thawed in a 37^{o}C water bath for approximately one minute, after which cells were transferred to the pre-warmed medium. The cell number was counted to reach 50 million by hematocytometer and trypan blue was used to check cell viability during the counting. MPCs were washed by 2x PBS and spun down at 400g for 5 minutes and resuspended in 2 ml saline. A small fraction of cells was replated in a T-150 flask to check the cell viability and percentage of Lac-z positive cells. Cells used for transplantation were >80% viable. MPCs conditioned medium in the subsequent experiments was harvested 24 h after culture. As a control, a portion of the medium was incubated for 24 h without MPCs.

Myocardial Ischemia/Reperfusion Model and transarterial stem cell injection Young Yorkshire female swine (~20 kg; Manthei Hog Farm, Elk River, MN) were anesthetized with pentobarbital (30 mg/kg iv), intubated and ventilated with a respirator with supplemental oxygen. Left heart catheterization was performed. Myocardial infarction was created by balloon occlusion of the left anterior descending coronary artery (LAD) distal to the second diagonal for 60 minutes followed by reperfusion after anticoagulation. The trans-arterial catheter (Microsyringe infusion catheter from Mercator MedSystems, CA) was then placed in the same coronary artery and either stem cells at 50 million cell/mL (n=6) or saline (n=6) were injected. The intra myocardial position of the needle was confirmed under fluoroscopy in the cardiac catheter Laboratory with contrast diluted in both placebo and cell injection to confirm delivery outside of vessel lumen. Five equal injections for a total of 50 million MPC were injected with final volume of one mL. If ventricular fibrillation occurred, electrical defibrillation was performed immediately. Animals received standard post-operative care including analgesia until they ate normally and became active.

MRI Methods Animals were examined at baseline, 1 week post infarction and then 4 weeks with MRI. MRI was performed on a 1.5 Tesla clinical scanner (Siemens Sontata, Siemens Medical Systems, Islen NJ) using a phased-array 4-channel surface coil and ECG gating. Animals were anesthetized with 1% isoflurane and positioned in a supine position within the scanner. The protocol consisted of: 1) localizing scouts to identify the long- and short-axis of

the heart, 2) short- and long-axis cine for the measurement of global cardiac function, and 3) delayed contrast-enhancement for the assessment of scar size. Steady-state free precession "True-FISP" cine imaging used the following MR parameters: TR = 3.1 ms, TE = 1.6 ms, flip angle = 79^{o}, matrix size = 256 x 120, field of view = 340 mm x 265 mm, slice thickness = 6 mm (4 mm gap between slices) and 16-20 phases were acquired across the cardiac cycle. Global function and regional wall thickness data were computed from the short-axis cine images using MASS (Medis Medical Imaging Systems, Leiden, The Netherlands) for the manual segmentation of the endocardial and epicardial surfaces at both end-diastole (ED) and end-systole (ED) from base to apex. Short-axis turboFLASH imaging, from base to apex, used TR = 16 ms, TE = 4 ms, TI ~ 220 ms, flip angle = 30^{o}, matrix size = 256 x 148, field of view = 320 mm x 185 mm, slice thickness = 6 mm (0 mm gap between slices) and two signal averages. The appropriate inversion time (TI) was chosen to adequately null the signal intensity (SI) of normal myocardium. Infarct size was calculated from the delayed contrast-enhanced images using MASS to manually segment regions of non-viable tissue. Infarct size was calculated as the ratio of the total scar area to the total LV area.

Spatially localized ^{31}P-MR spectroscopy technique Animals returned to the laboratory for final open chest MR spectroscopic study 4 weeks after myocardial infarction. Magnetic field shimming to improve the magnetic field homogeneity of the heart was achieved by the "auto-shim" scheme (Varian

Assoc. Inc., CA). Spatially localized ^{31}P NMR spectroscopy was performed using the RAPP-ISIS/FSW method [54, 89-91], which is the rotating-frame experiment using adiabatic plane-rotation pulses for phase modulation (RAPP)-imaging-selected in vivo spectroscopy (ISIS)/Fourier series window (FSW) method. Detailed experiments documenting voxel profiles, voxel volumes and spatial resolution attained by this method have been published previously. In this application of RAPP-ISIS/FSW, the signal origin was first restricted to a 12*12 mm two-dimensional column perpendicular to the LV wall. The signal was later localized into three well resolved and five partially resolved layers along the column and hence, across the LV wall. Localization along the column was based on B_1 phase encoding and employed a 9-term Fourier series window as previously describe [54, 89-91]. The phase encoded data were used to generate a voxel or a "window" that can be shifted arbitrarily by post data acquisition processing along the phase encode direction (in this case perpendicular to the surface coil and thus the heart wall); consequently, voxels were generated at different distances or "depths" from the outer LV wall. However, we normally present five voxels centered about 45°, 60°, 90°, 120°, and 135° phase angles as previously described. There is absolutely no overlap between the 135° voxel (corresponding to the subepicardium) and the 45° voxel (corresponding to the subendocardium). Whole wall spectra were obtained with the image-selected *in vivo* (ISIS) technique, defining a column 12*12 mm^2 perpendicular to the heart wall. The calibration of spectroscopic parameters was facilitated by placing a polyethylene capillary filled with 15 µl of 3 M/L phosphonoacetic acid into the

inner diameter of the surface coil. This phosphonoacetic acid standard was used only for calculating the 90 degree pulse length of the RAPP-ISIS method [54, 89-91]. The position of the voxels relative to the coil was set according to the B_1 strength at the coil center which was experimentally determined in each case by measuring the 90° pulse length for the phosphonoacetic acid standard contained in the reference capillary at the coil center. NMR data acquisition was gated to the cardiac and respiratory cycles using the cardiac cycle as the master clock to drive both the respirator and the spectrometer as previously described [54, 89-91]. The surface coil was constructed from a single turn copper wire 25 mm in diameter with each side of the coil leads soldered to a 33 pF capacitor. Complete transmural data sets were obtained in 10-minute time blocks using a repetition time of 6-7 seconds to allow for full relaxation for ATP and inorganic phosphate (Pi) and approximately 95% relaxation of the PCr resonance [54, 89-91]. The ratios of PCr to ATP (PCr/ATP) were calculated for each transmurally differentiated spectra set as previously described [54, 89-91]. All resonance intensities were quantified using integration routines provided by the SISCO software.

^{1}H- NMR spectroscopy technique ^{1}H NMR methods have been previously reported in detail [54, 92]. In brief, radiofrequency (RF) transmission and signal detection were performed with the dually tuned 28 mm diameter surface coil. A single-pulse-collection sequence with a frequency selective Gaussian excitation pulse (1ms) was used to selectively excite the N-δ proton resonance signal of the

proximal histidine in deoxymyoglobin (Mb- δ). This technique provided sufficient water suppression due to the large chemical shift difference between water and Mb- δ (>14 kHz). The NMR signal was optimized by adjusting the RF pulse power using the water signal as a reference. A short repetition time (TR = 25 ms) was used due to the short T_1 of Mb- δ. Each spectrum was acquired in 5 min (10,000 FIDs). Although the short T_1 of Mb- δ and fast acquisition prevent gating to the cardiac cycle, the signal loss due to motion is negligible compared to the inherently broad line width of the Mb- δ peak.

Surgical preparation for open chest MR spectroscopy study Detailed surgical preparations for MRS study are published previously [56, 77, 91]. Briefly, animals were anesthetized with pentobarbital (30 mg/kg followed by a 4 mg/kg/hr iv), intubated and ventilated with a respirator and supplemental oxygen. Arterial blood gases were maintained within the physiologic range by adjustments of the ventilator settings and oxygen flow. 3.0 mm OD heparin-filled polyvinyl chloride catheters were inserted into the ascending aorta (Ao) and inferior vena cava (IV). A sternotomy was performed, and the heart was suspended in a pericardial cradle. A third heparin-filled catheter was introduced into the LV through the apical dimple and secured with a purse string suture. A 25 mm diameter NMR surface coil was sutured onto the anterior wall of the LV adjacent to the infarct region. The pericardial cradle was then released, and the heart was allowed to assume its normal position in the chest. The surface coil leads were connected to a balanced-tuned external circuit and the animals positioned within the

magnet. Hearts with post infarction LV remodeling are very sensitive to alterations of loading conditions of the LV, and that subtle differences in LVEDP or LVSP could affect myocardial contractile performance measurements. In order to compensate for insensible fluid loss in the open chest studies, we routinely administer saline at rate of 1 ml/min i.v. during the entire experimental data acquisition. Ventilation rate, volume and inspired oxygen content were adjusted to maintain physiologic values for arterial PO_2, PCO_2 and pH. Aortic and LV pressures were monitored continuously throughout the study. Hemodynamic measurements were acquired simultaneously with the ^{1}H - and ^{31}P- MR spectra.

MR spectroscopy study protocol and hemodynamic measurements

Hemodynamic measurements were acquired simultaneously with the NMR spectra. Aortic and LV pressures were measured using pressure transducers positioned at mid-chest level [89-91] and recorded on an 8-channel recorder. After all the baseline data were obtained, animals received combined dobutamine and dopamine infusion (20 μg/kg/min. each) to induce a very high cardiac workstate. After waiting for approximately 5 minutes after the initiation of catecholamine infusion, all the spectroscopic and hemodynamic data were again measured under the high cardiac workstates.

Tissue preparation The LV was sectioned in a bread-loaf manner into 6 transverse sections (~ 10 mm in thickness) from apex to base. Even rings were subdivided into 12 circumferential specimens and fixed in zinc fixative (Anatech

LTD, Battle Creek, MI, USA) for Haematoxylin & Eosin (HE), immunofluorescence staining and engraftment evaluation.

Engraftment evaluation Each of the 12 pieces of cardiac tissue of a short axis ring were stained by X-gal (Invitrogen) and embedded in Tissue-Tek OCT (Fisher Scientific). Serial cryostat sections (10μm in thickness) were obtained from the whole transverse even rings. Engrafted MPCs were identified by counting the X-gal-positive nuclei in every 10th serial section of the whole transverse ring and then multiplying by 10 to obtain the total number of engrafted MPCs per ring. The total number of engrafted MPCs equals two fold x-gal staining positive cells in all three even rings. The engraftment rate of transplanted MPCs was calculated by dividing the total number of engrafted MPCs by 50×10^6 (the number of MPCs injected) and multiplying by 100%.

Immunohistochemistry Detailed immunohistochemistry methods are described previously [85, 93]. Briefly, cryostat sections (10μm thickness) were obtained for immunofluorescence staining to evaluate myocyte or endothelial differentiation of injected cells. Antibodies used included Troponin T (cardiac isoform Ab-1, Lab Vision Corp. Chicago, IL), α-sarcomeric actin, N-cadherin, and CD31 (Research Diagnostic Inc. Flanders, NJ). Nuclear counterstaining was performed with 4',6'-diamino-2-phenylindole (DAPI, Molecular Probes, Grand Island, New York).

Analysis of Myocardial Vascular Density Vascular density was assessed by staining with anti-CD31 (BD Biosciences, San Diego) antibody. The sections were visualized using fluorescence-labeled secondary antibody (Molecular Probes Inc., Eugene, OR). Images were taken at a magnification of X20 using an Olympus microscope (BX51/BX52; Tokyo). The number of capillaries were counted in a blind fashion in three fields per each section of the peri-infarct zone, and total of five sections per ring were analyzed (n = 4 for each group). The quality of the computer analysis (Image J) was checked against manual counting.

HL-1 myocyte culture and apoptosis HL-1 myocytes (from Claycomb Laboratory, University of Louisiana) were cultured as previously described [85]. Briefly HL-1 cells were plated onto fibronectin-gelatin-coated plates or flasks and cultured in Claycomb medium supplemented with 10% fetal bovine serum, 100 U/ml penicillin, 100 µg/ml streptomycin, 0.1 mM norepinephrine, and 2 mM L-glutamine. For the coculture experiment, HL-1 cells were plated in 12-well plates at a total density of 5 x 10^5 (1:3 ratio of MPCs to HL-1 cells) in half MPC medium and half Claycomb medium. Before being cocultured, HL-1 cells were labeled with Vybrant CFDA SE cell tracer kit (Molecular Probes). Labeled HL-1 cells were extensively washed and cocultured with MPCs. The coculture and HL-1 cells alone were treated with 40ng TNFα for 18 h. Apoptosis was assessed by staining with Hoechst 33342 (H33342) dye and then quantifying the percentage of

apoptotic nuclei (300 cells counted per sample) in the CFDA-labeled subset by identifying cells with H33342 staining [85].

Identification of angiogenic factors released from the stem cells The cultured MPCs were divided into two subgroups ($5x10^4$cell/per group). One MPC group was exposed to 2% oxygen (hypoxia). The other group was cultured in normoxic condition. Eighteen hours later, the unconcentrated supernatants were subjected to ELISA assay for VEGF and Insulin like growth factor (IGF) contents according to manufactures' instructions, respectively.

Mitochondrial membrane potential ($\Delta\psi m$) changes detection HL-1 cells were plated on chamber slides and the next day cells were stained with Hoechst 33342 (H33342) dye. After thoroughly washing three times, MPCs were plated onto the chamber slides (1:1 ratio). After 12 hours, the cells were treated with 40ng tumor necrosis factor α (TNFα) for 6 hours. Mitochondrial inner-membrane potential changes were evaluated using Mitochondria staining kit according to the manufacturer's directions (Sigma-aldrich, Saint Louis, Missouri).The cationic, lipophilic dye, JC-1 (5,5',6,6'-tetrachloro-1,1',3,3'-tetraethybenzimidazolocarbo-cyanine iodide) aggregates can be visualized in the mitochondria as bright red flurorescence, representing intact mitochondria and JC-1 monomers as green flurorescence, which represent disrupted mitochondria.

MPCs cocultured with neonatal cardiomyocytes and Cytochrome C release Primary cultures of cardiac myocytes were prepared by enzymatic digestion of ventricles obtained from neonatal (2 day old) Sprague-Dawley rats as previously described [93]. Coculture experiments were set up in the fibronectin-coated chamber slides at a total density of 2×10^4(1:1 ratio; cardiomyocytes: MPC) in MPCs medium supplemented with 2% FBS, 100 µg/ml of penicillin, and 250 µg/ml of streptomycin at 37 °C in humid air with 5% CO_2. Cytochrome C release was detected by immunofluroscence staining using anti-cytochrome C antibody after cardiomyocytes and the coculture cells were treated with 40 ng TNFα. Troponin T was used to stain cardiomyotyes. Double staining positive cardiomyocytes were detected and counted.

Statistics and Data analysis Anatomic data, wall stress data, capillary density and the *in vitro* apoptosis data were compared between the two groups (MI and MI + cell) using the Student t-test. The repeated measures ANOVA was applied to compare the measurements of systolic thickening fraction, ejection fraction and scar size across two treatment groups (MI and MI + cell) and different time points (before MI, 1 week, and 4 week after MI) and to compare the measurement of myocardial PCr/ATP and hemodynamic data across two treatment groups (MI and MI + cell) and two hemodynamic conditions (baseline and after inotropic stimulation). For comparison between the two treatment groups, the conventional significance level of type I error ($P < 0.05$) was used. The Bonferroni correction for the significance level was used to take into account

multiple comparisons. All values are expressed as mean ± standard deviation (SD). All statistical analyses were performed in Sigmastat version 3.5 (San Jose, CA).

The authors had full access to the data and take responsibility for its integrity. All authors have read and agree to the manuscript as written.

RESULTS

Anatomic and Hemodynamic Data Four of the 16 pigs with LAD occlusion and reperfusion died within the first 60 minutes after coronary occlusion due to ventricular fibrillation. The surviving 12 pigs were randomized to receive either MPC (n=6) or saline only (n=6). The anatomic data for the 12 swine with LAD ligation is summarized in Table 1. The degree of LVH as reflected by LVW/BW and RVW/BW was not significantly different between the MPC and saline group. The hemodynamic data at baseline and at increased workload are summarized in Table 2. Inotropic stimulation caused a significant increase in the heart rate and left ventricular systolic pressure and consequently rate-pressure product. However, there was no significant difference between the swine with cell treatment versus swine without cell treatment.

Global Functional Data The temporal changes in global function as measured by MRI are depicted in Figure 1. There was no significant difference between the two groups at baseline. At week 1, the distal LAD occlusion caused

a similar scar size in both groups with significant decrease in LV ejection fraction (EF), with no significant difference between the two groups. However, there was a remarkable LV chamber functional recovery from 1 week to 4 weeks after cell transplantation (EF, 46.3±6.6 vs. 33.3±3.1, $p<0.001$), which was not observed in the control group (Figure 1a). Thus, at week 4, the LVEF was significantly higher in the cell treated animals as compared to control animals (46.3±6.6 vs. 35.4±3.2, $p<0.001$) (Figure 1a). This functional improvement in the MPC treatment group was accompanied by a significant decrease in scar size at 4 weeks compared with saline group (4.8±1.9 vs. 8.8±2.1, $p=0.047$). It should be noted that there was a significant decrease in the scar size from week 1 to week 4 in the cell treated group (4.8±1.9 at 4 week vs. 9.2±3.5 at 1 week, $p<0.001$) (Figure 1b).

Regional Contractile Functional Data The left ventricle was divided into 16 segments. The apex was divided into 4, mid-LV into 6 and base into 6 segments. Distal LAD occlusion resulted in a thin walled infarct in the apex mainly in the anteroseptal segments (segments 1 and 2). The remaining apical segments (segments 3 and 4) are the border zone and the mid LV and base make up the remote zone. Systolic thickening fraction was measured as a surrogate marker of regional left ventricular contractile function. Distal LAD occlusion alone resulted in systolic bulging of the infarct zone at 1 week which persisted at 4 weeks (Table 3). MPC treatment resulted in increased systolic thickening fraction of the infarct and border zone at 4 weeks as compared to

control (Table 3). Moreover, the systolic thickening fraction in the infarct and border zone within cell treated animals was significantly increased at 4 weeks as compared to 1 week (Table 3). LV wall stress (σ) in different LV segments at 4 weeks was calculated according to the Laplace law, as previously described, using the following equation: $\sigma = PR/(2T)$ [57], where P is LV pressure, *R* is chamber radius, and T is wall thickness measured from CINE MRI images in the particular region of the LV. MPC treatment resulted in a significant decrease in wall stress in the infarct (300±16 mmHg in Control vs 208±20 mmHg in MPC treated, p=0.009) and border zone (242±18 mmHg in Control vs 174±14 mmHg in MPC treated animals, p=0.01).

Myocardial high-energy phosphate (HEP) and Pi levels Myocardial HEP and Pi levels are reflected by the PCr/ATP ratios as shown in Figure 2. The PCr/ATP ratio is significantly higher at 4 weeks in the pigs treated with MPC as compared to those without treatment (2.03±0.31 vs 1.53±0.28, p=0.009). After increased workload, the PCr/ATP ratio decreased in both groups but was still significantly higher in the cell treated pigs (1.80±0.24 vs 1.43±0.25, p=0.027). No deoxymyoglobin resonance peak was detected in either group using ^{1}H-MRS, which supports our previous findings that the border zone bioenergetic abnormalities in hearts with postinfarction LV remodeling are not caused by a persistent myocardial ischemia.

Cell engraftment and differentiation in Vivo Cell engraftment was determined by counting β-galactosidase staining positive cells in tissue sections and cell engraftment rate was calculated as a percentage of engrafted cells out of a total 50 million injected stem cells. Two additional pigs were sacrificed at 10 days post MI and cell transplantation to assess for engraftment at an earlier time period. Ten days after cell transplantation, the cell engraftment rate was about 5%. Most of the cells were retained in the infarcted area and only a small portion of the engrafted cells resided in the peri-infarct and remote areas (Figure 3a). Four weeks after cell transplantation, cell engraftment rate was remarkably decreased and reached 0.55% (n=6). To determine the differentiation of engrafted cells, tissue sections were double-stained for ß-galactosidase and cardiac-specific markers, including troponin T, α-sarcomeric actin, and N-cadherin. We found that approximately 2% of engrafted cells costained positive for ß-galactosidase and troponin T or α-sarcomeric actin 10 days after cell transplantation (Figure 3b, 3c). These double staining positive cells were only observed in the peri-infarct and remote areas. Among the cells that costained positive for ß-galactosidase or α-sarcomeric actin, we identified gap junctions between the cells as indicated by N-cadherin immunoflurescence staining (Figure 3b). These data suggest that transplanted MPCs engraft successfully and can undergo in vivo transdifferentiation into cardiomyocyte-like cells or form fused cells**.**

Vascular Density To determine the mechanisms underlying the beneficial effects of MPC transplantation, we investigated the effects of MPC transplantation on neovascularization and angiogenesis in the post-MI hearts. At 4 weeks after cell transplantation, immunofluorescence staining for CD31 antibody indicated significant angiogenesis in stem cell treated hearts, with more CD31 expressing capillaries being present in peri-infarct regions of cell treated compared with saline-treated hearts (Figure 4a). Quantitative evaluation of CD31-positive capillary numbers per high-power field (20x) indicated that vascular density was significantly greater in the MPC treated group than the saline-treated group (Figure 4a, b). However, few cells were staining positive for both the endothelial cell marker CD31 and ß-galactosidase (data not shown). These data suggest that transplanted MPCs may promote angiogenesis through a paracrine effect.

To further identify the angiogenic factors, we determined the levels of VEGF and IGF in the conditioned medium under different culture conditions. We found that MPCs can secrete detectable VEGF in normoxic conditions, which was significantly increased in response to hypoxia (Normoxia, 456.1+/-104.1pg/5x10^4cell; hypoxia, 1543.8+/-77.1pg/5x10^4cell, n=5, P<0.001). However, the IGF levels secreted under both conditions were too low to be detected. These data suggest that MPCs secrete VEGF that is an important angiogenic factor contributing to the observed cellular therapy associated beneficial effects.

The protective effect of MPCs on mitochondrial membrane potential.

To investigate the protective effect of MPCs on cardiomyocytes, HL-1 myocyte apoptosis was induced by inflammatory factor TNFα. Coculture of HL-1 cells with MPCs significantly inhibited TNFα induced apoptosis (HL-1+TNFα, 32+/-3; TNFα+coculture, 14+/-1%; n=6, p<0.001)(Figure 5a). To further determine its underlying mechanisms, the alteration in mitochondrial inner-membrane electrochemical potential was determined by staining with the cationic, lipophilic dye, JC-1. MPCs significantly inhibited TNFα induced HL-1 cell mitochondrial membrane potential changes (Figure 5b). Co-cultured MPCs with neonatal cardiomyocytes also inhibited TNFα induced cytochrome c release from neonatal cardiomyocytes (Figure 5c). These data suggest that the paracrine factors secreted by MPCs play a protective role in preventing myocytes from apoptosis.

DISCUSSION

The present study demonstrates that MPC transplantation through a trans-coronary arterial catheter approach is safe, feasible and effective. MPC transplantation is associated with increase in vascular density, inhibition of apoptosis and reduction of infarct size, which is accompanied by improvement in border zone and infarct zone contractile function, with consequent improvement in myocardial bioenergetics and global LV function. These functional beneficial effects were observed despite a low engraftment of MPCs at 4 weeks. In vitro, the MPCs significantly inhibited TNFα induced mitochondrial membrane potential

change and cytochrome C release from myocytes. Additionally, coculture of MPCs with HL-1 cells inhibited TNFα induced apoptosis. Thus, the MPC induced "trophic effect" results in structural changes that are characterized by increased vascular density, spared myocytes from apoptosis and decreased infarct size, which in turn, leads to the improvement of BZ myocardial contractile performance, amelioration of regional wall stress and myocardial bioenergetics.

Stem cell delivery via trans-arterial injection. Although clinical trials of intra-coronary artery infusion of stem cells have shown moderate LV functional improvement [41-42, 44, 46], a report of a dog study suggested that coronary artery infusion of stem cells resulted in blockage of small vessels, which in turn caused discrete micro-myocardial necrosis [87]. In the present study, we employed a trans-arterial catheter with a micro-needle that penetrates the coronary artery wall and injects stem cells directly into the myocardium that is exposed to ischemia and reperfusion. We found similar engraftment of stem cells as previous studies using open heart direct intra myocardial injection [77, 94]. These data demonstrate that trans-coronary injection of MPCs through this technique is safe and leads to the improvement in left ventricular function.

Contractile performance in the infarct border zone. Increased LV wall stress in the border zone has been implicated among the factors attributing for left ventricular remodeling after myocardial infarction [56, 95]. It has been shown in a porcine model that myocardial infarction leads to dyskinesis in the infarct

region and hypokinesis in the infarct border zone [56]. MPC transplantation caused an improvement in infarct and border zone systolic thickening fraction in the present study (Table 3), which in turn, effectively reduced wall stress (border zone wall stress was 242±18 mmHg in Control vs 174±14 mmHg in MPC treated animals, p=0.01) and consequently improved the mismatch of energy delivery and demand (Figure 2) [77, 94]. The contractile performance improvement in the BZ is likely based on the myocardial structural improvements that are characterized by increased vascular density (Figure 4) and reduced apoptosis (Figure 5) in the BZ, and myocyte differentiation (Figure 3).

Border Zone Myocardial Energetics Post infarction LV remodeling is associated with decreased high energy phosphates, PCr/ATP and expression of several proteins crucial to oxidative ATP production and these abnormalities are most severe in the borderzone [56].Our study confirmed these reports and showed that these abnormalities are worsened during catecholamine stimulation induced high cardiac workstate (Figure 2). The improved myocardial bioenergetics in response to the stem cell transplantation was also supported by the in vitro experiments indicating that mitochondrial inner-membrane electrochemical potential was significantly improved (Figure 5b), which could effectively increase the mitochondrial oxidative phosphorylation potential. This improvement in mitochondrial function may have an important role in cell survival and inhibition of the apoptotic pathway in resident cardiac progenitors.

Effect of cell transplantation on infarct size Sequential MRI functional assessment allowed us to conclude that the infarct size in swine treated with MPC decreased from 1 week to 4 week interval, while the scar sizes in swine without MPC treatment was maintained throughout the follow-up (Figure 1b). This reduction in scar size with stem cell treatment has been seen previously in other reports [78, 83]. The beneficial effects of MPC transplantation could be related to MPC differentiation into cardiomyocytes [11] or mobilization of endogenous progenitors to the injury site by paracrine effects [83]. Recently, it has been shown that endogenous cardiac progenitor cells upon activation can home to the infarcted myocardium and help in myocardial regeneration [96-99]. In the present study, less than 1% of transplanted MPC cells engrafted at 4 week, and even a smaller percentage expressed markers of cardiomyocytes. This suggests that the functional and bioenergetic improvements are likely secondary to paracrine effects. The data from the present study indicates a "trophic effect" that is the cytokines released from the engrafted stem cells act upon the host myocytes and spare them from apoptosis.

Stem cells induced Anti-Apoptosis effect Apoptosis does occur in failing hearts [100]. Mitochondrial release of cytochrome c has been implicated in apoptosis induced by TNF-α [101]. Mesenchymal stem cell transplantation has been shown to have significant anti-apoptosis effects [80, 82-83]. Data from the present study supports this hypothesis and further elucidates this finding by showing that MPC co-cultured with neonatal rat cardiomyocytes inhibits TNF-α

induced cytochrome c release. Mitochondria serve a central role in apoptotic pathways. It has been shown that the mitochondrial respiratory chain (MRC) complex I is inhibited in the early phase of TNFα induced apoptosis [101]. Inhibition of complex I can affect electron flow through the other complexes of the mitochondrial oxidative physporylation leading to cytochrome c release and caspase 3 activation followed by the reduction of mitochondrial membrane potential. The data from the present study demonstrates that the TNFα induced loss of mitochondrial membrane potential can be inhibited by stem cell treatment. The improvement in myocardial energetics *in vivo* with MPC treatment observed in the present study indicates that the impairment in mitochondrial respiratory chain, F0F1 ATP synthase and ATP production are ameliorated by MPC treatment.

Stem cell induced neovascularization We hypothesized that the mechanism for improvement in ventricular function in response to MPC transplantation is partially due to neovascularization. MPC treated animals demonstrated a significant increase in vascular density as compared to animals which received saline (Figure. 4). This generation of new coronary vessels after ischemic injury is very important clinically as it leads to increased blood flow to the infarct and border zone [102], and consequently spares ischemia threatened myocytes from apoptosis leading to improved ventricular function. The neovascularization is probably related to both an increase in angiogenesis and vasculogenesis. Previously, we reported that vasculogenesis as evidenced by

endothelial differentiation from MPC did contribute to the increased vascular density although only 3% of the engrafted MPCs differentiate into endothelial cells [77]. In our present study, we observed insignificant endothelial differentiation of transplanted MPCs 4 weeks after the cell transplantation. Thus, it seems that the endothelial differentiation from MPCs has minimal effect on vasculogenesis. However, it is possible that the MPC transplantation results in recruitment of endogenous cardiac or bone marrow endothelial progenitor cells (EPCs) that leads to vasculogenesis and contributes to the increased vascular density (Fig. 4 Panel B). In addition, it has been recently demonstrated that transplantation of cardiac progenitor cells (CPCs) induces neovascularization primarily through vasculogenesis [102]. Data from the present study demonstrates that MPCs secrete a significant level of VEGF under normoxic conditions, which was further increased in response to hypoxia. It has been previously reported that VEGF secretion by MSCs is a potent angiogenic factor to promote neovascularization as well as inhibit apoptosis [103]. Taken together, these data suggest that VEGF plays an important role in myocardial protection that is associated with MPC transplantation.

In summary, the present study demonstrates that trans-coronary artery injection of MPCs in a porcine model of ischemia/reperfusion resulted in improvement of myocardial contractile function, reduction of BZ wall stress, limitation of the scar size expansion and balance of myocardial energy delivery and demand. Since the engraftment rate is low and myogenic differentiation is

even lower, the beneficial effects are most likely related to the “trophic effects” of MPCs on the host myocardium, which include promotion of angiogenesis, maintenance of mitochondrial integrity, and inhibition of apoptosis of ischemia threatened and overstretched myocytes in the BZ myocardium.

FIGURE LEGENDS

Figure 1. The functional and structural improvements 4 weeks after MPC transplantation into myocardial infarction hearts. **A:** MPC transplantation into the border zone myocardium in a swine ischemia/reperfusion model significantly attenuated the deterioration of cardiac function. **B:** MPC transplantation into the border zone myocardium in a swine ischemia/reperfusion model significantly limited the scar size expansion following myocardial infarction at 4 weeks. Data are mean+/-SD; n=6 in each group. Pair-wise p values are derived from repeated measures ANOVA with Bonferroni correction.

Figure 2. MPCs transplantation into the border zone myocardium significantly improved LV bioenergetics as reflected by altered myocardial PCr/ATP 4 weeks after MI at baseline and high work states. Data are mean+/-SD; n=6 in each group. Pair-wise p values are derived from repeated measures ANOVA with Bonferroni correction.

Figure 3. Histological staining of the tissues from the heart 10 days after transplantation of retrovirus lacZ labeled swine MPCs. **A:** H&E staining of the tissues from the heart 10 days after transplantation of retrovirus lacZ labeled swine MPCs. Panel (a) shows that the engrafted cells (LacZ) are distributed in peri-infarct and remote regions (magnification, x100); panel (b) shows the same sections at high magnification (magnification, x400). **B:** Engraftment and

differentiation of Swine MPCs in vivo. Swine MPCs labled with LacZ were injected into myocardial infarcted hearts via a transmural catheter delivery and the tissues were harvested and dissected into 10μm sections. Dissected samples were stained for LacZ (dark blue), troponin T (green), and/or N-cadherin (red). Nuclei were stained by DAPI (blue). Upper panel: Low magnification. Lower panel: High magnification. **C:** Engraftment and differentiation of Swine MPCs in vivo. Dissected samples were stained for LacZ (blue) and alpha sarcomeric actin (Green). Nuclei were stained by DAPI (blue). Left Panel: low magnification; Right Panel: high magnification.

Figure 4. Transplantation of MPCs into myocardial infarction hearts significantly promoted angiogenesis which was probably mediated by release of VEGF. **A:** Immunoflurescence staining of tissues from myocardial infarction and MPC transplantation heart; **B:** Mean number of CD31 containing capillaries in border zone myocardium (n=6, $p<0.01$). Data are mean+/-SD.

Figure 5. The protective effect of MPCs on cardiomyocytes. **A:** Cocultured Swine MPCs with HL-1 cells significantly inhibited TNFα induced HL-1 cell apoptosis (n=6, $P<0.001$). Data are mean +/-SD. **B:** Swine MPCs cocultured with HL-1 cells significantly inhibited TNFα induced mitochondrial membrane potential changes. **C:** Swine MPCs cocultured with rat neonatal cardiomyocytes significantly inhibited TNFα induced cytochrome C release.

Table 1. Anatomic Data obtained 4 weeks after MI

	BW (kg)	LVW (g)	RVW (g)	LV/BW (g/kg)	RV/BW (g/kg)
MI (n=6)	33±5	97±13	33±8	2.96±0.24	1.00±0.15
MI + Cell (n=6)	32±6	98±23	34±6	3.01±0.27	1.06±0.12

Values are mean±SD; MI, myocardial infarction; n, number of pigs; BW, Body weight; LVW, Left ventricular weight; RVW, Right ventricular weight.

Table 2. Hemodynamic data obtained 4 weeks after MI

	HR (beats/min)	**Ao-S** (mmHg)	**Ao-D** (mmHg)	**Mean AoP** (mmHg)	**LVSP** (mmHg)	**LVEDP** (mmHg)	**RPP x 10^3** ($mmHg.min^{-1}$)
MI (n=6)							
Baseline	73±10	93±10	51±10	65±6	99±13	5±1	7.14±1.24
DB+DP	135±26	124±19	54±14	77±11	151±18	7.5±2.9	20.51±5.15
p-value within MI	<0.001	NS	NS	NS	0.009	NS	<0.001
MI + Cell (n=6)							
Baseline	100±28	95±18	63±21	74±19	108±26	5±1	11.02±5.12
DB+DP	148±23	110±29	63±16	79±19	148±28	6.7±2.6	21.58±3.87
p-value within MI+Cell	<0.001	NS	NS	NS	0.013	NS	0.001

Values are mean±SD; n, number of pigs; MI, myocardial infarction; DbDp, Dobutamine and Dopamine (each 20μg/kg/min intravenous); HR, heart rate; Ao-S, aortic systolic pressure; Ao-D, aortic diastolic pressure; LVSP, left ventricular systolic pressure; LVEDP, left ventricular end diastolic pressure; RPP, rate pressure product (HR x LVSP); NS, Not significant; Repeated Measures ANOVA p value is not significant for the effect of cell treatment with inotropic stimulation (p=0.353). Pair-wise comparisons within groups are listed in the table.

Table 3. Systolic thickening fraction 1 week and 4 weeks after the MI measured by MRI

	Infarct Zone		p-value within group	Border Zone		p-value within group	Remote Zone		p-value within group
	1 week	4 weeks		1 week	4 weeks		1 week	4 weeks	
MI	-4.3±1.5	-4.5±1.3	0.927	8.9±1.4	8.8±1.7	0.986	27.9±3.0	30.9±5.7	NS
MI + Cell	1.0±3.9	17.3±2.9	<0.001	12.3±2.8	24.1±5.5	0.005	28.7±4.6	34.2±4.9	NS
p-value between group	0.031	<0.001		0.229	<0.001		NS	NS	

Values are mean ± SD; n=6 in each group; Pair-wise p values are derived from repeated measures ANOVA with Bonferroni correction; NS=Not significant.

Fig. 1: The functional and structural improvements 4 weeks after MPC transplantation into MI hearts

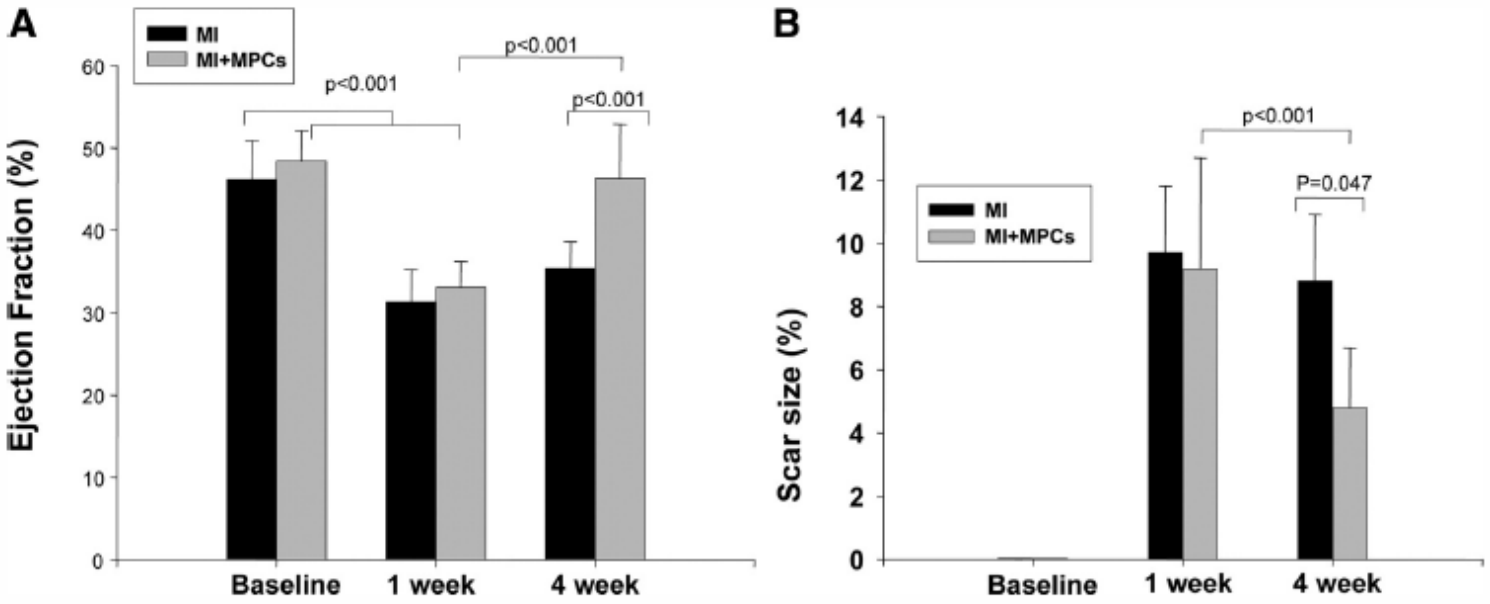

Fig. 2: MPC transplantation into the BZ myocardium significantly improved LV bioenergetics, as reflected by altered myocardial PCr/ATP 4 weeks after MI at baseline and in high work states

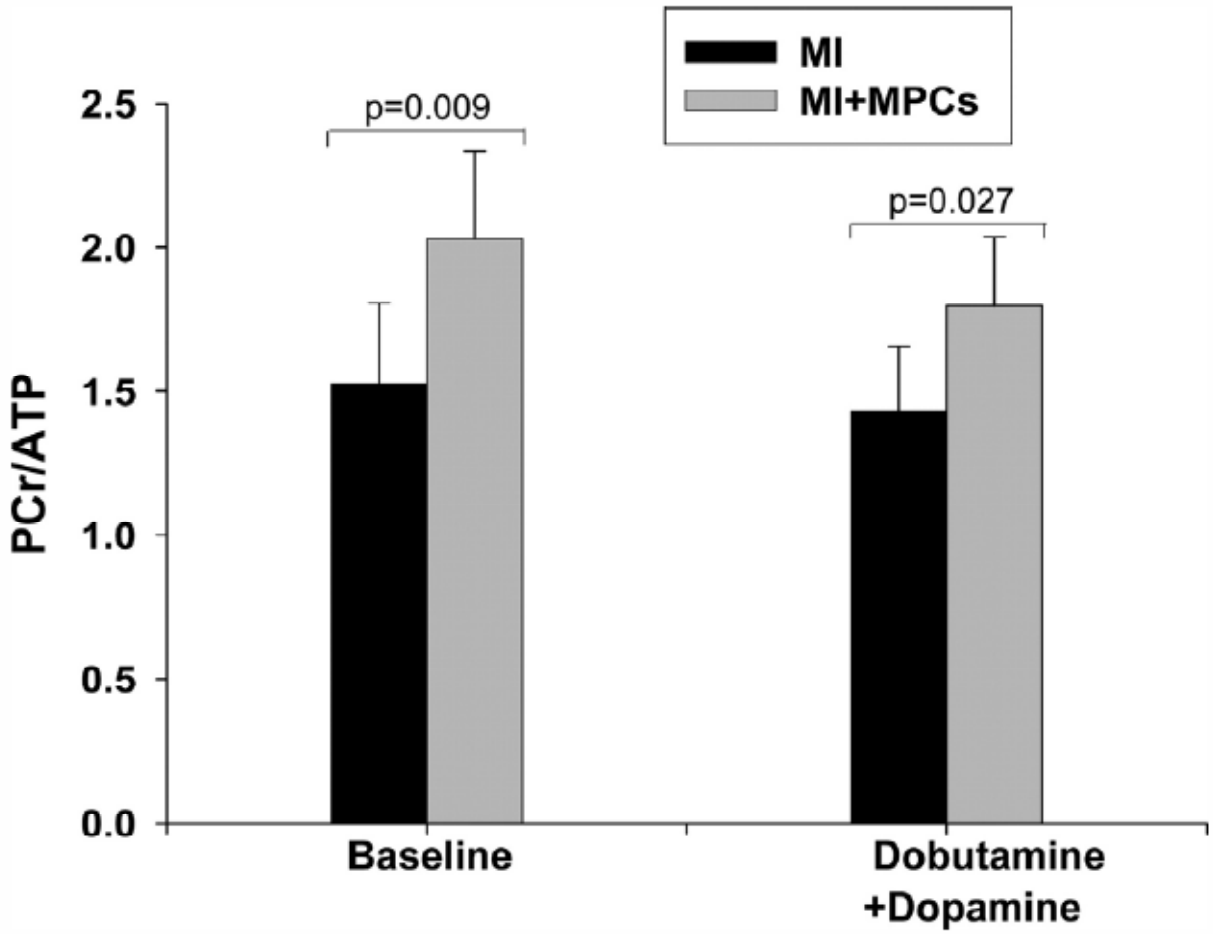

Fig. 3: Histologic staining of tissues from the heart 10 days after transplantation of retrovirus LacZ-labeled swine MPCs

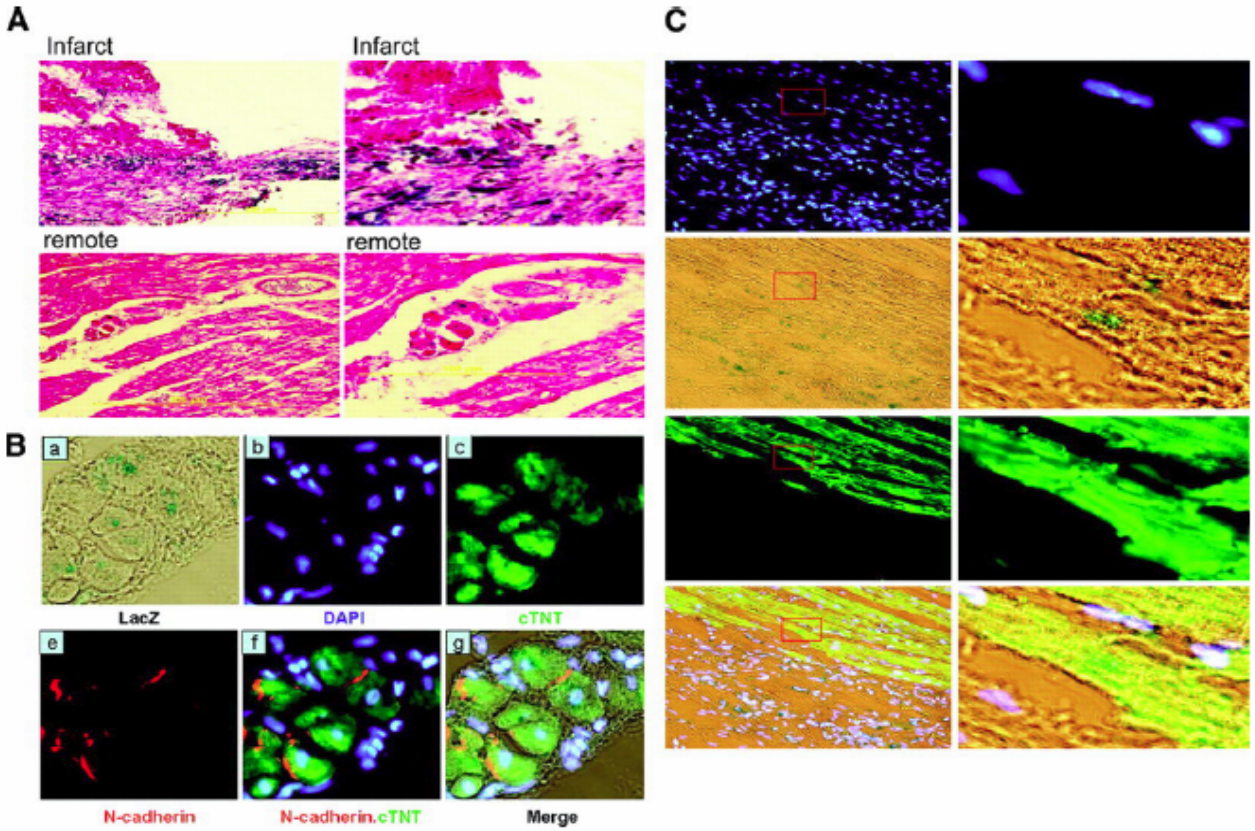

Fig. 4: Transplantation of MPCs into MI hearts significantly promoted angiogenesis, which was probably mediated by release of VEGF

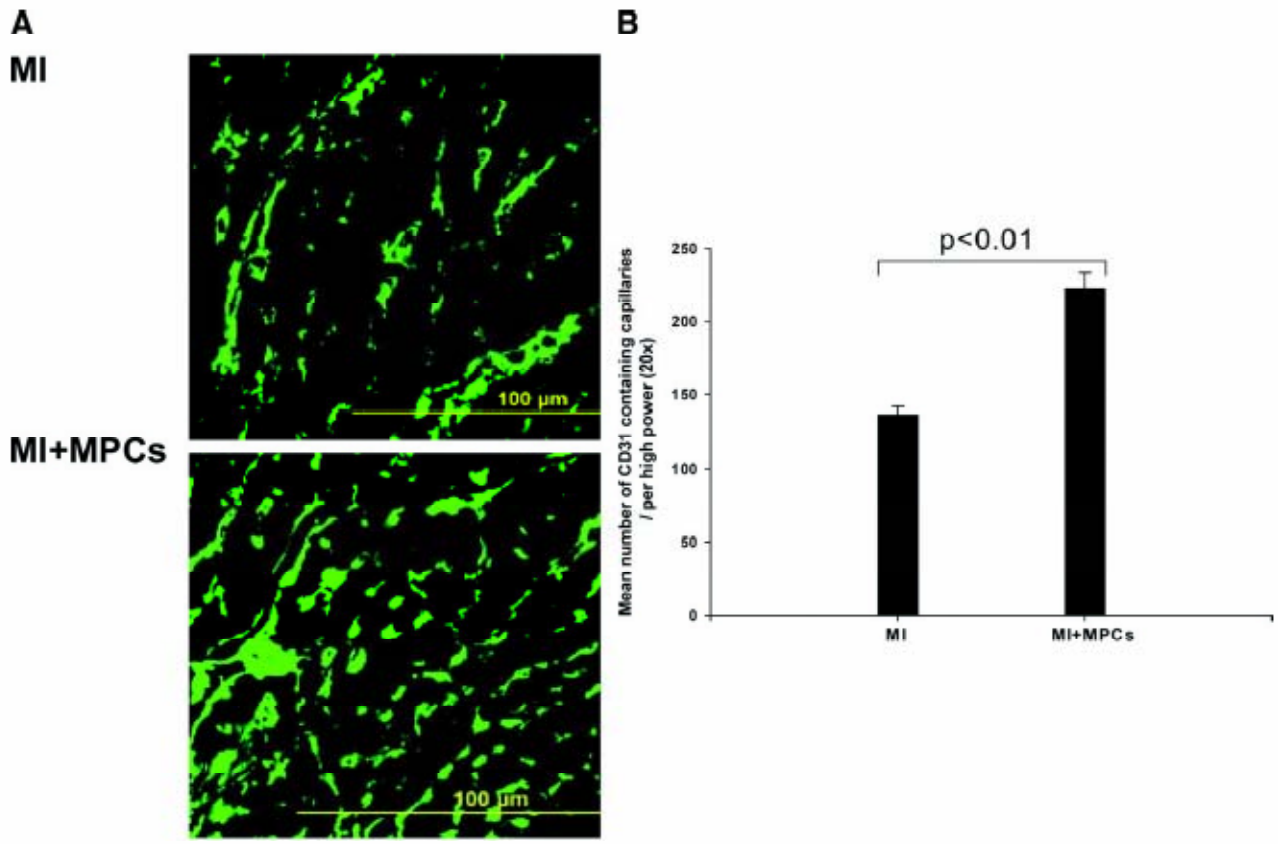

Fig. 5: The protective effect of MPCs on cardiomyocytes

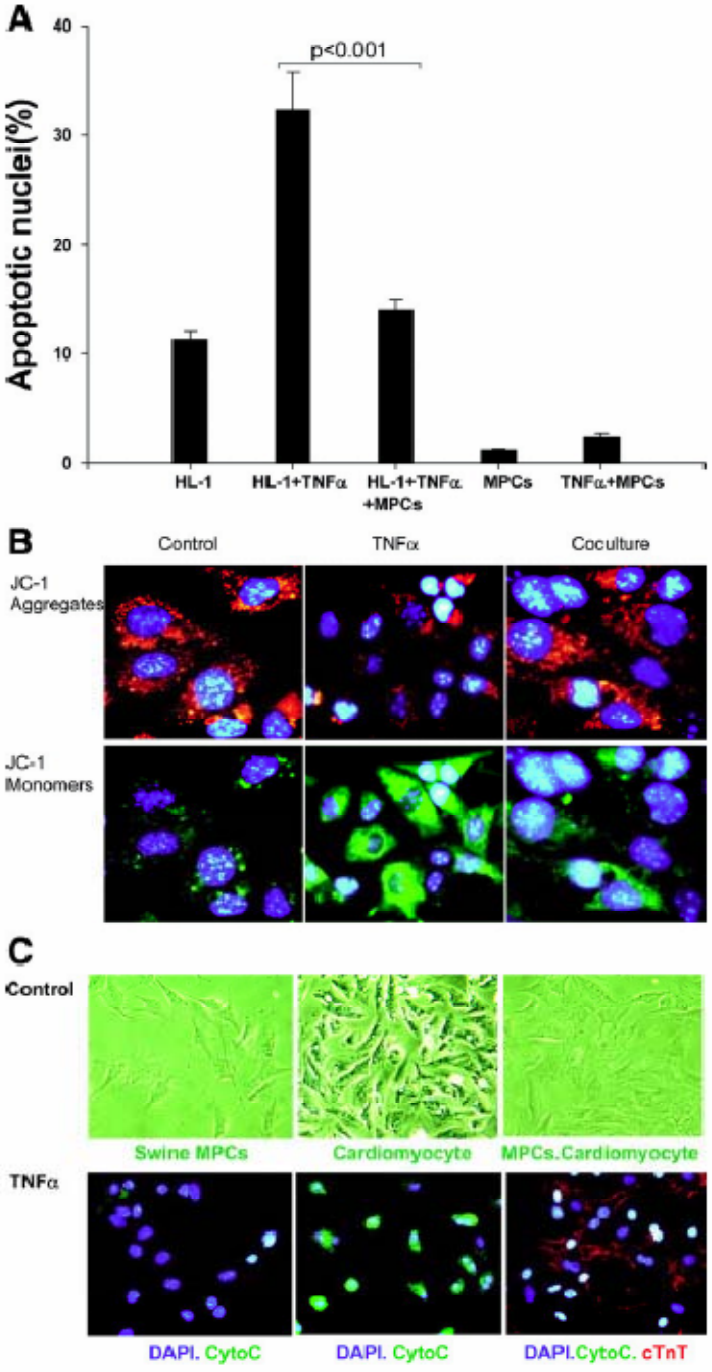

CHAPTER 4: LONG TERM FUNCTIONAL IMPROVEMENT AND GENE EXPRESSION CHANGES AFTER BONE MARROW DERIVED MULTIPOTENT PROGENITOR CELL TRANSPLANTATION IN MYOCARDIAL INFARCTION

Mohammad Nurulqadr Jameel, Qinglu Li, Abdul Mansoor,

Xiong Qiang, Aaron Sarver, Xiaohong Wang, Cory Swingen, Jianyi Zhang.

The study examined the long term outcome of cardiac stem cell transplantation in hearts with postinfarction left ventricular (LV) remodeling. Myocardial infarction (MI) was created by ligating the 1st and 2nd diagonal branches of the left anterior descending coronary artery in Miniature Swines. Intramyocardial injections of 50 million LacZ labeled bone marrow derived multipotent progenitor cells (MPC) was performed in the periscar region (Cell, n=7) immediately after MI, while in control animals (CONT, n=7) saline was injected. Functional outcome was assessed monthly for 4 months with MRI and ^{31}P MR spectroscopy. Engraftment was studied on histology and gene chip (Affymetrix) array analysis was used to study differential expression of genes in the two groups. MPC treatment resulted in improvement of ejection fraction as early as 10 days after MI (Cell, 43.4±5.1 % vs. CONT, 32.2±5.5 %; $p<0.05$). This improvement was seen each month and persisted to 4 months (Cell, 51.2±4.8 % vs. CONT, 35.7±5.0 %; $p<0.05$). PCr/ATP ratio improved with MPC transplantation, which was most pronounced at high cardiac workstates (Subendocardial PCr/ATP was 1.70±0.10 vs. 1.34±0.14, $p<0.05$). There was no significant difference in scar size (scar/LV area*100) at 10 days post infarction. However, at 4 months there was a significant decrease in scar size in the Cell group (Cell, 4.6±1.0 % vs. CONT, 8.6±2.4 %; $p<0.05$). No significant engraftment of MPC was observed. MPC transplantation was associated with a downregulation of mitochondrial oxidative enzymes and increased levels of MEF2a and ZFP91. In conclusion, MPC transplantation leads to long term

functional and bioenergetic improvement in a porcine model of postinfarction LV remodeling despite no significant engraftment of stem cells in the heart. MPC transplantation reduces regional wall stresses and infarct size and mitigates the adverse effects of LV remodeling as seen by a reduction in LV hypertrophy and LV dilatation and is associated with differential expression of genes relating to metabolism and apoptosis.

INTRODUCTION

Stem cell transplantation has emerged as a potential therapy for limiting post-infarction left ventricular (LV) remodeling and the consequent development of CHF in both animal [77-80] and clinical [39, 41-42, 44, 46] studies. Clinical studies have shown mixed results on LV function with stem cell therapy with some showing benefit [39, 41-42] and some no difference in left ventricular ejection fraction [43-44]. In the Bone marrow transfer to enhance ST-elevation infarct regeneration (BOOST) study, the treated group showed significant short term increase of LV ejection fraction at 6 months, but interestingly no difference between the two groups was present at 18 months [104]. Using a swine model of post myocardial infarction (MI) LV remodeling, we recently reported that transplantation of bone marrow derived multipotent progenitor cells (MPC) resulted in a significant improvement of cardiac function and correction of abnormal energy metabolism at one month following transplantation [77]. However, the long term effect after MPC treatment still needs to be defined. Dai *et al* showed in a rat myocardial infarction model that allogenic Mesenchymal stem cell (MSC) treatment led to an improvement in left ventricular function 4 weeks after transplantation but this improvement was lost at 6 months [37]. However, they did find stem cell engraftment as late as 6 months and showed that these cells expressed markers that suggested endothelium and muscle phenotypes [37]. Long term studies of any stem cell type in large animal models of myocardial infarction are relatively scarce.

The mechanisms underlying the beneficial effects of stem cell treatment are also not well defined. Our lab and others have demonstrated a very low engraftment rate and even lower cardiomyocyte differentiation rate a few weeks after bone marrow stem cell transplantation [77, 81, 105]. Therefore, the direct contribution of regenerated myocytes to the improved cardiac contractile function appears less likely. Dzau's group have shown a significant protection of stressed cardiomyocytes from apoptosis and consequent reduction in infarct size by injection of concentrated cell culture medium that was obtained from bone marrow derived MSCs with overexpression of Akt, or by injection of MSCs themselves into the myocardium at the time of acute myocardial infarction [81-83]. Thus, the mechanisms underlying the long term outcome after stem cell transplantation also require more elucidation.

The objectives of the present study are to determine the long term functional and bioenergetic outcome after MPC transplantation in a clinically relevant porcine model of postinfaction LV remodeling and whether these effects are related to persistent long term engraftment of MPC in the heart. We hypothesize that MPC transplantation leads to transient engraftment and secretion of factors that leads to long term myocardial gene expression changes which contributes to the beneficial functional outcome.

METHODS

All experiments were performed in accordance with the animal use guidelines of the University of Minnesota, and the experimental protocol was approved by the University of Minnesota Institutional Animal Care and Use Committee (IACUC). The investigation conformed to the *"Guide for the care and use of laboratory animals"* published by the National Institutes of Health (NIH publication No 85-23, revised 1985).

Study Design The study design is depicted in Fig.1. A total of 14 swine were randomized after myocardial infarction to receive either 50 million stem cells (n=7) or saline only (n=7). The pigs were followed for a total of 4 months after transplantation with MRI occurring at baseline, 10 days, 1 month and then subsequently each month for 4 months. At the end of the study open-chest NMR spectroscopy was performed and then after sacrifice histology and microarray analysis was done on the tissue samples.

Cell Culture Bone Marrow Derived Multipotent Progenitor Cells (MPCs) were expanded from one of the established swMAPC (swine multipotent adult progenitor cell) cell lines generated as described previously in detail[88]. MPCs at population doubling 80 (~PD70) were transduced with a Lac-Z Retrovirus (RV) supernatant (Lac-Z RV supernatants were generated by co-transfection of pVSV-G retroviral vector (BD Biosciences) and pCL-MFG-LacZ RV packaging vector

(Imgenex) using the calcium phosphate method (BD Bioscience, K2051-1) in GP-293 cell line (BD Bioscience)). Large scale expanded and LacZ transduced cells expressed low to non-detectable Oct-4 mRNA. These MPC cells have previously been shown to differentiate along different cell lineages [77].

The transduced swine cells were expanded using the following methods. Cells were cultured in 60% DMEM-LG / 40% MCDB-201 supplemented with 1x ITS, 0.5x LA-BSA, 0.1mM L-ascorbic acid 2-phosphate, 100U penicillin and 1,000U streptomycin, 50 nM dexamethasone and 2% pre-screened FBS with 10 ng/ml each human PDGF-BB and human EGF and passaged every 2 to 3 days through removal of the growth media and addition of 5 ml 0.25% trypsin per T150 flask. After rocking the flask to coat the bottom of the flask with trypsin, the cells were incubated at room temperature for 1 minute. Each flask was tapped lightly and 1 ml of FBS was then added. Cells were removed and cells were combined into a 50 ml conical tube. Flasks were rinsed with 10 ml PBS and this volume added to cells. Cells were pelleted through centrifugation at 400×g's for 5 minutes, and after removal of the supernatant the cells were resuspended in 1 ml of complete medium and counted using a hemacytometer. Flasks were routinely seeded at 500 cells/cm^2 in flasks coated with 10ng/ml fibronectin A with 10ml media per T 150 flask. After an initial placement of the flasks at 37 ºC, 5.5% CO_2 overnight, the media was removed and replaced with fresh media and cells incubated another 2 days before passaging.

MPCs were harvested, centrifuged and resuspended at 10 million cells / 1 ml cryo preservation solution that consists of 70% growth media, 20% FBS, and 10% DMSO in 1 mL cryovials. Cells were frozen at ~1^{o}C per minute to –80^{o}C and transferred into liquid nitrogen for long-term storage until of implantation. To thaw MPCs prior to grafting, basal media (expansion media without PDGF-BB, EGF, FBS, and penicillin/streptomycin) was pre-warmed to 37^{o}C, and 9 ml of the warmed media was placed into a 15 ml conical centrifuge tube. Vials of frozen MPC were thawed in a 37^{o}C water bath for approximately one minute, after which cells were transferred to the pre-warmed medium. The cell number was counted to reach 50 million by hematocytometer and trypan blue was used to check cell viability during the counting. MPC were washed by 2x PBS and spun down at 400g for 5 minutes and resuspended in 2 ml saline. A small fraction of cells was replated in a T-150 flask to check the cell viability and percentage of Lac-z positive cells. Cells used for transplantation were >80% viable.

Animal Model and stem cell delivery method Sinclair Miniswine (Sinclair Research Center, MO) were used for this study. Sinclair pigs are research purpose bread, and grow very slowly which allowed us to follow these animals for long term. These pigs have a shorter lifespan as compared to humans, so 4 months is equivalent to a longer follow-up in human years. The follow-up of 4 months was also chosen because the bore size of the 4.7T magnet for the magnetic resonance spectroscopy studies limits us to perform these studies on larger animals. The postinfarction LV remodeling model was created

as described before [53, 56]. Briefly, female Sinclair miniswine (5 months age, ~15 kg) were anesthetized with pentobarbital (30 mg/kg iv), intubated and ventilated with a respirator with supplemental oxygen. A left thoracotomy was performed, and the 1st and 2nd diagonal branches of the left anterior descending artery were dissected free and permanently occluded with a ligature. The ischemic myocardial region became cyanotic in response to the coronary artery occlusion. MPCs were injected directly into 5 regions of the peri-infarct border zone (BZ) (10 million cells per location; 50 million total diluted in 2 ml saline). Injection sites were marked with a stitch to allow identification of the areas for histological studies. Animals in the placebo group received 2 ml saline in 5 injections at similar BZ injection sites. Animals were observed in the open chest state for 60 minutes. If ventricular fibrillation occurred, electrical defibrillation was performed immediately. The chest was then closed. Animals received standard post-operative care including analgesia until they ate normally and became active.

MRI Methods MRI was performed on a 1.5 Tesla clinical scanner (Siemens Sontata, Siemens Medical Systems, Islen NJ) using a phased-array 4-channel surface coil and ECG gating. Animals were anesthetized with 1% isoflurane and positioned in a supine position within the scanner. The protocol consisted of: 1) localizing scouts to identify the long- and short-axis of the heart, 2) short- and long-axis cine for the measurement of global cardiac function, and 3) delayed contrast-enhancement for the assessment of scar size. Steady-state

free precession “True-FISP” cine imaging used the following MR parameters: TR = 3.1 ms, TE = 1.6 ms, flip angle = 79^{o}, matrix size = 256 x 120, field of view = 340 mm x 265 mm, slice thickness = 6 mm (4 mm gap between slices) and 16-20 phases were acquired across the cardiac cycle. Global function and regional wall thickness data were computed from the short-axis cine images using MASS (Medis Medical Imaging Systems, Leiden, The Netherlands) for the manual segmentation of the endocardial and epicardial surfaces at both end-diastole (ED) and end-systole (ED) from base to apex. Short-axis turboFLASH imaging, from base to apex, used TR = 16 ms, TE = 4 ms, TI ~ 220 ms, flip angle = 30^{o}, matrix size = 256 x 148, field of view = 320 mm x 185 mm, slice thickness = 6 mm (0 mm gap between slices) and two signal averages. The appropriate inversion time (TI) was chosen to adequately null the signal intensity (SI) of normal myocardium. Infarct size was calculated from the delayed contrast-enhanced images using MASS to manually segment regions of non-viable tissue. Infarct size was calculated as the ratio of the total scar area to the total LV area.

Spatially localized ^{31}P-MR spectroscopy technique Magnetic field shimming to improve the magnetic field homogeneity of the heart was achieved by the “auto-shim” scheme (Varian Assoc. Inc., CA). Spatially localized ^{31}P NMR spectroscopy was performed using the RAPP-ISIS/FSW method [54, 89-91], which is the rotating-frame experiment using adiabatic plane-rotation pulses for phase modulation (RAPP)-imaging-selected in vivo spectroscopy (ISIS)/Fourier series window (FSW) method. Detailed experiments documenting voxel profiles,

voxel volumes and spatial resolution attained by this method have been published previously. In this application of RAPP-ISIS/FSW, the signal origin was first restricted to a 12*12 mm two-dimensional column perpendicular to the LV wall. The signal was later localized into three well resolved and five partially resolved layers along the column and hence, across the LV wall. Localization along the column was based on B_1 phase encoding and employed a 9-term Fourier series window as previously describe [54, 89-91]. The phase encoded data were used to generate a voxel or a "window" that can be shifted arbitrarily by post data acquisition processing along the phase encode direction (in this case perpendicular to the surface coil and thus the heart wall); consequently, voxels were generated at different distances or "depths" from the outer LV wall. However, we normally present five voxels centered about 45°, 60°, 90°, 120°, and 135° phase angles as previously described. There is absolutely no overlap between the 135° voxel (corresponding to the subepicardium) and the 45° voxel (corresponding to the subendocardium). Whole wall spectra were obtained with the image-selected *in vivo* (ISIS) technique, defining a column 12*12 mm^2 perpendicular to the heart wall. The calibration of spectroscopic parameters was facilitated by placing a polyethylene capillary filled with 15 µl of 3 M/L phosphonoacetic acid into the inner diameter of the surface coil. This phosphonoacetic acid standard was used only for calculating the 90 degree pulse length of the RAPP-ISIS method [54, 89-91]. The position of the voxels relative to the coil was set according to the B_1 strength at the coil center which was experimentally determined in each case by measuring the 90° pulse length

for the phosphonoacetic acid standard contained in the reference capillary at the coil center. NMR data acquisition was gated to the cardiac and respiratory cycles using the cardiac cycle as the master clock to drive both the respirator and the spectrometer as previously described [54, 89-91]. The surface coil was constructed from a single turn copper wire 25 mm in diameter with each side of the coil leads soldered to a 33 pF capacitor. Complete transmural data sets were obtained in 10-minute time blocks using a repetition time of 6-7 seconds to allow for full relaxation for ATP and inorganic phosphate (Pi) and approximately 95% relaxation of the PCr resonance [54, 89-91]. The ratios of PCr to ATP (PCr/ATP) were calculated for each transmurally differentiated spectra set as previously described [54, 89-91]. All resonance intensities were quantified using integration routines provided by the SISCO software.

^{1}H- NMR spectroscopy technique ^{1}H NMR methods have been previously reported in detail [54, 92]. In brief, radiofrequency (RF) transmission and signal detection were performed with the dually tuned 28 mm diameter surface coil. A single-pulse-collection sequence with a frequency selective Gaussian excitation pulse (1ms) was used to selectively excite the N-δ proton resonance signal of the proximal histidine in deoxymyoglobin (Mb- δ). This technique provided sufficient water suppression due to the large chemical shift difference between water and Mb- δ (>14 kHz). The NMR signal was optimized by adjusting the RF pulse power using the water signal as a reference. A short repetition time (TR = 25 ms) was used due to the short T_1 of Mb- δ. Each

spectrum was acquired in 5 min (10,000 FIDs). Although the short T_1 of Mb- δ and fast acquisition prevent gating to the cardiac cycle, the signal loss due to motion is negligible compared to the inherently broad line width of the Mb- δ peak.

Surgical preparation for open chest MR spectroscopy study Detailed surgical preparations for MRS study are published previously [56, 77, 91]. Briefly, animals were anesthetized with pentobarbital (30 mg/kg followed by a 4 mg/kg/hr iv), intubated and ventilated with a respirator and supplemental oxygen. Arterial blood gases were maintained within the physiologic range by adjustments of the ventilator settings and oxygen flow. 3.0 mm OD heparin-filled polyvinyl chloride catheters were inserted into the ascending aorta (Ao) and inferior vena cava (IV). A sternotomy was performed, and the heart was suspended in a pericardial cradle. A third heparin-filled catheter was introduced into the LV through the apical dimple and secured with a purse string suture. A 25 mm diameter NMR surface coil was sutured onto the anterior wall of the LV adjacent to the infarct region. The 31P and 1H coils were placed in the periscar region 1cm away from the infarct site and adjacent to the injection sites. The pericardial cradle was then released, and the heart was allowed to assume its normal position in the chest. The surface coil leads were connected to a balanced-tuned external circuit and the animals positioned within the magnet. Hearts with post infarction LV remodeling are very sensitive to alterations of loading conditions of the LV, and that subtle differences in LVEDP or LVSP could affect myocardial contractile

performance measurements. In order to compensate for insensible fluid loss in the open chest studies, we routinely administer saline at rate of 1 ml/min i.v. during the entire experimental data acquisition. Ventilation rate, volume and inspired oxygen content were adjusted to maintain physiologic values for arterial PO_2, PCO_2 and pH. Aortic and LV pressures were monitored continuously throughout the study. Hemodynamic measurements were acquired simultaneously with the ^{1}H - and ^{31}P- MR spectra.

MR spectroscopy Study protocol and hemodynamic measurements

Hemodynamic measurements were acquired simultaneously with the NMR spectra. Aortic and LV pressures were measured using pressure transducers positioned at mid-chest level [89-91] and recorded on an 8-channel recorder. After all the baseline data were obtained, animals received combined dobutamine and dopamine infusion (20 μg/kg/min. each) to induce a very high cardiac workstate. After waiting for approximately 5 minutes after the initiation of catecholamine infusion, all the spectroscopic and hemodynamic data were again measured under the high cardiac workstates.

Tissue preparation Myocardial drill biopsies from BZ and RZ were taken with a pre-cooled biopsy drill and quickly (within 5 seconds) frozen in liquid nitrogen [54, 89-91] for subsequent microarray analysis. BZ tissue samples were taken at least 3 mm away from the edge of the infarct to avoid contamination with scar tissue. The remainder of the LV was sectioned in a bread-loaf manner into 6

transverse sections (~ 10 mm in thickness) from apex to base. Even rings were subdivided into 12 circumferential specimens and fixed in zinc fixative (Anatech LTD, Battle Creek, MI, USA) for Haematoxylin & Eosin (HE), immunofluorescence staining and engraftment evaluation.

Engraftment evaluation Each of the 12 pieces of cardiac tissue of a short axis ring were stained by X-gal (Invitrogen) and embedded in Tissue-Tek OCT (Fisher Scientific). Serial cryostat sections (10μm in thickness) were obtained from the whole transverse even rings. Engrafted MPCs were identified by counting the X-gal-positive nuclei in every 10th serial section of the whole transverse ring and then multiplying by 10 to obtain the total number of engrafted MPCs per ring. The total number of engrafted MPCs equals two fold x-gal staining positive cells in all three even rings. The engraftment rate of transplanted MPCs was calculated by dividing the total number of engrafted MPCs by 50 x 10^6 (the number of MPCs injected) and multiplying by 100%.

RNA isolation Tissue was placed in TRIzol reagent and homogenized using a rotor-stator homogenizer. Homogenates were transferred to a Phase Lock Gel (PLG) Heavy tube (Eppendorf), chloroform was added, and the mixture was centrifuged. Supernatants were collected, and isopropanol was added to precipitate the RNA. The RNA pellet was washed with 80% ethanol, then air-dried before dissolving in 100 μl of RNase-free H_2O. RNA was further purified using the RNeasy Mini protocol according to the manufacturer's directions

(Qiagen). The integrity of each RNA sample was validated using an Agilent Bioanalyzer 2100 (Agilent Technologies, Palo Alto, CA) to measure the ratio of 28s/18s ribosomal RNA.

Double-stranded cDNA synthesis Total RNA of 5 µg was used in the synthesis of double-stranded cDNA based on Affymetrix protocol with a T7-$(dT)_{24}$ primer and 200 U/µl of SuperScript II RT. Second-strand synthesis was performed according to the manufacturer's directions.

In vitro transcription-synthesis of biotin-labeled cRNA Biotin-labeled RNA targets were obtained by using the Enzo BioArray High Yield RNA Transcript Labeling Kit via in vitro transcription from bacteriophage T7 RNA polymerase promoters according to the manufacturer's directions (Enzo). The cRNA was then fragmented according to the Affymetrix protocol. Quality and fragmentation of cRNA was confirmed with gel electrophoresis.

Target hybridization and probe array wash and stain Hybridization cocktail for single standard probe array (Porcine Genome Array, Affymetrix) was made by mixing 15 µg of fragmented cRNA with control oligonucleotide B2, 20x eukaryotic hybridization controls, herring sperm DNA (10 mg/ml), acetylated BSA (50 mg/ml) 2x hybridization buffer, and RNase-free water. Hybridization was performed in our Affymetrix Core Facility.

Microarray Data analysis Array data was normalized using GC-RMA method using genedata refiner software. Significance Analysis of Microarrays

(SAM) [106] was used to identify probes whose expression was modified following stem cell transplantation and showed a fold change greater than 1.7 and a False Discovery Rate (FDR) of less than 20%. Probes were mapped to human genes using the annotation described by Tsai et al [107]. Normalized and raw data is available at GEO under the entry GSE14643.

Data analysis Data were analyzed with repeated measures ANOVA. A value of $p<0.05$ was considered significant. The Bonferroni correction for significance level was used to take into account multiple comparisons. All statistical analyses were performed in Sigmastat version 3.5 (San Jose, Calif). All results are presented as mean ± SD unless otherwise specified. The authors had full access to the data and take responsibility for its integrity. All authors have read and agree to the manuscript as written.

RESULTS

Anatomic Data The anatomic data for the 14 swine is summarized in Table 1. MPC transplantation resulted in a significant decrease in left ventricular hypertrophy as reflected by a decrease in LVW/BW (2.86±0.12 vs. 3.33±0.16, $p< 0.05$) and RVW/BW (1.03±0.08 vs. 1.34±0.10, $p<0.05$) in the cell treated pigs as compared to the saline treated pigs after 4 months.

Hemodynamic Data The hemodynamic data at baseline and at increased workload are summarized in Table 2. Inotropic stimulation caused a significant increase in the heart rate, mean aortic pressure and left ventricular systolic pressure and consequently rate pressure product. However, there was no significant difference between the swine with cell treatment versus swine without cell treatment.

Functional Data The temporal changes in ejection fraction as measured by MRI are depicted in Figure 2. There was no significant difference between the two groups at baseline. However, the cell treated group showed a significant improvement in ejection fraction which was seen as early as 10 days (43.4±5.1 % vs. 32.2±5.5 %, $p<0.05$) after MPC transplantation and persisted up to 4 months (51.2±4.8 % vs. 35.7±5.0 %, $p<0.05$). In addition, the MPC treatment resulted in reduction of the left ventricular dilatation seen at 4 months after myocardial infarction in the saline treated animals, as depicted by significantly lower left ventricular end-diastolic (16.9±1.8 ml vs. 22.2±4.8 ml, $p<0.05$) and left ventricular end-systolic volume (8.9±2.3 ml vs. 14.1±2.5 ml, $p<0.05$) in the MPC treated group at 4 month follow-up (Table 3). The initial scar size was similar at 10 days in both groups; however, there was a significant decrease in scar size in the MPC treated animals from 10 days to 4 months (4.6±1.0 % at 4 months vs. 8.3±1.5 % at 10 days, $p<0.05$), which was also significantly smaller than the scar size in control animals at 4 months (4.6±1.0 % vs. 8.6±2.4 %, $p<0.05$) (Figure 3).

Myocardial high-energy phosphate (HEP) and Pi levels Myocardial HEP and Pi levels are reflected by the PCr/ATP ratios as shown in Table 4. The subendocardial and subepicardial myocardial PCr/ATP ratios were significantly higher at 4 months in the pigs treated with MPC as compared to those without treatment. After increased workload, the PCr/ATP ratio decreased in both groups but was still significantly higher in the cell treated pigs. No deoxymyoglobin resonance peak was detected in either groups using ^{1}H-MRS, which supports our previous findings that the border zone bioenergetic abnormalities in hearts with postinfarction LV remodeling is not caused by a persistent myocardial ischemia.

Cell engraftment There was no engraftment of MPC observed at 4 months after transplantation in any of the cell treated animals.

Microarray analysis As there was no long term engraftment, it was postulated that the MPC engraft transiently after transplantation and exert a paracrine effect by secretion of factors that may lead to long term gene expression changes that may ultimately lead to improved long term outcome. Gene expression profiles were collected from seven MPC treated animals and six control animals (one animal did not have quality RNA for array analysis) using the Affymetrix Porcine Gene chip array containing over 23000 probe sets. SAM analysis identified a number of genes that were differentially expressed in the heart of the MPC treated animals (Fig.4). There were 41 genes that were down-

regulated after MPC transplantation and 11 genes that were upregulated (Table 5). There was down-regulation of several mitochondrial oxidative enzymes including 3 different subunits of complex I of the respiratory chain which were decreased by 0.59, 0.58 and 0.57 fold, respectively. The levels of ZFP91 (a member of the zinc finger family of proteins associated with Ciliary Neurotrophic factor) were increased by 3.62 fold. Similarly, Myocyte Enhancer Factor 2a (MEF2a) was upregulated by 1.7 fold.

DISCUSSION

The present study demonstrates that MPC transplantation leads to long term functional and bioenergetic improvement in a clinically relevant porcine model of postinfarction LV remodeling despite no significant engraftment of MPCs at 4 months in the heart. Stem cell transplantation resulted in an overall improved long term remodeling of the left ventricle following MI with a decrease in LV hypertrophy and amelioration of LV dilatation. This was associated with a reduction in scar size at 4 months. MPC transplantation also resulted in long term differential expression of genes which included a downregulation of mitochondrial oxidative enzymes and upregulation of MEF2a and ZFP91.

Long term improvement in ventricular function The present study unequivocally demonstrates that MPC transplantation leads to long term improvement in ventricular function in a large preclinical animal model. This is an

important finding, as clinical studies have shown mixed outcomes after stem cell transplantation with some showing benefit [39, 41-42] and some no difference in left ventricular ejection fraction [43-44]. In the Bone marrow transfer to enhance ST-elevation infarct regeneration (BOOST) study, the treated group showed significant short term increase of LV ejection fraction at 6 months, but interestingly no difference between the two groups was present at 18 months [104]. Similarly, in a rat model of myocardial infarction allogenic MSC treatment led to an improvement in left ventricular function 4 weeks after transplantation but this improvement was lost at 6 months [37]. In the present study, MPC transplantation also mitigated the adverse long term effects of ventricular remodeling. This was seen as a reduction in LV hypertrophy (Table 1) and LV dilatation (Table 3) in the MPC treated animals.

Myocardial Energetics Post infarction LV remodeling is associated with decreased high energy phosphates, PCr/ATP and expression of several proteins crucial to oxidative ATP production and these abnormalities are most severe in the borderzone [56]. Our study confirmed these reports and showed that these abnormalities are worse in the subendocardial layers and further worsened during catecholamine stimulation induced high cardiac workstate (Table 4). Previously, we have shown improvement in myocardial energetics 1 month following MPC transplantation which is related to reduction in wall stress and consequent improvement in the mismatch of energy delivery and demand [77]. In the present study, we demonstrate that this improvement in myocardial

energetics persist up to 4 months after transplantation (Table 4). In hearts with cardiac hypertrophy we have previously reported that myocardial PCr/ATP ratio is significantly decreased, which is linearly related to the severity of hypertrophy and LV dysfunction, and is independent from a persistent myocardial ischemia [89-90, 108-109]. These LVH hearts are also associated with a significant lower myocardial total creatine level [89-90, 108, 110], which in principle can cause the reduction of the myocardial creatine phosphate level. In the heart, creatine is not synthesized in myocytes, and is up taken by the cell via the creatine transporters against a significant concentration gradient [111-112]. The reduction of myocardial total creatine content in the LVH hearts was found to be caused by the decrease of myocardial creatine transporter [111-112]. In the present study we do not have direct evidence on whether the improvement of the PCr/ATP is accompanied by the increase of myocardial total creatine content or creatine transporter protein expression.

Lack of long term engraftment of MPCs The functional and bioenergetic improvement occurred despite no long term engraftment of stem cells in pig hearts at 4 months. We have previously shown that there is a very low engraftment rate and even lower cardiomyocyte differentiation rate 1 month following MPC transplantation [77]. Thus, it seems that there is transient engraftment of MPCs in the myocardium which decreases with time and is not present at 4 months. This conclusion is supported by other groups which have found transient engraftment of MSCs with very little differentiation as early as 3

days after transplantation in a mice model of myocardial infarction [81]. In contrast, Amado *et al* have shown that MSC transplantation in a porcine model of myocardial infarction led to engraftment of these cells at 2 months which was associated with a decrease in scar size and improvement in left ventricular function [78]. In a rat model of myocardial infarction, MSC engraftment was seen up to 6 months follow-up [37]. These cells expressed muscle specific markers but did not fully differentiate into a cardiac phenotype. In another study, intravenous injection of human MSC in a mice MI model resulted in functional improvement with no engraftment in the heart after 3 weeks [105]. These data support the conclusion of the present study that host myocardial structural (Fig 3) and genomic expression changes (Table 5) are associated with the observed chamber functional improvements (Fig 2). We have also previously shown an increase in vascular density in the border zone one month following cell transplantation [113].

Effect of cell transplantation on infarct size Sequential MRI functional assessment allowed us to conclude that the infarct size in swine treated with MPC decreased from 1 week to 4 month interval, while the scar sizes in swine without MPC treatment was maintained throughout the follow-up (Figure 3). This reduction in scar size with stem cell treatment has been seen previously in other reports [78, 83]. The beneficial effects of MPC transplantation could be related to MPC differentiation into cardiomyocytes [11] or mobilization of endogenous progenitors to the injury site by paracrine effects [83]. As we did not observe any

engraftment of MPCs at 4 months, the functional and bioenergetic improvements are likely secondary to paracrine effects that may include sparing of native cardiomyocytes from apoptosis.

Downregulation of mitochondrial oxidative enzymes MPC transplantation was associated with downregulation of several different subunits of the respiratory chain (Table 5). The LV dysfunction of failing hearts is associated with oxidative stress caused by excess reactive oxygen species (ROS) production in the cytoplasm and the electron transport chain of mitochondria in myocytes[114]. In the present study, the observed reduction of several different subunits of the respiratory chain oxidative enzymes (Table 5) in hearts with MPC transplantation may result in reduction of the oxidative stress, which could in turn, reduce the myocardial apoptosis that we have observed recently using the same cell type for the transplantation and the same animal model [113].

We have previously reported that LV bulging of the infarct zone was accompanied by a significant increase of regional LV wall stress of the infarct zone and peri-infarct border zone [56]. This particular increase of regional wall stresses and its associated severe bioenergetic abnormality was significantly ameliorated by the MPC transplantation [77, 94]. In the present study, we reasoned that the decreased bulging of the LV scar area resulted in reduction of the regional wall stress and energy demand, which in turn, resulted in the

differential expression of several different subunits of the respiratory chain enzymes (Table 5).

Increased levels of ZFP91 ZFP91 is a member of the zinc finger family of proteins and its expression was increased by 3.62 fold in hearts with MPC transplantation. Apart from the monocistronic transcript originating from this locus, a co-transcribed variant composed of ZFP91 and CNTF (Ciliary neurotrophic factor) sequence has been identified. CNTF promotes survival and decreases apoptosis in neurons and islet cells and has also been shown to reverse cardiac hypertrophy in mice [115-116].

Upregulation of MEF2a The expression of Myocyte Enhancer Factor 2a (MEF2a) was increased by 1.7 fold in hearts with MPC transplantation. MEF2a is the predominant MEF2 gene product expressed in postnatal cardiac muscle. MEFs play an important role in myogenesis [117]. MEF2a is also important for maintaining appropriate mitochondrial content and cyto-architectural integrity in the post-natal heart [118]. We postulate that MPC treatment may cause an activation of endogenous cardiac stem cells and MEF2a may play a role in their differentiation into cardiomyocytes.

In summary, the present study demonstrates that MPC transplantation leads to long term functional and bioenergetic improvement in a porcine model of postinfarction LV remodeling despite no significant engraftment of stem cells in

the heart. MPC transplantation also mitigates the adverse effects of LV remodeling as seen by a reduction in LV hypertrophy and LV dilatation. These beneficial effects are accompanied by a significant reduction in infarct size. It was also shown that MPC transplantation results in differential expression of certain genes including mitochondrial oxidative enzymes, ZFP91 and MEF2a which may play a role in long term functional improvement after transplantation.

FIGURE LEGENDS

Figure 1. Study Design.

Figure 2. Long term improvement in ventricular function after MPC transplantation. **A:** MPC transplantation leads to an improvement in Ejection Fraction as early as 10 days after cell transplantation that persists up to 4 months ($p<0.05$). **B:** Tabulated form of the Ejection Fraction data from 10 day, 1month, 2 month, 3 month and 4 month MRI.

Figure 3. Long term reduction in scar size after MPC transplantation.

Figure 4. Heatmap showing all differentially expressed transcripts found using affymetrix array analyses of heart tissue with and without exposure to stem cells. Expression levels are normalized to the average value of the untreated heart tissue and are log transformed. The names associated with each probe are the human names obtained from the annotation described in the methods section. The probe names can be found in table 5. Normalized and raw data is available at GEO under the entry GSE14643.

TABLES

Table 1. Anatomic Data obtained 4 months after MI

	BW (kg)	LVW (g)	RVW (g)	LV/BW (g/kg)	RV/BW (g/kg)
MI (n=7)	16.5±3.7	54.2±5.6	22.0±3.9	3.33±0.16	1.34±0.10
MI + Cell (n=7)	14.3±2.1	41.0±6.0*	14.5±3.2*	2.86±0.12*	1.03±0.08*

Values are mean±SD; MI, myocardial infarction; n, number of pigs; BW, Body weight; LVW, Left ventricular weight; RVW, Right ventricular weight. *, $p<0.05$ vs. MI.

Table 2. Hemodynamic data obtained 4 months after MI

	HR (beat/min)	Mean AoP (mmHg)	LVSP (mmHg)	LVEDP (mmHg)	RPP x 10^3 ($mmHg.min^{-1}$)
Baseline					
MI	117±19	80±5	100±16	7±1	11.7±2.4
MI + Cell	110±13	76±8	97±12	5±1	10.6±1.2
Db + Dp					
MI	150±7*	97±7*	155±16*	8±2	23.3±2.7*
MI + Cell	142±14*	101±8*	156±21*	5±2	22.1±3.3*

Values are mean±SD; MI, myocardial infarction; DbDp, Dobutamine and Dopamine (each 20µg/kg/min intravenous); HR, heart rate; Mean AoP, mean aortic pressure; LVSP, left ventricular systolic pressure; LVEDP, left ventricular end diastolic pressure; RPP, rate pressure product (HR x LVSP); *, $p<0.05$ vs. Baseline.

Table 3. Ventricular volumes

	LVEDV (ml)		LVESV (ml)	
	MI	MI + Cell	MI	MI + Cell
Baseline	16.4±2.4	14.7±2.9	7.9±1.4	6.7±1.4
10 day	15.8±2.9	14.9±3.1	10.7±3.0	8.4±1.7
1 month	16.3±2.5	16.7±2.7	10.5±1.9	9.0±1.1
2 month	17.4±3.5	16.7±1.5	11.5±2.5	9.0±0.2
3 month	19.6±6.3	16.2±2.5	13.3±5.3	8.2±1.2
4 month	22.2±4.8	16.9±1.8*	14.1±2.5	8.9±2.3*

Values are mean±SD; MI, myocardial infarction; LVEDV, left ventricular end-diastolic volume; LVESV, left ventricular end-systolic volume; *, $p<0.05$ vs. MI.

Table 4. Myocardial PCr/ATP ratio 4 months after MI

	Epi	Endo
Baseline		
MI	1.94±0.10	1.65±0.15
MI + Cell	2.17±0.10*	1.90±0.14*
Db + Dp		
MI	1.62±0.17†	1.34±0.14†
MI + Cell	1.91±0.06*†	1.70±0.10*†

Values are mean±SD; MI, myocardial infarction; DbDp, Dobutamine and Dopamine (each 20μg/kg/min intravenous); Epi, Subepicardium; Endo, Subendocardium; *, $p<0.05$ vs. MI; †, $p<0.05$ vs. Baseline.

Table 5. SAM table listing genes that had statistically significant differential expression after MPC transplantation

Gene Name	Gene Description	GeneCards Accession	Fold Change
	Downregulated after MPC transplantation		
Ssc.26278.1.S1_at	importin 13	IPO13	0.55
Ssc.18764.1.A1_at	integrin beta 1 binding protein 3	ITGB1BP3	0.56
Ssc.3563.1.S1_at	PCTAIRE protein kinase 1	PCTK1	0.59
Ssc.23233.1.S1_a_at	Transcribed locus, strongly similar to XP_536737.1 PREDICTED: similar to mitochondrial carrier protein MGC4399 [Canis familiaris]	NP_115691	0.49
Ssc.16937.1.A1_at	tumor protein p53 inducible nuclear protein 2	TP53INP2	0.53
Ssc.23233.1.S1_a_at	glutathione peroxidase 1	GPX1	0.49
Ssc.16849.1.S1_at	follistatin-like 3 (secreted glycoprotein)	FSTL3	0.48
Ssc.2329.1.A1_at	glycogen synthase 1 (muscle)	GYS1	0.57
Ssc.9914.1.A1_at	creatine kinase, brain	CKB	0.52
Ssc.23508.1.S1_at	endoplasmic reticulum-golgi intermediate compartment (ERGIC) 1	Q969X5	0.57
Ssc.13255.1.A1_at	serine/arginine repetitive matrix 2	SRRM2	0.45
Ssc.11779.1.S1_at	folate receptor 1 (Adult)	FOLR1	0.52
Ssc.21553.1.S1_at	hepatoma-derived growth factor (high-mobility group protein 1-like)	HDGF	0.57
Ssc.1819.1.S1_at	trafficking protein particle complex 1	TRAPPC1	0.58

Ssc.22694.1.S1_at	NADH dehydrogenase (ubiquinone) 1 beta subcomplex, 6, 17kDa	NDUFB6	0.59
Ssc.5886.1.S1_at	mitochondrial ribosomal protein S17	MRPS17	0.56
Ssc.25389.1.S1_at	histidine rich calcium binding protein	HRC	0.43
Ssc.9125.1.S1_at	myosin, light chain 9, regulatory	MYL9	0.54
Ssc.12999.1.S1_at	glutathione S-transferase pi 1	GSTP1	0.53
Ssc.12207.1.A1_at	Transcribed locus, weakly similar to XP_425282.1 PREDICTED: similar to MGC68763 protein [Gallus gallus]	NP_542408	0.57
Ssc.14392.1.A1_at	microseminoprotein, beta-	MSMB	0.51
Ssc.2339.1.S1_at	D-dopachrome tautomerase	DDT	0.48
Ssc.2514.1.S1_at	Chromosome 11 open reading frame 31	C11orf31	0.46
Ssc.2447.1.A1_at	Chromosome 17 open reading frame 49	Q8IXM2	0.56
Ssc.12576.1.A1_at	Transcribed locus, strongly similar to XP_548156.1 PREDICTED: similar to CG3420-PA [Canis familiaris]	-	0.58
Ssc.23542.1.A1_at	NADH dehydrogenase (ubiquinone) 1 beta subcomplex, 11, 17.3kDa	NDUFB11	0.58
Ssc.26100.1.S1_at	NADH dehydrogenase (ubiquinone) 1 beta subcomplex, 7, 18kDa	NDUFB7	0.57
Ssc.27967.1.A1_at	polymerase (RNA) II (DNA directed) polypeptide L, 7.6kDa	POLR2L	0.48
Ssc.21753.1.S1_at	Ubiquitously-expressed transcript	UXT	0.52
Ssc.3197.1.S1_at	Transcribed locus, moderately similar to XP_533944.1 PREDICTED: similar to QIL1 [Canis familiaris]	NP_991330	0.51
Ssc.2261.1.S1_at	APC11 anaphase promoting complex	ANAPC11	0.56

	subunit 11 homolog (yeast)		
Ssc.24290.1.S1_at	biogenesis of lysosomal organelles complex-1, subunit 1	BLOC1S1	0.53
Ssc.3675.1.A1_at	calmodulin 2 (phosphorylase kinase, delta)	CALM2	0.54
Ssc.21117.1.A1_at	Transcribed locus, strongly similar to XP_213214.2 PREDICTED: similar to mitochondria-associated granulocyte macrophage CSF signaling molecule [Rattus norvegicus]	MAGM_HUMAN	0.55
Ssc.7580.1.A1_at	chromosome 17 open reading frame 61	Q8N2U0	0.56
Ssc.19954.1.S1_at	Transcribed locus, moderately similar to NP_060694.1 hypothetical protein FLJ10803 [Homo sapiens]	-	0.57
Ssc.17618.1.S1_at	Clone Clu_6860.scr.msk.p1.Contig4, mRNA sequence	Q8NAX4	0.56
Ssc.19477.1.A1_at	trafficking protein particle complex 5	TRAPPC5	0.58
Ssc.5035.1.S1_at	mitochondrial ribosomal protein S18A	MRPS18A	0.56
Ssc.19928.1.S1_a_at	deoxyuridine triphosphatase	DUT	0.54
Ssc.14361.1.A1_at	olfactomedin 1	OLFM1	0.56

Upregulated after MPC transplantation

Ssc.24458.1.A1_at	KIAA1429	Q69YN4	1.83
Ssc.10473.1.A1_at	zinc finger protein 91 homolog (mouse)	ZFP91	3.62
Ssc.8896.1.A1_at	GDP-mannose 4,6-dehydratase	GMDS	1.76
Ssc.21898.1.S1_at	ERO1-like (S. cerevisiae)	ERO1L	1.86

Ssc.25201.1.A1_at	regulating synaptic membrane exocytosis 2	RIMS2	2.09
Ssc.29206.1.A1_at	chromosome 19 open reading frame 2	C19orf2	2.56
Ssc.13545.1.A1_at	chromosome 21 open reading frame 66	C21orf66	2.15
Ssc.18307.1.A1_at	RNA binding motif protein 25	RBM25	2.38
Ssc.12654.2.A1_at	myocyte enhancer factor 2A	MEF2A	1.70
Ssc.8247.1.A1_at	opioid binding protein/cell adhesion molecule-like	OPCML	1.71
Ssc.27217.2.A1_at	zinc finger protein 354A	ZNF354A	1.84

SAM, Significance Analysis of Microarrays. Normalized and raw data is available at GEO under the entry GSE14643.

Fig. 1.

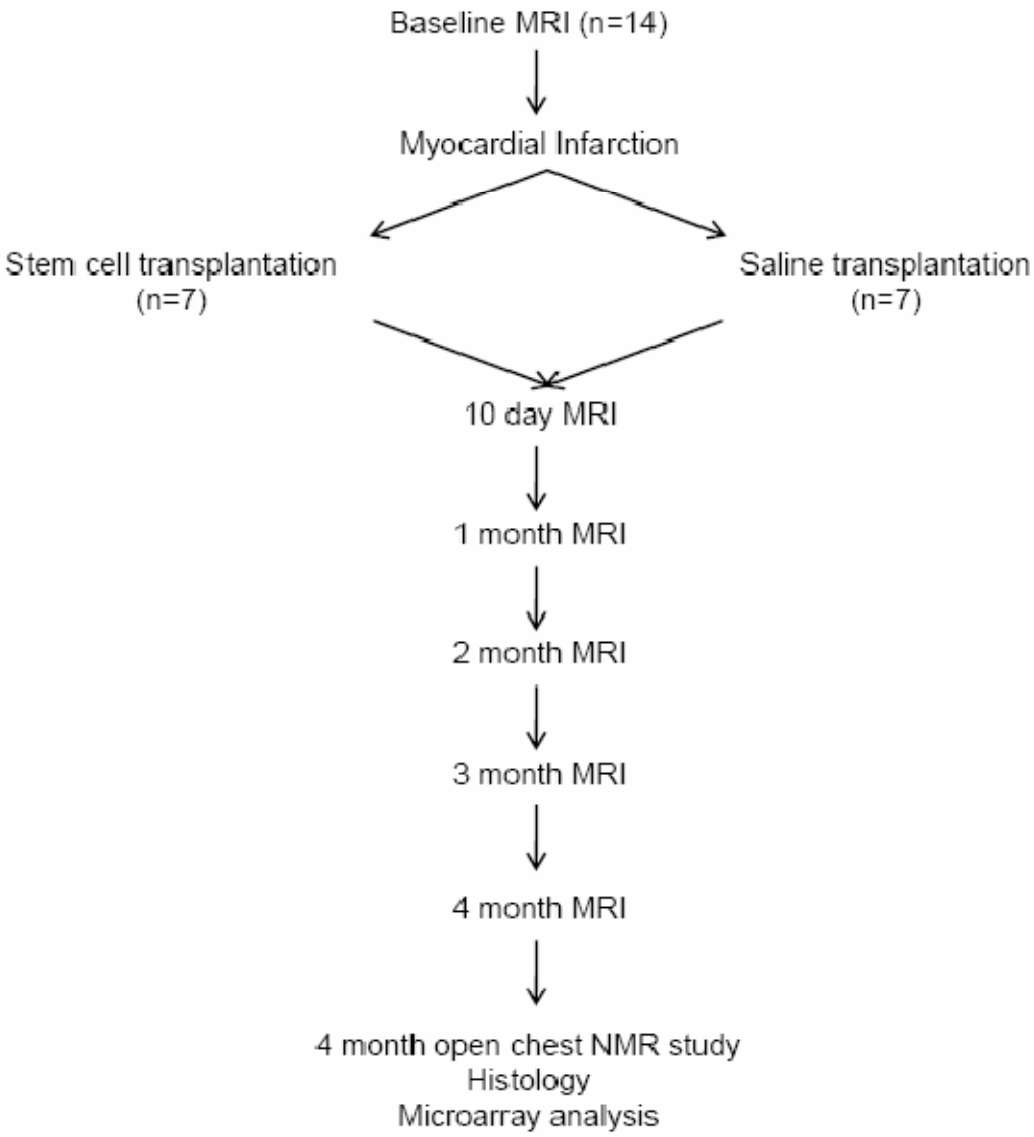
Baseline MRI (n=14)
Myocardial Infarction
Stem cell transplantation
(n=7)
Saline transplantation
(n=7)
10 day MRI
1 month MRI
2 month MRI
3 month MRI
4 month MRI
4 month open chest NMR study
Histology
Microarray analysis

Fig. 2.

A.

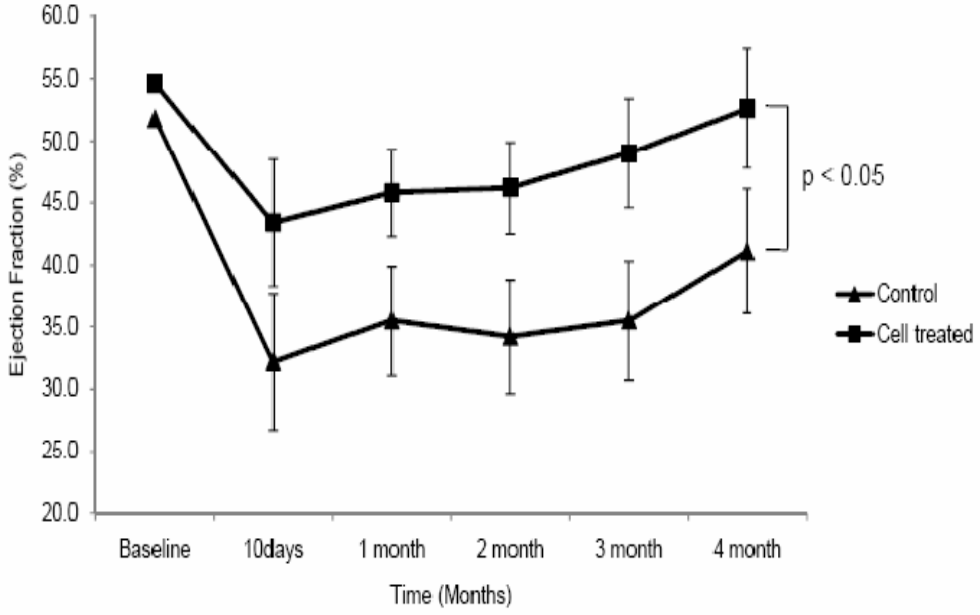

B.

	Control (n=7)	Cell Treated (n=7)
Baseline	51.8±5.0	54.6±3.0
10 day	32.2±5.5	43.4±5.1*
1 month	35.5±4.4	45.8±3.5*
2 month	33.4±4.6	46.2±3.7*
3 month	33.1±4.8	49.0±4.4*
4 month	35.7±5.0	51.2±4.8*

Fig. 3.

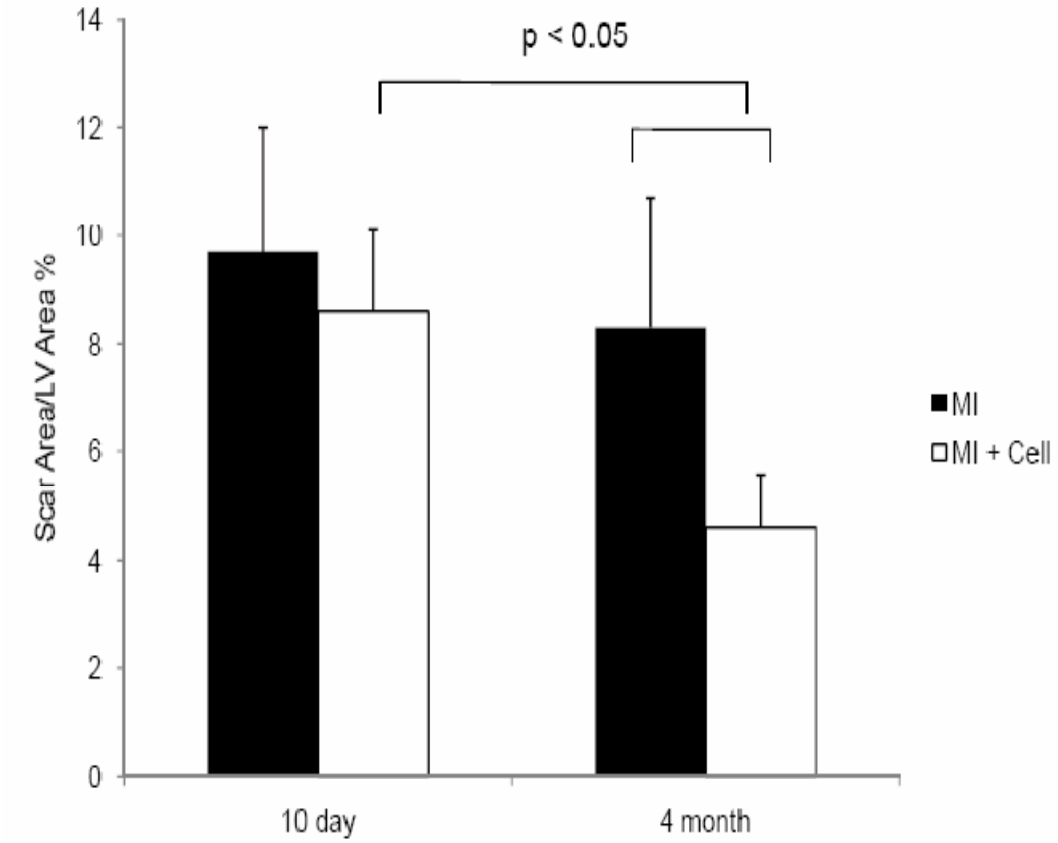

Fig. 4.

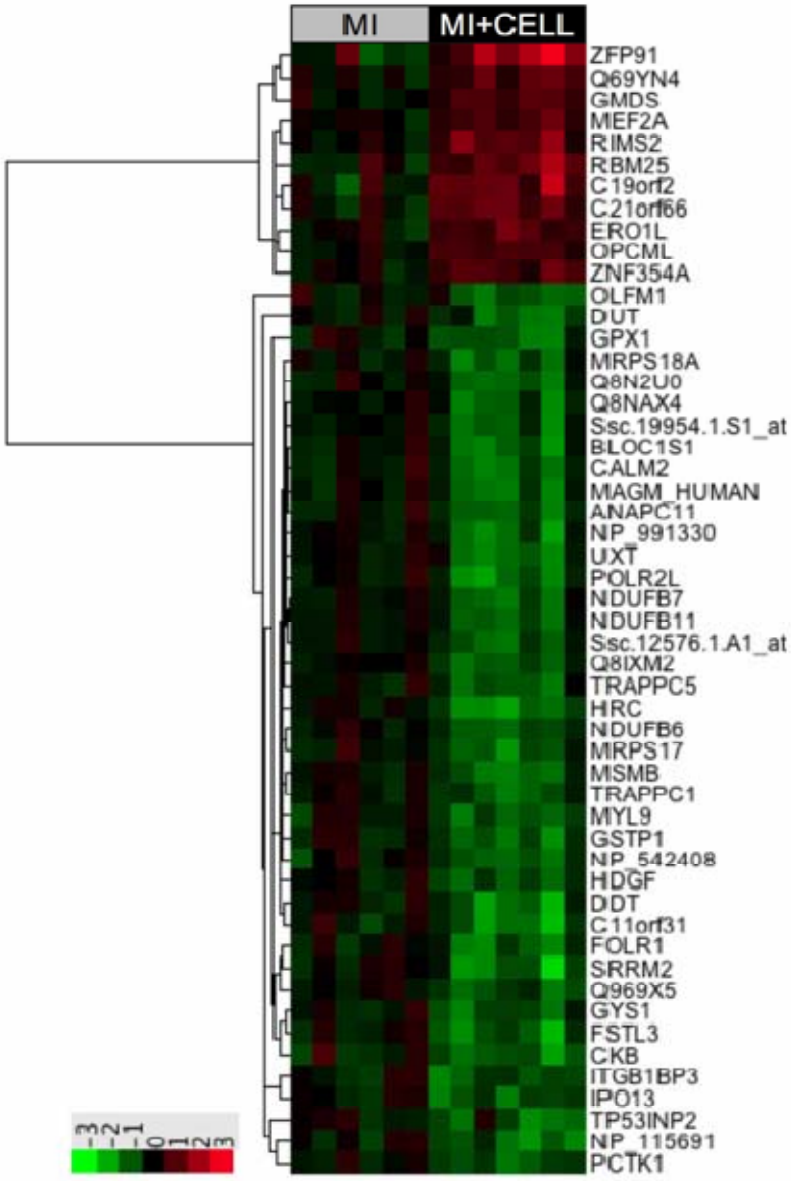
MI
MI+CELL
ZFP91
Q69YN4
GMDS
MEF2A
RIMS2
RBM25
C19orf2
C21orf66
ERO1L
OPCML
ZNF354A
OLFM1
DUT
GPX1
MRPS18A
Q8N2U0
Q8NAX4
Ssc.19954.1.S1_at
BLOC1S1
CALM2
MAGM_HUMAN
ANAPC11
NP_991330
UXT
POLR2L
NDUFB7
NDUFB11
Ssc.12576.1.A1_at
Q8IXM2
TRAPPC5
HRC
NDUFB6
MRPS17
MSMB
TRAPPC1
MYL9
GSTP1
NP_542408
HDGF
DDT
C11orf31
FOLR1
SRRM2
Q969X5
GYS1
FSTL3
CKB
ITGB1BP3
IPO13
TP53INP2
NP_115691
PCTK1
3
2
1
0
1
2
3

CHAPTER 5: LONG TERM PRESERVATION OF MYOCARDIAL ENERGETICS IN CHRONICALLY HIBERNATING MYOCARDIUM

Mohammad Nurulqadr Jameel , Qinglu Li , Abdul Mansoor, Qiang Xiong,

Cory Swingen, Jianyi Zhang.

We previously reported that the myocardial energetic state, as defined by PCr/ATP, was preserved at baseline in a swine model of chronic myocardial ischemia with a mild reduction of myocardial blood flow (MBF) 10 weeks after placement of an external constrictor on the LAD. It remains to be seen whether this stable energetic state is maintained at a longer term follow-up. Hibernating Myocardium (HB) was created in mini-pigs (n=7) by the placement of an external constrictor (1.25 mm i.d) on the LAD. Function was assessed with MRI at regular intervals for 6 months. At 6 months, myocardial energetics in the HB was assessed by ^{31}P-MRS and myocardial oxygenation was examined from the deoxymyoglobin signal (Mb-δ) using ^{1}H-MRS during baseline (BL), coronary vasodilation with adenosine (AD) and high cardiac work load (HWL) with dopamine and dobutamine (DpDb). MBF was measured with radiolabeled microspheres. At BL, systolic thickening fraction was significantly lower in the HB as compared to remote region (34.4±9.4 *vs* 50.1±10.7, p=0.006). This was associated with a decreased MBF in the HB as compared to remote region (0.73±0.08 ml/min.g *vs* 0.97±0.07 ml/min.g, p=0.03). The HB PCr/ATP ratio at BL was normal. DpDb resulted in a significant increase in RPP, which caused a 2 fold increase in MBF in the HB and a 3 fold increase in the remote region. The systolic thickening fraction increased with DpDb that was significantly higher in the remote region than HB ($p<0.05$). The HWL was associated with a significant reduction in the HB PCr/ATP ratio ($p<0.02$) but this response was similar to normal myocardium. Thus, HB has stable baseline myocardial energetics despite a reduction in MBF and regional LV function. More importantly, HB has a

reduced contractile reserve but has a similar energetic response to high cardiac workload as normal myocardium.

Introduction

In clinical practice, hibernating myocardium refers to areas of regional dysfunction, decreased blood flow and absence of scar in patients with coronary artery disease which are thought to recover after revascularization [63-65]. Hibernating myocardium is characterized by a balance between matched reductions in myocardial blood flow and function [119-120]. The acute perfusion contraction matching in short term hibernation is maintained up to 90 minutes after the initiation of moderate ischemia and is not sustained over several hours [119-120]. In animal models, chronic hibernating myocardium can be created by constriction of a proximal coronary artery that leads to progressive reduction in myocardial blood flow and regional dysfunction [66-76]. Perfusion contraction matching in this model probably develops from a single or repetitive bouts of stress induced ischemia and reperfusion in the presence of severe coronary stenosis [119-120]. Thus, there is a temporal progression from chronic stunning to hibernation in which the reduced resting blood flow is the result rather than the cause of chronic contractile dysfunction [66-76]. Decreased myocardial oxygen consumption has been observed in hibernating myocardium at rest and during increased myocardial oxygen demand which contrasts with findings in short term hibernating myocardium [72, 121]. Chronic hibernating myocardium demonstrates alteration in metabolism with an increase in glucose uptake and glycogen storage [69, 73-74]. The energetic state in the hibernating myocardium has been studied previously with diverse results [75, 122-124].

Our laboratory specializes in studying myocardial energetic states in vivo with NMR spectroscopy. Energetic state refers to delta G which is the free energy of ATP hydrolysis [125]. ΔG_{ATP} (kJ/mol) = $\Delta G° - RT\ ln\ ([ATP]/[ADP][Pi])$, where ΔG^{o} (− 30.5 kJ/mol) is the value of ΔG_{ATP} under standard conditions of molarity, temperature, pH, and $[Mg^{2+}]$, *R* is the gas constant (8.3 J/mol K), and *T* is temperature (Kelvin). Delta G is linearly related to the myocardial PCr/ATP [125]. The set point of the driving force and the efficiency of mitochondria ATP production (mtOXPHOS) are reflected by the myocardial PCr/ATP (delta G). In chronic heart failure or acute myocardial ischemia, the myocardial energetic state is decreased that is reflected by a decrease in PCr/ATP [50-51, 53, 56, 90, 126-127]. In a short term follow-up of animals with chronic hibernation, we showed that despite a reduction in myocardial blood flow and regional function, the hibernating myocardium has well preserved myocardial energetics [75].

The aim of the present study is three fold. Firstly, we aim to create a model of chronic hibernation in mini-pigs to allow us to study the energetic state in chronic hibernating myocardium up to 6 months. Our second objective is to determine sequential measurements of myocardial blood flow in this model with MR imaging to assess for sequential changes in blood flow and its correlation with regional function. Thirdly, and most importantly, we hypothesize that chronic hibernating myocardium will maintain a stable energetic state for up to 6 months at baseline and with increased work load.

Methods

All experiments were performed in accordance with the animal use guidelines of the University of Minnesota, and the experimental protocol was approved by the University of Minnesota Institutional Animal Care and Use Committee (IACUC). The investigation conformed to the *"Guide for the care and use of laboratory animals"* published by the National Institutes of Health (NIH publication No 85-23, revised 1985).

Animal Preparation

Sinclair Miniswines (Sinclair Research Center, MO) were used for this study. Sinclair pigs are research purpose bread, and grow very slowly which allowed us to follow these animals for long term. A chronic hibernation myocardium model was created in seven mini-pigs. Briefly, female Sinclair miniswine (5 months age) were anesthetized with pentobarbital (30 mg/kg iv), intubated and ventilated with a respirator with supplemental oxygen. A left thoracotomy was performed. The left anterior descending coronary artery (LAD) was dissected free, and a C-shaped titanium occluder (3 mm in length and 1.25 mm in internal diameter) was secured around the proximal vessel and gently closed with suture. In all animals, the pericardium and chest were closed in layers. Animals received standard post-operative care including analgesia until they ate normally and became active.

Regional Function Measurements

Ventricular function was assessed using MRI before surgery and then at 2 weeks, 1 month, 4 month and 6 month after instrumentation. MRI was performed on a 1.5 Tesla clinical scanner (Siemens Sontata, Siemens Medical Systems, Islen NJ) using a phased-array 4-channel surface coil and ECG gating as previously described in detail [50]. Animals were anesthetized with 1% isoflurane and positioned in a supine position within the scanner. The protocol consisted of: 1) localizing scouts to identify the long- and short-axis of the heart, 2) short- and long-axis cine for the measurement of global cardiac function, and 3) delayed contrast-enhancement for the assessment of scar size. Steady-state free precession "True-FISP" cine imaging used the following MR parameters: TR = 3.1 ms, TE = 1.6 ms, flip angle = 79^{o}, matrix size = 256 x 120, field of view = 340 mm x 265 mm, slice thickness = 6 mm (4 mm gap between slices) and 16-20 phases were acquired across the cardiac cycle. Global function and regional wall thickness data were computed from the short-axis cine images using MASS (Medis Medical Imaging Systems, Leiden, The Netherlands) for the manual segmentation of the endocardial and epicardial surfaces at both end-diastole (ED) and end-systole (ED) from base to apex. End-diastole and end-systole were determined by evaluating the largest and smallest ventricular volumes during a cycle. Short-axis turboFLASH imaging, from base to apex, used TR = 16 ms, TE = 4 ms, TI ~ 220 ms, flip angle = 30^{o}, matrix size = 256 x 148, field of view = 320 mm x 185 mm, slice thickness = 6 mm (0 mm gap between slices) and two signal

averages. The appropriate inversion time (TI) was chosen to adequately null the signal intensity (SI) of normal myocardium. The LV papillary muscles, as well as the LV short and long axis were used as landmarkers for the cardiac MRI and indentifying the LAD region. The spatial resolution of the MRI measurements is very high (approximately 1-2 mm).

Myocardial Blood Flow with First Pass Perfusion MRI

Sequential myocardial blood flow measurements were obtained before surgery and then at 2 weeks, 1 month, 4 month and 6 month after instrumentation. Perfusion imaging was performed with a bolus injection of 0.025 mmol/kg of gadolinium (Gd)-diethylenetriamine pentaacetic acid (DTPA) at 5 ml/s through a power injector. We chose this dose to be in the linear range of Gd-DTPA concentration and signal intensity (SI) within the blood pool. A saturation-recovery gradient echo imaging with an echo-train readout was used. The field of view was 30 cm^2, matrix was 1.4 × 1.4 mm, and short-axis slice thickness was 8 mm, the repetition time = 6.3 ms, echo time = 1.3 ms, flip angle = 20°, and the echo train = 4. During bolus transit, 3 to 4 short-axis images were acquired per 1 R-R interval gated to the electrocardiographic signal of the animal over 40 to 60 heart beats.

Perfusion images were analyzed offline with an interactive data language-based software program (Cine Tool GEMS, Milwaukee, Wisconsin). Time intensity curves (TIC) were generated from both the left ventricular blood pool to obtain

the arterial input function to the coronary circulation and from the myocardial tissue. These were 1.0 to 1.5 cm^2 in area to coincide with volume of the pathologic sections. The concept of deconvolution of arterial input function with a shaped function to fit the tissue enhancement curve was employed as first described by L. Axel, Tissue mean transit time from dynamic computed tomography by a simple deconvolution technique [128], and adapted to CMR [129]. A Fermi function is used to deconvolve the arterial input function to fit the myocardial TIC in a region of interest. Perfusion scans were acquired for 40 R-R intervals, and the entire myocardial TIC was used to generate the fit with the arterial input function. The resultant amplitude of the Fermi function after the fit reflects absolute MBF [128-129]. Signal noise was calculated for each study by measuring the SD of the mean SI to a region of interest outside the chest cavity. This was done to separate the impact of noise from tissue SI. The contrast enhancement ratio was calculated by: (peak enhancement − pre-contrast) SI/pre-contrast SI, during FP perfusion.

Myocardial blood flow measurement with microspheres

Myocardial blood flow was measured using radionuclide labeled microspheres 15 μm in diameter labeled with 4 different radioisotopes (^{51}Cr, ^{85}Sr, ^{95}Nb and ^{46}Sc) during the terminal NMR study at 6 month follow-up. Microsphere suspension containing $2x10^6$ microspheres was injected through the left atrial catheter while a reference sample of arterial blood was withdrawn from the aortic catheter at a rate 15 ml/min beginning 5 seconds before the microsphere injection and

continuing for 120 seconds. Radioactivity in the myocardial and blood reference specimens was determined using a gamma spectrometer (Packard Instrument Company, Downers Grove, IL) at window settings chosen for the combination of radioisotopes used during the study. Activity corrected for overlap between isotopes and for background was used to compute blood flow as ml/g of myocardium/minute.

Surgical preparation for open chest MR spectroscopy study

Detailed surgical preparations for MRS study are published previously [56, 77, 91]. Briefly, animals were anesthetized with pentobarbital (30 mg/kg followed by a 4 mg/kg/hr iv), intubated and ventilated with a respirator and supplemental oxygen. Arterial blood gases were maintained within the physiologic range by adjustments of the ventilator settings and oxygen flow. 3.0 mm OD heparin-filled polyvinyl chloride catheters were inserted into the ascending aorta (Ao) and inferior vena cava (IV). A sternotomy was performed, and the heart was suspended in a pericardial cradle. A third heparin-filled catheter was introduced into the LV through the apical dimple and secured with a purse string suture. A 25 mm diameter NMR surface coil was sutured onto the anterior wall of the LV. The pericardial cradle was then released, and the heart was allowed to assume its normal position in the chest. The surface coil leads were connected to a balanced-tuned external circuit and the animals positioned within the magnet. In order to compensate for insensible fluid loss in the open chest studies, we routinely administer saline at rate of 1 ml/min i.v. during the entire experimental

data acquisition. Ventilation rate, volume and inspired oxygen content were adjusted to maintain physiologic values for arterial PO_2, PCO_2 and pH. Aortic and LV pressures were monitored continuously throughout the study. Hemodynamic measurements were acquired simultaneously with the ^{1}H - and ^{31}P- MR spectra.

MR spectroscopy Study protocol and hemodynamic measurements

Hemodynamic measurements were acquired simultaneously with the NMR spectra. Aortic and LV pressures were measured using pressure transducers positioned at mid-chest level [89-91] and recorded on an 8-channel recorder. After all the baseline data were obtained, animals received adenosine to cause maximal vasodilation and the measurements were repeated. This was following by combined dobutamine and dopamine infusion (20 μg/kg/min. each) to induce a very high cardiac workstate. After waiting for approximately 5 minutes after the initiation of catecholamine infusion, all the spectroscopic and hemodynamic data were again measured under the high cardiac workstates.

^{31}P-NMR Spectroscopy Technique

^{31}P-NMR spectroscopy has been used to study myocardial energetics [130]. NMR spectroscopy was performed at 6 month follow-up in a 4.7T magnet. Magnetic field shimming to improve the magnetic field homogeneity of the heart was achieved by the “auto-shim” scheme (Varian Assoc. Inc., CA). Spatially

localized ^{31}P NMR spectroscopy was performed using the RAPP-ISIS/FSW method [54, 89-91], which is the rotating-frame experiment using adiabatic plane-rotation pulses for phase modulation (RAPP)-imaging-selected in vivo spectroscopy (ISIS)/Fourier series window (FSW) method. Detailed experiments documenting voxel profiles, voxel volumes and spatial resolution attained by this method have been published previously. In this application of RAPP-ISIS/FSW, the signal origin was first restricted to a 12*12 mm two-dimensional column perpendicular to the LV wall. The signal was later localized into three well resolved and five partially resolved layers along the column and hence, across the LV wall. Localization along the column was based on B_1 phase encoding and employed a 9-term Fourier series window as previously describe [54, 89-91]. The phase encoded data were used to generate a voxel or a "window" that can be shifted arbitrarily by post data acquisition processing along the phase encode direction (in this case perpendicular to the surface coil and thus the heart wall); consequently, voxels were generated at different distances or "depths" from the outer LV wall. However, we normally present five voxels centered about 45°, 60°, 90°, 120°, and 135° phase angles as previously described. There is absolutely no overlap between the 135° voxel (corresponding to the subepicardium) and the 45° voxel (corresponding to the subendocardium). Whole wall spectra were obtained with the image-selected *in vivo* (ISIS) technique, defining a column 12*12 mm^2 perpendicular to the heart wall. The calibration of spectroscopic parameters was facilitated by placing a polyethylene capillary filled with 15 µl of 3 M/L phosphonoacetic acid into the inner diameter of the surface

coil. This phosphonoacetic acid standard was used only for calculating the 90 degree pulse length of the RAPP-ISIS method [54, 89-91]. The position of the voxels relative to the coil was set according to the B_1 strength at the coil center which was experimentally determined in each case by measuring the 90° pulse length for the phosphonoacetic acid standard contained in the reference capillary at the coil center. NMR data acquisition was gated to the cardiac and respiratory cycles using the cardiac cycle as the master clock to drive both the respirator and the spectrometer as previously described [54, 89-91]. The surface coil was constructed from a single turn copper wire 25 mm in diameter with each side of the coil leads soldered to a 33 pF capacitor. Complete transmural data sets were obtained in 10-minute time blocks using a repetition time of 6-7 seconds to allow for full relaxation for ATP and inorganic phosphate (Pi) and approximately 95% relaxation of the PCr resonance [54, 89-91]. The ratios of PCr to ATP (PCr/ATP) were calculated for each transmurally differentiated spectra set as previously described [54, 89-91]. All resonance intensities were quantified using integration routines provided by the SISCO software.

CK kinetics measurement with ^{31}P MRS saturation transfer

A double-tuned (200 MHz for ^{1}H and 81 MHz for ^{31}P) surface coil (diameter, 28 mm) was used for RF transmission and signal detection. A chemical shift selective (CHESS) pulse sequence was employed to saturate the ATP γ

resonance [131]; this sequence consisted of a 90° Sinc RF excitation pulse followed by a short half-sine gradient pulse in all three orthogonal axes to enhance the dephasing of transverse magnetization. This CHESS sequence was applied repetitively to ensure complete saturation of the ATP γ resonance. The repetition time for signal acquisition of 12 s provided fully relaxed ATP γ and PCr resonances. Control spectra were acquired with the saturation carrier frequency setting on the opposite side of the PCr resonance with a frequency difference identical to that between PCr and ATP γ. The relative change of the PCr resonance intensity between the saturated and control spectra is proportional to the forward rate constant (k_f) in the exchange reaction between PCr and ATP. All spectra were recorded with a spectral width of 6,000 Hz. The forward rate of CK (k_f: PCr → ATP γ) and the intrinsic longitudinal relaxation time for PCr (T_1) were calculated based on the two-site chemical exchange model as follows: $k_f = (\Delta M/M_0)/T_i$ and $1/T_1 = 1/T_i - k_f$, where k_f and T_1 represent the pseudo first-order rate constant and the intrinsic longitudinal relaxation time of PCr, respectively; $\Delta M = M_0 - M_{infinite}$, where M_0 and $M_{infinite}$ represent the magnetization at saturation zero and infinite times, respectively; and T_i is the time constant that describes the integral of PCr magnetization decay as the time of saturation of ATP γ increased from 0 to infinity. The CK forward flux rate ($Flux_f$) was calculated as the product of k_f and the myocardial PCr concentration ($Flux_f = k_f$ [PCr]). Each set of spectra for saturation transfer measurements required ~6.2 min.

^{1}H- NMR spectroscopy technique

^{1}H NMR spectroscopy was performed on 4.7T and the methods have been previously reported in detail [54, 92]. In brief, radiofrequency (RF) transmission and signal detection were performed with the dually tuned 28 mm diameter surface coil. A single-pulse-collection sequence with a frequency selective Gaussian excitation pulse (1ms) was used to selectively excite the N-δ proton resonance signal of the proximal histidine in deoxymyoglobin (Mb- δ). This technique provided sufficient water suppression due to the large chemical shift difference between water and Mb- δ (>14 kHz). The NMR signal was optimized by adjusting the RF pulse power using the water signal as a reference. A short repetition time (TR = 25 ms) was used due to the short T_1 of Mb- δ. Each spectrum was acquired in 5 min (10,000 FIDs). Although the short T_1 of Mb- δ and fast acquisition prevent gating to the cardiac cycle, the signal loss due to motion is negligible compared to the inherently broad line width of the Mb- δ peak.

Statistics

Statistical analysis was performed using 2-way ANOVA (hibernating vs. remote, baseline vs. time) with post-hoc analysis. For comparison between the two treatment groups, the conventional significance level of type I error ($P < 0.05$) was used. The Bonferroni correction for the significance level was used to take

into account multiple comparisons. All values are expressed as mean ± standard deviation (SD). All statistical analyses were performed in Sigmastat version 3.5 (San Jose, CA).

Results

Resting Myocardial Blood Flow in Hibernating Myocardium

A titanium c-shaped occluder device with an internal diameter of 1.25mm was placed over the proximal LAD. MR Angiography was performed to determine the progression in severity of stenosis over time. It showed that at 1 month there is approximately 75% stenosis and it progresses to >90% stenosis of the proximal LAD at 4 months but was not completely occluded. There was a gradual decline of myocardial blood flow (MBF) in the anterior region of the heart. Resting MBF data obtained with Perfusion MRI is summarized in Fig. 1. There was a trend towards decreased MBF in the LAD territory as compared to Remote region at 1 month (1.08±0.06 $ml.min^{-1}.g^{-1}$ vs 1.32±0.05 $ml.min^{-1}.g^{-1}$, p=0.06). At 4 month, the LAD region had significantly decreased MBF than the Remote region (0.78±0.05 $ml.min^{-1}.g^{-1}$ vs 1.22±0.04 $ml.min^{-1}.g^{-1}$, p=0.008) which persisted up to the 6 month follow-up (0.75±0.04 $ml.min^{-1}.g^{-1}$ vs 1.14±0.08 $ml.min^{-1}.g^{-1}$, p=0.01).

Coronary Flow Reserve in Hibernating Myocardium

During the final terminal study at 6 months, MBF was measured by injection of microspheres at baseline and after intravenous adenosine administration (Fig. 2). The baseline MBF data correlated with the perfusion MRI data obtained at baseline at 6 months. This demonstrates that at baseline, hibernating myocardium has decreased MBF as compared to remote myocardium (0.73±0.08 $ml.min^{-1}.g^{-1}$ vs 0.97±0.07 $ml.min^{-1}.g^{-1}$, $p < 0.05$). Moreover, subendocardial blood flow (0.62±0.06 $ml.min^{-1}.g^{-1}$ vs 1.20±0.06 $ml.min^{-1}.g^{-1}$, $p < 0.05$) showed the most dramatic decrease in the hibernating myocardium with subsequent decrease in the endo/epi ratio. After adenosine vasodilation, MBF was critically impaired in the LAD region and only increased minimally (0.73±0.08 $ml.min^{-1}.g^{-1}$ vs 1.04±0.12 $ml.min^{-1}.g^{-1}$, p=NS) as compared to the more than 3 fold increase in MBF in the remote region (0.97±0.07 $ml.min^{-1}.g^{-1}$ vs 3.22±0.25 $ml.min^{-1}.g^{-1}$, p=0.0007) (Fig. 2). Coronary Flow Reserve (CFR= MBF after maximal hyperemia with adenosine/MBF at rest) was calculated and was significantly lower in HB as compared to remote region (1.38±0.12 in HB vs 3.36±0.14 in remote myocardium, $p<0.05$).

Ventricular Function in Hibernating Myocardium

The weights of the animal were 20±3 kg at 6 months. Serial measurements of ventricular volumes, ventricular mass and ejection fraction have been

summarized in Table 1. These demonstrate that the global left ventricular function was normal in all the animals throughout the follow-up period. There was no evidence of myocardial infarction by delayed enhanced MRI. None of the animals developed clinical heart failure and LVEDP was normal in all animals at 6 months (2.8±3.3mmHg) and none of the animals had LVEDP greater than 10. There were two animals that died from sudden cardiac death and thus mortality was 22% over a period of 6 months. Regional ventricular function is summarized in Fig. 3. Systolic Thickening Fraction was significantly decreased in the LAD region as compared to Remote region at 1 month (36.2±7.0% vs 52.4±7.2%, p=0.04). This persisted at 4 month (34.2±7.8% vs 52.8±8.2%, p=0.02) and 6 month (34.4±7.2% vs 50.1±7.6%, p=0.02).

Response to Increased Cardiac Workload in Hibernating Myocardium

Even though that the resting myocardial blood flow and function in the hibernating myocardium was decreased, all the animals had an appropriate hemodynamic response to inotropic stimulation. Intravenous administration of dopamine and dobutamine resulted in a significant increase in heart rate (101.6±14.9 vs 153±32.7, p=0.019), left ventricular systolic pressure (103.8±16.5 mmHg vs 160±40.5 mmHg, p=0.04) and consequently Rate Pressure Product ($10.6\pm2.3 \times 10^3$ vs $25.0\pm10.8 \times 10^3$, p=0.04) (Table 2). This increase in workload was associated with only a 53.4% increase in MBF in the hibernating myocardium as compared to a 222% increase in MBF in the remote myocardium

(Fig 4). The thickening fraction was similar at baseline in the hibernating myocardium and remote myocardium. Thickening fraction increased significantly in the remote area after inotropic stimulation as compared to baseline ($p<0.05$). Moreover, thickening fraction was significantly higher in the remote area as compared to hibernating myocardium after inotropic stimulation (84.1±10.4% vs 42.2±8.6%, $p=0.006$). However, there was no significant difference between the thickening fraction at baseline and increased workload in the hibernating myocardium.

Myocardial Energetics in Hibernating Myocardium

Transmural High Energy Phosphate (HEP) measurements in the hibernating myocardium are summarized in Table 3. In addition, these have been compared to normal minipig controls and historical normal controls [54, 131]. This shows that the hibernating myocardium has normal energetic state at baseline as reflected by the PCr/ATP ratio. The subepicardial, subendocardial and full thickness PCr/ATP ratios in the hibernating myocardium are 2.33±0.09, 1.88±0.06 and 2.25±0.21 respectively which are similar to normal minipigs and historical pig controls. As shown, there is a significant decrease in PCr/ATP ratio with inotropic stimulation (1.84±0.23 vs 2.25±0.21, $p=0.03$) but this decrease is similar to what is observed in normal myocardium at a similar work-load [54]. The increased workload was associated with a 20.4±0.12% decrease in ATP production rate via Creatine Kinase which is again similar to previous

observations in normal pigs at increased workload [54]. Transmural myocardial oxygenation, by in vivo H1-MRS myoglobin saturation levels, demonstrated no myoglobin desaturation in the hibernating myocardium at rest or with increased cardiac workload. Thus, myocardial ischemia is not observed in hibernating myocardium despite a depression in myocardial blood flow and reduction in wall thickening.

The CK forward flux rate ($Flux_f$) was calculated as the product of k_f and the myocardial PCr concentration ($Flux_f = k_f$ [PCr]), where [PCr]=[ATP] x PCr/ATP. ATP concentration in hibernating myocardium has been previously reported by Canty et al as 20.1±1.0 μmol/g dry weight [123]. Under baseline conditions in our study, the PCr/ATP ratio and kf were 2.25±0.21 and 0.40±0.04 sec^{-1}. Thus, $Flux_f$ was calculated as 18.1±2.1 μmol g^{-1} sec^{-1}. This value is similar to what has been reported for normal pigs (20.3±2.4 μmol g^{-1} sec^{-1}) [53].

Discussion

This study describes the longest follow up of experimental chronic hibernation in a pre-clinical large animal model. It utilized cardiac MRI to demonstrate the temporal changes in blood flow and regional function in hibernating myocardium to elucidate the exact timing of development of the phenomenon of hibernating myocardium in these animals. More importantly, it reveals that the myocardial energetic state as reflected by PCr/ATP ratio is normal under baseline conditions

up to 6 months in hibernating myocardium despite a reduction in perfusion reserve and regional function. Furthermore, the decrease in PCr/ATP ratio with increased workload in hibernating myocardium is similar to normal myocardium.

Creation of Hibernating Myocardium animal model

Our previous study of myocardial energetics in hibernating myocardium was limited to a follow-up period of 10 weeks because of the large size of the farm pigs which were not able to fit in the bore size of the magnet used for Magnetic Resonance studies [75]. Thus, in the current study we used Mini-swine which grow at a slower rate and thus do not attain a large size despite a longer follow-up period. This allowed us to follow the function and blood flow in the hibernating myocardium up to six months and study the myocardial energetics in the hibernating myocardium at this longer follow-up. A titanium c-shaped occluder device with an internal diameter of 1.25mm was placed over the proximal LAD, which is smaller than the 1.4mm size used in the farm pig study [75]. MR Angiography was performed to determine the progression in severity of stenosis over time. It showed that at 1 month there is approximately 75% stenosis and it progresses to >90% stenosis of the proximal LAD at 4 month but it was not completely occluded. It has been shown previously that hibernating myocardium develops regardless of whether the chronic stenosis was eventually totally occluded or remained patent; however, the inotropic reserve that was recruited by epinephrine depended on coronary reserve and was greater with a patent

artery in that study [132]. There was no evidence of myocardial infarction by late enhanced gadolinium MR imaging and on gross visualization at the time of sacrifice at 6 months. Focal myocardial damage exceeding 5% of myocardium within the region of interest seems to be necessary for detection of LGE in vivo in an experimental model of coronary microembolization [133]. Thus, smaller areas of fibrosis cannot be excluded in the present study.

Temporal changes in Myocardial Blood Flow in Hibernating Myocardium

A unique feature of our study was the ability to examine the serial changes of myocardial blood flow non-invasively using quantitative MR perfusion imaging techniques. This showed that the myocardial blood flow in the hibernating myocardium started to decline at 1 month. Thus, the absolute MBF in the hibernating myocardium was significantly lower than the remote region at 4 and 6 month follow up. CMR perfusion imaging has been used to demonstrate decreased resting MBF in patients with CAD and regional LV dysfunction [134]. There is excellent correlation between microsphere and MRI myocardial blood flow measures. We have previously shown that hypoperfused regions, identified with microspheres, on the first-pass MR images displayed significantly decreased signal intensities compared with normally perfused myocardium ($P < .0007$) [135]. Moreover, flow estimates by first pass MR imaging averaged 1.2 mL/min/g +/- 0.5 (n = 29), compared with 1.3 mL/min/g +/- 0.3 obtained with tracer microspheres in the same tissue specimens at the same time. In the present

study, MBF in control myocardium at 6 months is 1.14±0.08 and 0.97±0.07 by MR perfusion imaging and microspheres respectively, while in hibernating myocardium at 6 months the MBF is 0.75±0.04 and 0.73±0.08. We believe it is the first time sequential MBF measurements have been obtained in an animal model of chronic hibernating myocardium. Transmural MBF measurements at 6 months using microsphere also showed that the subendocardial layer had the most significant decrease in MBF with a subsequent decrease in the endo/epi MBF ratio. The myocardial perfusion reserve was also markedly diminished in the hibernating myocardium as shown previously [72].

It is interesting to note that systolic thickening fraction was maintained in hibernating myocardium between 1 and 6 months (Figure 3), whereas the MBF gradually continued to decrease by an additional 25% (Figure 1), which suggests that the hibernating myocardium is becoming more efficient between 1 and 6 months (maintaining the same function while being provided less blood flow). Assuming the mitochondrial OXPHOS is unchanged between 1-6 months, this observation would suggest that similar amount of myocardial thickening contraction requires less supporting ATP in Month 6 as compared to Month 1. The mechanism for this observation warrants future studies such as using tagged MRI to track 3D regional myocardial motion vectors in modeling the efficiency of LV ejection [136-137]

Preserved Baseline Myocardial Energetics in chronic hibernating myocardium

In short term hibernation myocardium, sequential biopsy-based measurements of ATP, creatine phosphate, creatine, and inorganic phosphate revealed a decrease in the free energy change of ATP hydrolysis during early ischemia with a subsequent recovery during continued 90 min ischemia [127]. A key feature of this study is that the myocardial energetic state as measured by in vivo NMR spectroscopy is stable in chronic hibernating myocardium. Energetic state refers to delta G which is the free energy of ATP hydrolysis [125]. ΔG_{ATP} (kJ/mol) = $\Delta G° - RT\ ln\ ([ATP]/[ADP][Pi])$, where ΔG^o (− 30.5 kJ/mol) is the value of ΔG_{ATP} under standard conditions of molarity, temperature, pH, and $[Mg^{2+}]$, *R* is the gas constant (8.3 J/mol K), and *T* is temperature (Kelvin). Delta G is linearly related to the myocardial PCr/ATP [125]. The set point of the driving force and the efficiency of mitochondria ATP production (mtOXPHOS) are reflected by the myocardial PCr/ATP (delta G). In chronic heart failure or acute myocardial ischemia, the myocardial energetic state is decreased as reflected by a decrease in PCr/ATP [90, 126]. Baseline high energy phosphate levels have been previously studied in animal models of hibernating myocardium and human hibernating myocardium with differing results [75, 122-124]. Elsasser et al studied 16 patients with coronary artery disease and left ventricular dysfunction who had documented hibernating myocardium detected by thallium-201 scintigraphy, radionuclide ventriculography and low-dose dobutamine

echocardiography [122]. All these patients had improvement of LV function with revascularization [122]. Myocardial biopsy specimens from the hibernating myocardium regions revealed significant depression of creatine phosphate, adenosine triphosphate and creatine, a significant increase in lactate levels and acidosis [122]. They concluded that hibernating myocardium demonstrated a decrease in free energy of ATP hydrolysis and thus is energy depleted [122]. Wiggers at al studied the myocardial energetics in 25 patients with CAD and LV dysfunction but these authors further categorized the dysfunctional myocardium into reversible (hibernating) and irreversible based on improvement after revascularization [124]. Biopsy specimens revealed similar ATP/ADP ratio, lactate levels and glucose uptake in hibernating and remote myocardium; however, the irreversible myocardium had significantly decreased ATP/ADP ratio and glucose uptake and significantly increased lactate levels [124]. In contrast to Elsasser's paper, these authors concluded that the energy stores in hibernating myocardium are well preserved [122, 124]. One of the reasons for this discrepancy could be the increased fibrosis (30%) in the hibernating myocardial specimens in the Elsasser study [122]. In a porcine model of chronic hibernating myocardium, Hu et al report normal baseline total creatine, creatine phosphate and ATP/ADP in biopsy specimens from hibernating myocardium 3 months after placement of an ameroid occluder [123]. These authors did observe a global reduction of absolute ATP, ADP and Total adenine nucleotide (TAN) levels in the hibernating myocardium but despite these reductions the overall energetic state as determined by the ATP/ADP and CP levels was preserved [123]. Our group

has the unique opportunity to study the myocardial energetics in vivo with NMR spectroscopy as opposed to measuring the levels of HEP in vitro in biopsy specimens. We previously have shown that the myocardial energetic state as determined by PCr/ATP ratio is maintained at 10 weeks in a porcine model of chronic hibernating myocardium [75]. We unfortunately were not able to perform a longer follow-up on these animals because of their large size. In the current study, a mini-pig model of chronic hibernating myocardium allowed us to study the myocardial energetics up to 6 months follow-up. We demonstrate that the transmural PCr/ATP ratio is normal in hibernating myocardium at 6 months reflecting a stable energetic state despite a reduction in regional blood flow and function. Furthermore, H1 NMR spectroscopy did not reveal any deoxymyoglobin showing that these tissues are not ischemic despite a reduction in blood flow. The preservation of a stable energetic state reflects the ability of hibernating myocardium to balance the supply and demand and this may be achieved by intrinsic downregulation of its metabolic needs. Using a proteomic approach, Page et al have shown that hibernating myocardium developed a significant downregulation of many mitochondrial proteins such as proteins involved in the major entry points to oxidative metabolism (eg, pyruvate dehydrogenase complex and Acyl-CoA dehydrogenase) and enzymes involved in electron transport (eg, complexes I, III, and V) [138].

Response to increased work load in hibernating myocardium

The animals with hibernating myocardium demonstrated an appropriate hemodynamic response to inotropic stimulation with a subnormal increase in blood flow and regional function. It has been shown previously in a short term hibernation model that inotropic stimulation with dobutamine for 5 minutes increases contractile function without increasing blood flow and disrupts the recovery of creatine phosphate and lactate consumption. If inotropic stimulation is maintained for 90 minutes, the metabolic deterioration is followed by myocardial infarction [139]. In our present study, the increased work load was associated with a decrease in the PCr/ATP ratio which is similar to the decrease seen in normal myocardium previously at a similar workload (RPP approximately 23000). Thus, the hibernating myocardium has a “stable” energetic state, that is similar to normal myocardium. The decreased PCr/ATP ratios during dobutamine infusion probably reflect a change in the kinetics of oxidative phosphorylation or intermediary metabolic steps rather than a myocyte oxygenation–related limitation of ATP synthetic capacity. In contrast to this response in chronic hibernating myocardium, we have previously demonstrated a dramatic decrease in PCr/ATP ratio after dobutamine stimulation in animals with moderate acute coronary artery stenosis. At this level of acute coronary artery stenosis with a state of abolished coronary flow reserve and a minor decrease of myocardial blood flow, there is mild reduction of PCr/ATP at basal cardiac workstate (PCr/ATP~ 1.99), but a marked further reduction of PCr/ATP (to ~1.40) during

higher cardiac workstate [140]. It is possible that intrinsic changes in the mitochondria that reduce oxidant damage within hibernating myocardium preserve energy at high work states. Hu et al have shown that hibernating myocardium has a significant reduction in mitochondrial function in vitro as reflected by a significant reduction in the respiratory control ratio mainly due to a decrease in state 3 respiration [123]. This was also shown by McFalls et al who studied isolated mitochondria from hibernating myocardium and demonstrated a decreased respiratory control ratio [76]. They further demonstrated that the reduction in oxidant damage may also be related to an increase in uncoupling protein 2 in hibernating myocardium [76].

Conclusion

Thus, long term chronic hibernating myocardium has a relatively well preserved stable energetic state despite a reduction in regional blood flow and function. This is probably related to an intrinsic down-regulation in the mitochondrial function which minimizes oxidative stress and leads to a balanced supply and demand at baseline and increased work load.

Figure Legends

Fig 1. Temporal changes in Myocardial blood flow in chronic hibernating myocardium as measured by First Pass Perfusion MRI. *, $p < 0.05$.

Fig 2. Myocardial Perfusion Reserve is diminished in chronic hibernating myocardium. A. Transmural MBF data at 6 months using microsphere method. Values are Mean±SD, *, $p<0.05$ as compared to Remote; †, $p<0.05$ as compared to Baseline. B. Graphical display of the full thickness MBF changes with adenosine in remote and hibernating myocardium.

Fig 3. Temporal changes in regional ventricular function in chronic hibernating myocardium.. A. Tabular summary of wall thickness and systolic thickening fraction. Values are Mean±SD. ESWT, end-systolic wall thickness; EDWT, end-diastolic wall thickness; *, $p<0.05$ as compared to remote. B. Graphical display of systolic thickening fraction over time. *, $p<0.05$.

Fig 4. Response to increased cardiac work load in chronic hibernating myocardium.

Table 1: Ventricular volumes, mass and ejection fraction

Time Period	EDV (ml)	ESV (ml)	SV (ml)	EF (%)	LVED Mass (g)
Baseline	16.9±2.6	7.6±1.8	9.3±0.8	55.1±2.2	35.20±2.2
2 week	19.6±1.3	8.9±1.0	10.7±0.5	55.5±2.5	36.10±2.4
1 month	16.7±2.6	7.7±1.9	9.0±1.1	55.2±4.5	36.42±2.8
4 month	26.9±3.1*	11.3±0.1*	15.5±3.2*	57.2±2.6	40.63±3.8*
6 month	26.9±4.3*	11.9±2.2*	15.1±2.5*	56.2±3.6	44.12±3.6*

Values are Mean±SD. *, $p<0.05$ as compared to Baseline.

Table. 2: Hemodynamic Data

	Baseline	Increased Workload	p-value
Heart Rate (bpm)	101.6±14.9	153±32.7	0.019
LVSP (mmHg)	103.8±16.5	160±40.5	0.04
RPP (x 10^3)	10.6±2.3	25.0±10.8	0.04

Values are Mean±SD; RPP, Rate Pressure Product.

Table 3: Transmural High Energy endocardial/epicardial PCr/ATP ratios

	Epi	Endo	FT
Hibernating Myocardium			
Baseline	2.33±0.09	1.88±0.06	2.25±0.21
Increased Work Load	1.94±0.10*	1.65±0.14*	1.84±0.23*
Control (Minipigs)			
Baseline	2.13±0.08	1.97±0.06	2.06±0.06
Historical Control (Normal Pigs)			
Baseline	2.23±0.08	1.92±0.08	2.18±0.06
Increased Work Load	1.73±0.09*	1.64±0.09*	1.70±0.08*

Values are Mean±SD; *, $p < 0.05$ as compared to baseline within group.

Fig. 1

A.

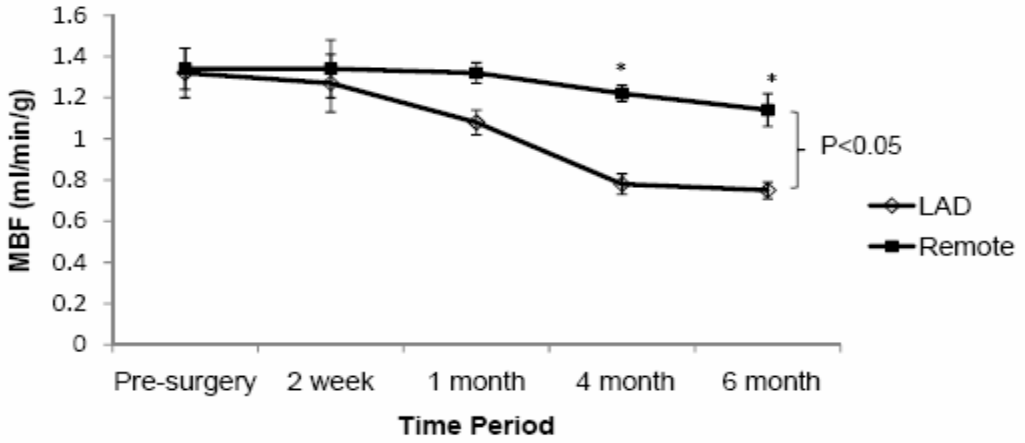

B.

Time Period	Myocardial Blood Flow (ml/min/g) (First Pass Perfusion MRI)		P-value
	LAD	Remote	
Baseline	1.32±0.12	1.34±0.10	0.98
2 week	1.27±0.14	1.34±0.14	0.86
1 month	1.08±0.06	1.32±0.05	0.06
4 month	0.78±0.05	1.22±0.04	0.008
6 month	0.75±0.04	1.14±0.08	0.01

Fig. 2

A.

Transmural MBF (ml/min/g) at 6 months (Microsphere Method)				
	Epi	Endo	FT	Endo/Epi
Remote				
Baseline	0.91±0.05	1.20±0.06	0.97±0.07	1.3±0.1
Adenosine	3.34±0.26†	3.02±0.22†	3.22±0.25†	0.9±0.1†
HB (LAD)				
Baseline	0.85±0.06	0.62±0.06*	0.73±0.08*	0.7±0.1*
Adenosine	1.22±0.12*	0.70±0.10*	1.04±0.12*	0.6±0.1*

B.

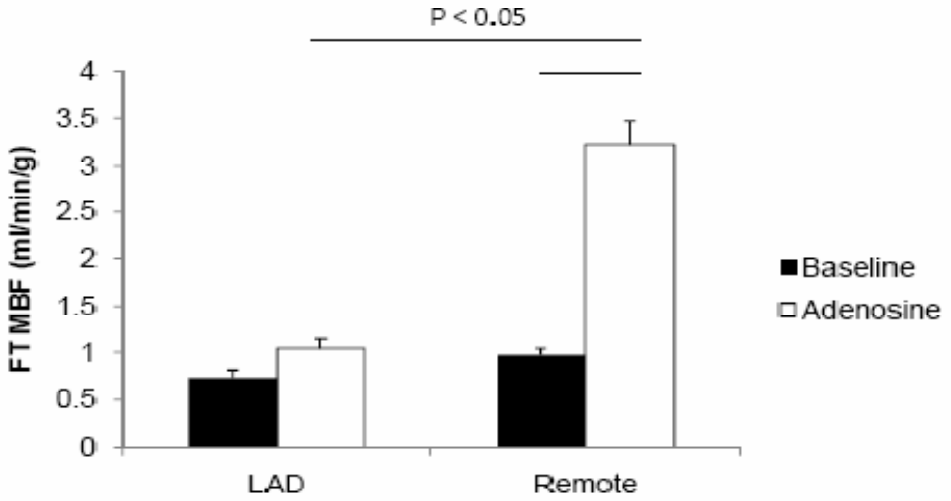

Fig. 3

A.

Time Period	ESWT		EDWT		Systolic Thickening Fraction (%)	
	LAD	Remote	LAD	Remote	LAD	Remote
Baseline	12.1±0.2	12.3±0.3	7.9±0.2	7.9±0.2	52.9±6.4	54.9±8.4
2 week	12.3±0.3	12.2±0.3	8.2±0.2	8.0±0.3	50.4±7.8	52.6±6.2
1 month	11.2±0.2*	12.4±0.2	8.2±0.2	8.1±0.1	36.2±7.0*	52.4±7.2
4 month	11.0±0.2*	12.5±0.3	8.2±0.3	8.2±0.2	34.2±7.8*	52.8±8.2
6 month	11.0±0.3*	12.3±0.2	8.2±0.2	8.2±0.3	34.4±7.2*	50.1±7.6

B.

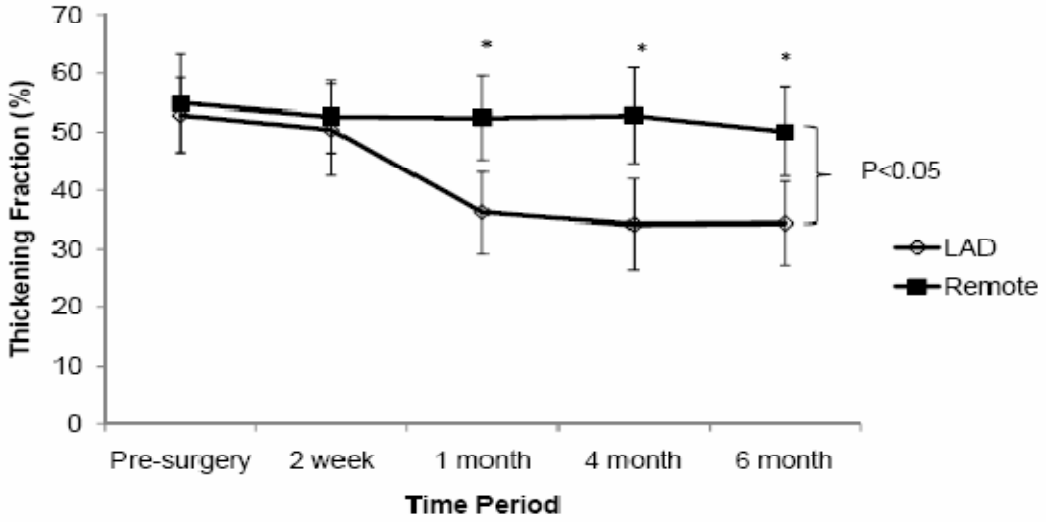

Fig. 4

A.

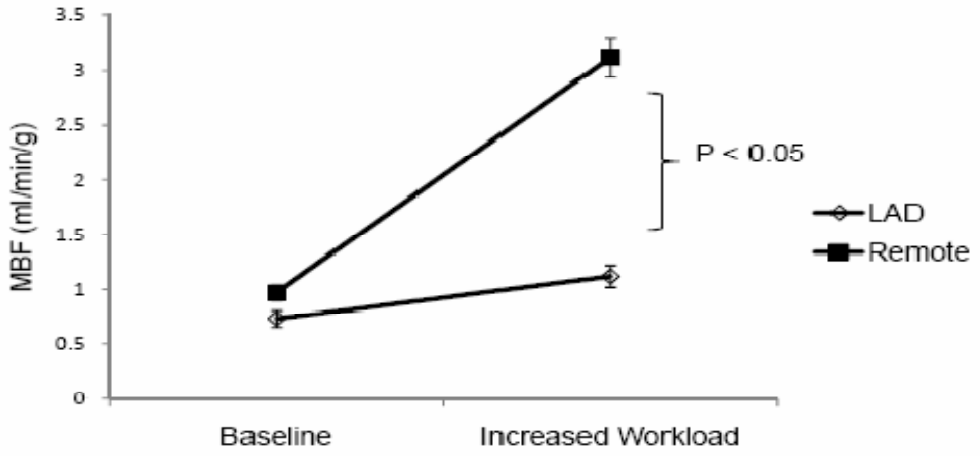
MBF (ml/min/g)
3.5
3
2.5
2
1.5
1
0.5
0
P < 0.05
LAD
Remote
Baseline
Increased Workload

B.

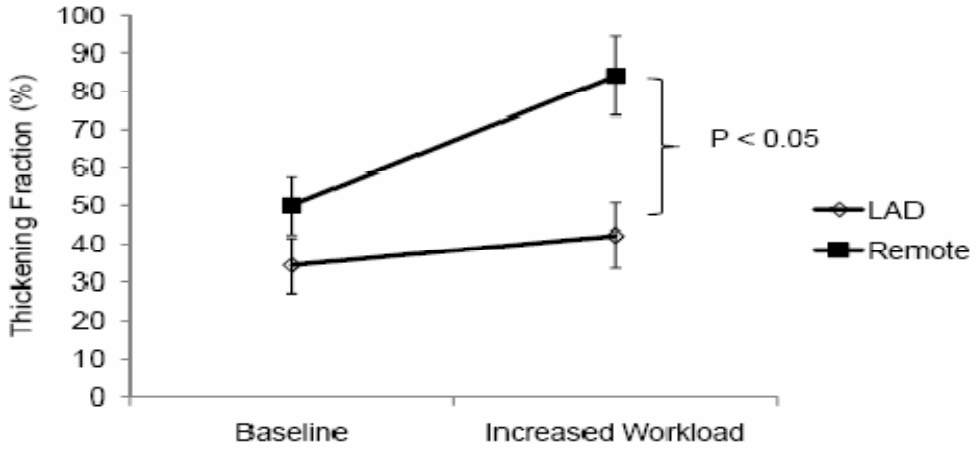
Thickening Fraction (%)
100
90
80
70
60
50
40
30
20
10
0
P < 0.05
LAD
Remote
Baseline
Increased Workload

CHAPTER 6: ATP SENSITIVE K^+ CHANNELS ARE CRITICAL FOR MAINTAINING MYOCARDIAL PERFUSION AND HIGH ENERGY PHOSPHATES IN THE FAILING HEART

Mohammad N Jameel, MD, Qinglu Li, BS, Abdul Mansoor, MD, PhD, Xiong Qiang, MS, Robert Bache, MD, Jianyi Zhang, MD, PhD.

Congestive heart failure (CHF) is associated with intrinsic alterations in mitochondrial oxidative phosphorylation which are independent of ischemia and manifest as an increase in myocardial cytosolic free ADP. ATP sensitive K^+ channels (K_{ATP}) act as metabolic sensors that are important for maintaining coronary blood flow (CBF) and in mediating the response of the myocardium to stress. Coronary adenosine receptors (AdR) are not normally active but cause vasodilation during myocardial ischemia. This study examined the myocardial energetic response to inhibition of K_{ATP} and AdR in CHF. CHF (as evidenced by LVEDP > 25 mmHg) was produced in adult mongrel dogs (n=12) by rapid ventricular pacing (220-250) for 4 weeks. CBF was measured with radiolabeled microspheres in open chest dogs during baseline (BL), AdR blockade with 8-Phenyltheophylline (8-PT; 5mg/kg iv) and K_{ATP} blockade with Glibenclamide (GLB; 20 μg/kg/min ic), while high energy phosphates were examined with ^{31}P magnetic resonance spectroscopy (MRS). Myocardial oxygenation was examined from the deoxymyoglobin signal using ^{1}H MRS (Mb-δ). During basal conditions Mb-δ was undetectable while phosphocreatine (PCr)/ATP (1.78±0.15) was significantly lower than in previously studied normal dogs (2.42±0.11). 8-PT caused a ≈ 21% increase in CBF (0.71±0.07 at BL *vs* 0.90±0.15 ml/min-g with 8-PT) with no change in PCr/ATP (1.65±0.17 with 8-PT *vs* 1.78±0.15 at BL, p=NS). GLB resulted in a 32.7±0.1% decrease in CBF (to 0.58±0.07 ml/min-g, p=0.02) that was associated with a decrease in PCr/ATP (1.11±0.11 with GLB *vs* 1.65±0.17 with 8-PT, p<0.0001). The pseudo-first-order rate constant of ATP

production via CK (k_f) did not change during GLB. However, the ATP production rate via CK was reduced by 35±0.08% during GLB, and this was accompanied by a significant increase in P_i/PCr and a Mb-δ signal indicating tissue hypoxia. Thus, in the failing heart without coronary artery disease, the balance between myocardial ATP demands (or oxygen demands) and delivery are critically dependent on functioning K_{ATP} channels but not AdR.

Introduction

ATP sensitive potassium (K_{ATP}) channels are present on the sarcolemma of coronary vascular smooth muscle cells and cardiac myocytes and on the mitochondrial inner membrane and play an important role in the cardiovascular system [141-144]. The opening of the K_{ATP} channels on vascular smooth muscle cells results in an outward flux of potassium causing hyperpolarization of the sarcolemma that subsequently closes voltage-dependent calcium channels, leading to a decreased influx of calcium, thereby causing vasodilation [145]. K_{ATP} channel activity is modulated by metabolic signals, with an increase in ADP/ATP ratio near the sarcolemma, acidosis, and hypoxia all directly activating K_{ATP} channels [146]. Intracoronary glibenclamide (inhibitor of K_{ATP} channels) in doses of 10–50 $\mu g \cdot kg^{-1} \cdot min^{-1}$ causes coronary vasoconstriction with a 20–55% decrease in basal coronary blood flow (CBF) in open-chest dogs or awake resting dogs, resulting in reduced coronary venous oxygen tension at a given level of myocardial oxygen consumption (MVO_2) [147-150]. The decrease in CBF produced by K_{ATP} channel blockade is associated with a decrease in regional systolic wall thickening [147-149]. We have previously shown that the decrease in CBF produced by glibenclamide causes a decrease in PCr/ATP and an increase in inorganic phosphate that is associated with a prominent deoxymyoglobin resonance which is substantially greater than when a similar decrease of coronary flow was produced by a stenosis [61]. These findings

suggested that reduction of CBF with an arterial stenosis was associated with a decrease of myocardial energy demands and that this response to hypoperfusion was inhibited by K_{ATP} channel blockade [61]. Mitochondrial K_{ATP} channels mediate cardioprotection presumably by mediating K^+ influx along mitochondrial inner membrane potential ($\Delta\Psi m$) and causing a decrease in $\Delta\Psi m$, matrix swelling and regulation of reactive oxygen species (ROS) generation [151]. We have previously shown that glibenclamide decreases MVO_2 by a decrease in CBF and oxygen availability rather than due to a primary reduction of mitochondrial respiration [61, 152].

Adenosine is a potent vasodilator, but it does not participate in regulation of coronary flow under physiological conditions [153]. However, adenosine does contribute to coronary vasodilation when there is an insufficient supply of oxygen [154]. Thus, adenosine receptor blockade with intravenous 8-phenyltheophylline caused a decrease in the total volume of excess flow during reactive hyperemia following a brief total coronary artery occlusion in dogs [153].

Congestive Heart Failure (CHF) is associated with a decrease in CBF that is matched to a decrease in MVO_2 suggesting a down-regulation of energy utilization [60]. K_{ATP} channel blockade with intracoronary glibenclamide resulted in a decrease in CBF and MVO_2 without a change in the relationship between CBF and MVO_2 in CHF animals [62]. On the other hand, adenosine receptor

blockade in CHF caused a significant increase in CBF that occurred secondary to an increase in MVO_2 [62].

Our group has studied high energy phosphate metabolism in animals with congestive heart failure using in vivo NMR spectroscopy [51, 131, 155]. This has revealed significant bioenergetic abnormalities in animals with CHF which are characterized by a lower ATP, CP, creatine and PCr/ATP ratio [51, 131, 155]. The myocardial calculated free ADP levels were also significantly increased in CHF hearts [51, 131, 155]. The increase in myocardial free ADP is associated with reductions in mitochondrial F0F1-ATPase protein expression[51]. CK-M and CK-mito protein levels were decreased along with significant decreases in CK flux rate [51, 131, 155]. Furthermore, in CHF hearts, the low basal PCr/ATP occurred in the absence of myocardial hypoxia, indicating that the HEP abnormalities were not the result of insufficient oxygen availability [51, 131, 155].

The aim of the present study was to investigate the bioenergetic response to K_{ATP} channel blockade and adenosine receptor blockade in animals with pacing induced heart failure using in vivo NMR spectroscopy.

Methods

All experiments were performed in accordance with the animal use guidelines of the University of Minnesota, and the experimental protocol was approved by the University of Minnesota Research Animal Resources Committee. The investigation conformed to the *"Guide for the care and use of laboratory animals"* published by the National Institutes of Health (NIH publication No 85-23, revised 1985).

Surgical Instrumentation and Production of CHF

Studies were performed in 12 adult mongrel dogs of either sex weighing 20-27 kg. CHF was produced by rapid ventricular pacing in 6 adult mongrel dogs as previously described [60, 62]. Briefly, animals were premedicated with acepromazine (10 mg IM), anesthetized with sodium pentobarbital (30 to 35 mg/kg IV), intubated, and ventilated with room air supplemented with oxygen to maintain arterial blood gasses in the physiological range. A left thoracotomy was performed in the fifth intercostal space. A heparin-filled polyvinyl chloride catheter (3.0 mm OD) was introduced into the internal thoracic artery and advanced until the tip was positioned in the ascending aorta. The pericardium was opened, and the heart was suspended in a pericardial cradle. A second catheter was placed into the left atrium through the atrial appendage and secured with a purse-string

suture. A similar catheter was introduced into the right atrium, manipulated into the coronary sinus ostium, and advanced until the catheter tip could be palpated in the great cardiac vein at the origin of the anterior interventricular vein to permit venous blood sampling from the myocardial region perfused by the left anterior descending coronary artery (LAD). A fluid-filled catheter and a high-fidelity Konigsberg micromanometer were placed in the left ventricle at the apex and secured in place. The proximal LAD was dissected free, and a Doppler velocity probe (Craig Hartley) was placed around the vessel. A heparin-filled silicone rubber catheter (0.75 mm ID) was introduced into the artery distal to the occluder [156]. Finally, a unipolar epicardial pacing lead (Medtronic Inc) was screwed into the right ventricle, and the pericardium was then loosely closed. All catheters and electrical leads were tunneled subcutaneously to exit at the base of the neck. The thoracotomy was closed in layers and evacuated of air. A programmable pacing generator modified to allow rapid pacing (Medtronic 5385) was placed in a subcutaneous pocket in the lateral chest wall and connected to the pacing lead. Catheters were flushed daily with heparin to maintain patency and were protected with a nylon vest. One week after surgery the pacemaker was activated at 220 bpm. This rate was continued or increased to 250 bpm if evidence of CHF was not present within 3 weeks. Resting hemodynamics and CBF were assessed weekly in normal sinus rhythm 1 hour after the pacemaker was deactivated. CHF was deemed to have developed when LV end-diastolic pressure was > 25mmHG.

Experimental preparation for MRS study.

Detailed surgical preparations for MRS study are published previously [56, 77, 91]. Briefly, the dogs were anesthetized with sodium pentobarbital (30-35 mg/kg bolus followed by 4 mg/kg/hr, i.v.), intubated and ventilated with a respirator with supplemental oxygen to maintain arterial blood gases within the physiologic range. A heparin-filled polyvinyl chloride catheter, 3.0 mm o.d., was introduced into the right femoral artery and advanced into the ascending aorta. A left thoracotomy was performed through the fourth intercostal space and the heart suspended in a pericardial cradle. A heparin-filled catheter (3.0 mm o.d.) was introduced into the left ventricle through the apical dimple and secured with a purse string suture. A similar catheter was inserted into the left atrium through the atrial appendage. A home made intra-cardiac vein catheter (0.3 mm o.d) was inserted directly into the great cardiac vein for coronary vein blood sampling. The region of the left ventricle that became cyanotic upon inflation of the LAD occluder was determined by visual inspection and a 28 mm diameter MRS surface coil was sutured onto the pericardium overlying the ischemic area. The pericardial cradle was then released and the heart allowed to assume its normal position. The surface coil leads were connected to a balanced tuned circuit and the animals were placed in the magnet.

MRS spectroscopy-general methods

Measurements were performed in a 40 cm bore 4.7 Tesla magnet interfaced with a SISCO (Spectroscopy Imaging Systems Corporation, Fremont, CA) console. The left ventricular pressure signal was used to gate MRS data acquisition to the cardiac cycle, while respiratory gating was achieved by triggering the ventilator to the cardiac cycle between data acquisitions [157-158]. ^{31}P and ^{1}H-MRS frequencies were 81 MHz and 200.1 MHz, respectively.

MRS deoxy-myoglobin methods.

^{1}H NMR methods have been previously reported in detail [54, 92]. The method for ^{1}H-MRS detection of the proximal histidyl N-δ proton resonance of Mb-δ has also been described [159]. Briefly, a single-pulse collection sequence with a Gaussian pulse (1 ms) was used to selectively excite the N-δ proton signal of the proximal histidyl of Mb-δ. This frequency selective pulse provided sufficient water suppression due to the large chemical shift difference between the water resonance and Mb-δ (>14 kHz). A short repetition time (TR=35 ms) was used due to the short T_1 value of Mb-δ. Each spectrum is acquired within 6 min (10,000 FID). Although the short T_1 of Mb-δ and the fast acquisition prevent gating of data acquisition to the cardiac cycle, signal loss as a result of heart motion was negligible because of the inherently broad line width of the Mb-δ

peak. Although the Mb-δ resonance is temperature sensitive, the chemical shift of this resonance which appeared at 71-72 ppm (relative to H_2O), remained virtually constant during the study protocol. No other resonances were detected within a 10 ppm region. In phantom studies we have established that the detection sensitivity for Mb-δ is essentially flat across the wall of the left ventricle. Therefore, the Mb-δ resonance reflects average whole wall Mb-δ without the need for correction for differences in sensitivity in the deeper myocardial layers as is the case for HEP measurements (see below).

Spatially localized ^{31}P MRS technique.

^{31}P MR spectra were acquired in late diastole with a pulse repetition time of 6-7 seconds. This repetition time allowed full relaxation for ATP and Pi resonances, and approximately 90% relaxation for the PCr resonance. PCr resonance intensities were corrected for this minor saturation. RF transmission and signal detection were performed with a 28 mm diameter surface coil. A capillary containing 15 µl of 3M phosphonoacetic acid was placed at the coil center to serve as a reference. The proton signal of the water resonance was used to homogenize the magnetic field and to adjust the position of the animal in the magnet so that the coil was at or near the magnet and gradient isocenter. This was accomplished using a spin-echo experiment with a readout profile. The information gathered in this step was also utilized to determine the spatial

coordinates for spectroscopic localization. Chemical shifts were measured relative to PCr which was assigned a chemical shift of -2.55 ppm relative to 85% phosphoric acid at 0 ppm. Spatial localization across the left ventricular wall was performed with the RAPP-ISIS/FSW method. The technical details of this method including voxel profiles, voxel volume, and the accuracy of spatial localization obtained in phantom studies and in vivo have been published elsewhere [158, 160-161]. Briefly, signal origin was restricted using B_0 gradients and adiabatic inversion pulses to an 18 mm x 18 mm column coaxial with the surface coil and perpendicular to the left ventricular wall. Within this volume, the signal was further localized using the B_1 gradient to 5 voxels spanning the left ventricular wall from epicardium to endocardium. Each set of spatially localized transmural spectra consisted of a total of 96 scans accumulated in a 10 minute block. Resonance intensities were quantified using integration routines provided by SISCO software. The values for PCr and ATP in each voxel were normalized to those present in the basal state and the PCr /ATP ratio was determined for each voxel. Pi resonances were also measured and ratio of Pi/ PCr was calculated.

The Mb-δ resonance detected using the present methodology represents an unweighted average of the Mb- δ content across the entire LV wall. A comparable whole wall measurement of HEP levels does not exist, because the sensitivity for detection of the phosphorus resonance decreases as a function of

distance from the surface coil. Therefore, average whole wall values of HEP were obtained by averaging the HEP contents in the subepicardial, midwall and subendocardial voxels that were acquired with our spatially localized spectroscopy technique [161]. This technique corrects voxel HEP content measurements for the decrease sensitivity which occurs with increasing distance from the surface coil, thereby yielding true average whole wall PCr and ATP contents.

Myocardial blood flow measurements

Myocardial blood flow was measured using radionuclide labeled microspheres, 15 μm in diameter labeled with 4 different radioisotopes (^{51}Cr, ^{85}Sr, ^{95}Nb and ^{46}Sc). Microsphere suspension containing $2x10^6$ microspheres was injected through the left atrial catheter while a reference sample of arterial blood was withdrawn from the aortic catheter at a rate 15 ml/min beginning 5 seconds before the microsphere injection and continuing for 120 seconds. Radioactivity in the myocardial and blood reference specimens was determined using a gamma spectrometer (Packard Instrument Company, Downers Grove, IL) at window settings chosen for the combination of radioisotopes used during the study. Activity corrected for overlap between isotopes and for background was used to compute blood flow as ml/g of myocardium/minute.

Study protocol.

Aortic and left ventricular pressures were measured with fluid filled pressure transducers positioned at mid-chest level and recorded on an 8-channel direct writing recorder (Coulbourne Instrument Company, Lehigh Valley, PA). Left ventricular pressure was recorded at normal and high gain for measurement of end-diastolic pressure. Hemodynamic measurements and ^{31}P and ^{1}H MRS spectra were first obtained under basal conditions. Midway through the 20 min data acquisition period, a microsphere injection was performed for determination of myocardial blood flow. After completion of baseline measurements, adenosine receptor blockade was produced by administration of 8-Phenyltheophylline (8-PT; 5mg/kg iv). This dose has been previously shown to produce >90% inhibition of the coronary vasodilator response to adenosine while causing minimal phosphodiesterase inhibition. Hemodynamic measurements and ^{31}P and ^{1}H MRS spectra were acquired under 8-PT infusion along with another microsphere injection. This was followed by intracoronary infusion glibenclamide at 20 μg/kg/min. After 10 minute was allowed to achieve steady state conditions, ^{31}P and ^{1}H MRS spectra.

Data analysis.

Hemodynamic data were measured from the chart recordings. ^{31}P spectra were analyzed as described above. Transmural blood flow distribution was determined from the microsphere measurements. Data were analyzed with one-way analysis of variance for repeated measures. A value of $p<0.05$ was considered significant. When a significant result was found, individual comparisons were made using the method of Sheffé.

Results

Hemodynamic Data

Rapid ventricular pacing resulted in heart failure in all the dogs with a documented LV end-diastolic pressure of greater than 25 mmHg. Hemodynamic measurements during each experimental condition in anaesthetized dogs are shown in Table 1. At baseline, these heart failure dogs had a lower mean aortic pressure, lower LV systolic pressure and higher LV end-diastolic pressure as compared with normal dogs previously studied in our laboratory [61]. Infusion of 8-PT resulted in a significant increase in heart rate and consequently higher rate pressure product. Infusion of glibenclamide caused no further change in heart rate, mean aortic pressure or LV systolic pressure but increased LV end-diastolic

pressure from 19±2 to 29±2 mmHg ($p<0.05$), suggesting a deterioration in LV function as previously demonstrated in normal dogs after K+ATP channel blockade [61].

Myocardial Blood Flow

Table 2 summarizes the myocardial blood flow (MBF) data under different experimental conditions. Resting mean MBF was 0.71±0.07 ml/min-g with a subendocardial-to-subepicardial ratio of 1.17±0.08. Adenosine receptor blockade caused an approximately 21% increase in mean MBF (0.71±0.07 at BL *vs* 0.90±0.15 ml/min-g with 8-PT, $p<0.05$) with no change in the transmural gradient. On the other hand, subsequent K+ATP channel blockade resulted in a 32.7±0.1% decrease in MBF (0.90±0.15 ml/min-g with 8-PT *vs* 0.58±0.07 ml/min-g with 8-PT+GLIB, $p<0.05$). The reduction of blood flow produced by glibenclamide was more pronounced in the subepicardium than in the subendocardium resulting in a significant increase in the subendocardial-to-subepicardial ratio from 1.13±0.14 to 1.42±0.15 ($p<0.05$). This is in contrast to previously studied dogs with coronary occlusion in which the decrease in MBF is most marked in the subendocardium with a decrease in the subendocardial-to-subepicardial flow ratio [61].

Transmural Myocardial High Energy Phosphates and Oxygenation

Spectra obtained during baseline conditions demonstrated prominent resonances corresponding to PCr and the three phosphates of ATP, whereas P_i was below the limit of detectability. Transmural high energy phosphate levels during different experimental conditions are depicted in Table 3. The PCr/ATP ratio during baseline conditions was 1.78±0.15 with the subendocardial layer showing the lowest ratio. This was significantly lower than previously studied normal dogs (2.42±0.11) and was not the result of ischemia as no deoxymyoglobin (Mb-δ) was detected. Adenosine receptor blockade caused no significant change in the PCr/ATP ratio despite an increase in myocardial blood flow. However, glibenclamide resulted in a significant decrease of PCr but no change of ATP, resulting in a significant decrease in the PCr/ATP ratio (1.11±0.11 with 8-PT+GLIB *vs* 1.65±0.17 with 8-PT, $p<0.05$). The transmural gradient was maintained with the subendocardium showing the worst energetic state despite a more prominent decrease in blood flow in the subepicardium. This was accompanied by a significant increase in ΔP_i/PCr and appearance of Mb-δ signal indicating tissue hypoxia.

Creatine Kinase Flux

The Creatine Kinase kinetics data is depicted in Table 4. The pseudo-first-order rate constant of ATP production via CK (k_f) did not change during either adenosine receptor or K+ATP channel blockade. However, the ATP production rate via CK was reduced by 35±0.08% during K+ATP channel blockade (Normalized CK flux rate with 8-PT was 1.13±0.26 *vs* 0.73±0.08 with 8-PT+GLIB, $p<0.05$).

Discussion

This is the first report examining the effect of adenosine and K+ATP channel blockade on myocardial energetics in the failing heart. We demonstrate that adenosine receptor blockade did not improve myocardial energetics in the failing heart despite an increase in myocardial blood flow. On the other hand, K+ATP channel blockade in the failing heart is associated with a significant decreases in the PCr/ATP ratio and the ATP production rate via CK which is associated with a decrease in myocardial blood flow and tissue hypoxia. Thus, in failing hearts without coronary artery disease, the balance between myocardial ATP demands (or oxygen demands) and delivery are critically dependent on functioning K_{ATP} channels but not on adenosine receptors.

Myocardial Energetics in Heart Failure

Our results confirm our previous findings that heart failure is associated with a decrease in PCr/ATP ratio that is not the result of ischemia [51, 131, 155]. It has been shown that this decrease in PCr/ATP ratio is associated with a decrease in CK flux [51, 131, 155] and change in substrate utilization with decreased fatty acid oxidation [162].

Adenosine Receptor Blockade in Heart Failure

We have previously shown that in the failing heart adenosine receptor blockade causes an increase in myocardial blood flow that appears to be secondary to an increase in myocardial oxygen consumption [62]. However, 8-PT did not alter the relationship between myocardial oxygen consumption and coronary venous pO_2, implying that it did not alter metabolic signaling between myocardial myocytes and the coronary resistance vessels [62]. The present study confirms our previous report of an increase in MBF with adenosine receptor blockade. More importantly, it shows that 8-PT did not have any impact on myocardial energetics, supporting the notion that adenosine receptors do not play a role in maintaining the metabolic balance between myocardial ATP demands (or oxygen demands) and delivery in the failing heart.

K+ATP channel blockade in Heart failure

We have previously shown that in normal animals K_{ATP} channel blockade inhibits the decrease in myocardial energy demands in response to hypoperfusion [61]. Our present study demonstrates that glibenclamide results in a significant reduction in PCr/ATP ratio and ATP production rate in failing hearts that is associated with tissue hypoxia. This is probably related to an inability to decrease myocardial oxygen consumption in response to a decrease in blood flow. This implies that K_{ATP} channels play a pivotal role in maintaining the balance between ATP demand and delivery in the failing hearts.

Conclusion

K_{ATP} channels but not adenosine receptors are important in maintaining the balance between oxygen delivery and demand in the failing heart.

Table 1. Hemodynamic Data

	HR (Beats/min)	MAP (mmHg)	LVSP (mmHg)	LVEDP (mmHg)	RPP (Beats.mmHg. min^{-1} $x10^{-3}$)
Baseline	102±8	82±4	102±5	19±2	10.4±0.8
8-PT	120±10*	88±7	104±6	20±2	12.6±1.3*
8-PT + GLIB	121±11*	86±8	100±7	29±2*†	12.2±1.1*

Values are means ± SE. 8-PT, 8-Phenyltheophylline at 5mg/kg intravenous; GLIB, Glibenclamide at 20 μg/kg/min intracoronary; HR, Heart rate; MAP, Mean Aortic Pressure; LVSP, Left ventricular systolic pressure; LVEDP, Left ventricular end-diastolic pressure; RPP, rate pressure product; *, $p<0.05$ vs. baseline; †, $p<0.05$ vs. 8-PT.

Table 2. Myocardial Blood Flow

	EPI	MID	ENDO	Mean	Endo/Epi
Baseline	0.64±0.07	0.75±0.08	0.74±0.08	0.71±0.07	1.17±0.08
8-PT	0.83±0.12*	0.92±0.17*	0.94±0.18*	0.90±0.15*	1.13±0.14
8-PT+GLIB	0.47±0.05*†	0.63±0.11†	0.65±0.08†	0.58±0.07*†	1.42±0.15†

Values are means ± SE. 8-PT, 8-Phenyltheophylline at 5mg/kg intravenous; GLIB, Glibenclamide at 20 µg/kg/min intracoronary; EPI, subepicardium; MID, midmyocardium; ENDO, subendocardium; *, $p<0.05$ vs. baseline; †, $p<0.05$ vs. 8-PT.

Table 3: Myocardial high-energy phosphate levels

	PCr/ATP			ΔPi/PCr	Normalized PCr	Normalized ATP
	EPI	ENDO	Mean	Mean	Mean	Mean
Baseline	1.90±0.14	1.62±0.15	1.78±0.15	0	1	1
8-PT	1.68±0.12	1.36±0.11	1.65±0.17	0	0.92±0.06	0.99±0.08
8-PT +GLIB	1.34±0.06*†	0.81±0.23*†	1.11±0.15*†	0.63±0.26*†	0.65±0.09*†	1.02±0.09

Values are means ± SE. 8-PT, 8-Phenyltheophylline at 5mg/kg intravenous; GLIB, Glibenclamide at 20 μg/kg/min intracoronary; Pi, Inorganic phosphate; PCr, Phosphocreatine; ATP, Adenosine Triphosphate; EPI, subepicardium; ENDO, subendocardium; *, $p<0.05$ vs. baseline; †, $p<0.05$ vs. 8-PT.

Table 4. Creatine Kinase Kinetics

	ΔM/M	Tau (sec)	T1 (sec)	k_f (sec^{-1})	Normalized CK flux rate
Baseline	0.64±0.07	1.37±0.12	4.33±0.84	0.47±0.06	1
8-PT	0.62±0.07	1.17±0.14	3.28±0.37	0.58±0.14	1.13±0.26
8-PT+GLIB	0.66±0.06	1.47±0.07	4.55±0.82	0.48±0.04	0.73±0.08*

Values are means ± SE. 8-PT, 8-Phenyltheophylline at 5mg/kg intravenous; GLIB, Glibenclamide at 20 μg/kg/min intracoronary; ΔM/M, relative change of PCr resonance intensity; Tau, time constant that fits the integral of PCr magnetization decay as the time of saturation of ATPγ increased from 0 to infinite; T1, longitudinal relaxation time; k_f, forward rate constant of creatine kinase; *, $p<0.05$ vs. baseline.

CHAPTER 7: CONCLUSIONS

In the current thesis, we demonstrated that trans-coronary artery injection of bone marrow derived multiprogenitor cells in a clinically relevant porcine model of ischemia/reperfusion is safe, feasible and effective. Stem cell transplantation resulted in improvement of ventricular function at 4 weeks after myocardial infarction. Cell transplantation was associated with an increase in vascular density, inhibition of apoptosis and reduction of infarct size, which was accompanied by improvement in border zone and infarct zone contractile function, with consequent improvement in myocardial bioenergetics and global LV function. These functional beneficial effects were observed despite a low engraftment of stem cells at 4 weeks. In vitro, the stem cells significantly inhibited TNFα induced mitochondrial membrane potential change and cytochrome C release from myocytes. Additionally, coculture of stem cells with HL-1 cells inhibited TNFα induced apoptosis. Thus, the beneficial effects of stem cell transplantation are most likely related to the “trophic effects” of cells on the host myocardium, which include promotion of angiogenesis, maintenance of mitochondrial integrity, and inhibition of apoptosis of ischemia threatened and overstretched myocytes in the border zone myocardium.

In subsequent experiments, we demonstrated that stem cell transplantation leads to long term functional and bioenergetic improvement in a clinically relevant

porcine model of postinfarction LV remodeling despite no significant engraftment of cells at 4 months in the heart. Stem cell transplantation resulted in a decrease in LV hypertrophy and amelioration of LV dilatation. This was associated with a reduction in scar size at 4 months. Cell transplantation also resulted in long term differential expression of genes which included a downregulation of mitochondrial oxidative enzymes and upregulation of MEF2a and ZFP91. Thus, stem cell transplantation reduces regional wall stresses and infarct size and mitigates the adverse effects of LV remodeling as seen by a reduction in LV hypertrophy and LV dilatation and is associated with differential expression of genes relating to metabolism and apoptosis.

We have also created a model of chronic hibernation in mini-pigs by placing a titanium c-shaped occluder device over the proximal LAD and described the longest follow up of experimental chronic hibernation in a pre-clinical large animal model. These studies utilized cardiac MRI to demonstrate the temporal changes in blood flow and regional function in hibernating myocardium to elucidate the exact timing of development of the phenomenon of hibernating myocardium in these animals. More importantly, we concluded that the myocardial energetic state as reflected by PCr/ATP ratio, is normal under baseline conditions up to 6 months in hibernating myocardium despite a reduction in perfusion reserve and regional function. Furthermore, the decrease in PCr/ATP ratio with increased workload in hibernating myocardium is similar to normal myocardium. This is

probably related to an intrinsic down-regulation in the mitochondrial function which minimizes oxidative stress and leads to a balanced supply and demand at baseline and increased work load.

Finally, we examined the effect of adenosine and K+ATP channel blockade on myocardial energetic in the failing heart. We demonstrate that adenosine receptor blockade has no effect on myocardial energetics in the failing heart despite an increase in myocardial blood flow. On the other hand, K+ATP channel blockade in the failing heart is associated with a significant decrease in the PCr/ATP ratio and ATP production rate via CK which is associated with a decrease in myocardial blood flow and tissue hypoxia. Thus, in failing hearts without coronary artery disease, the balance between myocardial ATP demands (or oxygen demands) and delivery are critically dependent on functioning K_{ATP} channels but not adenosine receptors.

BIBLIOGRAPHY

1. Weir, R.A. and J.J. McMurray, *Epidemiology of heart failure and left ventricular dysfunction after acute myocardial infarction.* Curr Heart Fail Rep, 2006. **3**(4): p. 175-80.
2. Anversa, P. and B. Nadal-Ginard, *Myocyte renewal and ventricular remodelling.* Nature, 2002. **415**(6868): p. 240-3.
3. Ferrari, G., et al., *Muscle regeneration by bone marrow-derived myogenic progenitors.* Science, 1998. **279**(5356): p. 1528-30.
4. Krause, D.S., et al., *Multi-organ, multi-lineage engraftment by a single bone marrow-derived stem cell.* Cell, 2001. **105**(3): p. 369-77.
5. Mezey, E., et al., *Turning blood into brain: cells bearing neuronal antigens generated in vivo from bone marrow.* Science, 2000. **290**(5497): p. 1779-82.
6. Bittner, R.E., et al., *Recruitment of bone-marrow-derived cells by skeletal and cardiac muscle in adult dystrophic mdx mice.* Anat Embryol (Berl), 1999. **199**(5): p. 391-6.
7. Jackson, K.A., et al., *Regeneration of ischemic cardiac muscle and vascular endothelium by adult stem cells.* J Clin Invest, 2001. **107**(11): p. 1395-402.
8. Orlic, D., et al., *Bone marrow cells regenerate infarcted myocardium.* Nature, 2001. **410**(6829): p. 701-5.
9. Murry, C.E., et al., *Haematopoietic stem cells do not transdifferentiate into cardiac myocytes in myocardial infarcts.* Nature, 2004. **428**(6983): p. 664-8.

10. Balsam, L.B., et al., *Haematopoietic stem cells adopt mature haematopoietic fates in ischaemic myocardium.* Nature, 2004. **428**(6983): p. 668-73.

11. Rota, M., et al., *Bone marrow cells adopt the cardiomyogenic fate in vivo.* Proc Natl Acad Sci U S A, 2007. **104**(45): p. 17783-8.

12. Caplan, A.I., *Mesenchymal stem cells.* J Orthop Res, 1991. **9**(5): p. 641-50.

13. Prockop, D.J., *Marrow stromal cells as stem cells for nonhematopoietic tissues.* Science, 1997. **276**(5309): p. 71-4.

14. Phinney, D.G., et al., *Donor variation in the growth properties and osteogenic potential of human marrow stromal cells.* J Cell Biochem, 1999. **75**(3): p. 424-36.

15. Pittenger, M.F., et al., *Multilineage potential of adult human mesenchymal stem cells.* Science, 1999. **284**(5411): p. 143-7.

16. Pittenger, M.F. and B.J. Martin, *Mesenchymal stem cells and their potential as cardiac therapeutics.* Circ Res, 2004. **95**(1): p. 9-20.

17. Majumdar, M.K., et al., *Characterization and functionality of cell surface molecules on human mesenchymal stem cells.* J Biomed Sci, 2003. **10**(2): p. 228-41.

18. Haynesworth, S.E., M.A. Baber, and A.I. Caplan, *Cell surface antigens on human marrow-derived mesenchymal cells are detected by monoclonal antibodies.* Bone, 1992. **13**(1): p. 69-80.

19. Alhadlaq, A. and J.J. Mao, *Mesenchymal stem cells: isolation and therapeutics.* Stem Cells Dev, 2004. **13**(4): p. 436-48.

20. Minguell, J.J., A. Erices, and P. Conget, *Mesenchymal stem cells.* Exp Biol Med (Maywood), 2001. **226**(6): p. 507-20.

21. Fukuda, K., *Molecular characterization of regenerated cardiomyocytes derived from adult mesenchymal stem cells.* Congenit Anom (Kyoto), 2002. **42**(1): p. 1-9.

22. Makino, S., et al., *Cardiomyocytes can be generated from marrow stromal cells in vitro.* J Clin Invest, 1999. **103**(5): p. 697-705.

23. Fukuda, K., *Use of adult marrow mesenchymal stem cells for regeneration of cardiomyocytes.* Bone Marrow Transplant, 2003. **32 Suppl 1**: p. S25-7.

24. Tomita, S., et al., *Bone marrow stromal cells contract synchronously with cardiomyocytes in a coculture system.* Jpn J Thorac Cardiovasc Surg, 2002. **50**(8): p. 321-4.

25. Hakuno, D., et al., *Bone marrow-derived regenerated cardiomyocytes (CMG Cells) express functional adrenergic and muscarinic receptors.* Circulation, 2002. **105**(3): p. 380-6.

26. Bartholomew, A., et al., *Mesenchymal stem cells suppress lymphocyte proliferation in vitro and prolong skin graft survival in vivo.* Exp Hematol, 2002. **30**(1): p. 42-8.

27. Le Blanc, K., et al., *Mesenchymal stem cells inhibit and stimulate mixed lymphocyte cultures and mitogenic responses independently of the major histocompatibility complex.* Scand J Immunol, 2003. **57**(1): p. 11-20.

28. Tse, W.T., et al., *Suppression of allogeneic T-cell proliferation by human marrow stromal cells: implications in transplantation.* Transplantation, 2003. **75**(3): p. 389-97.

29. Zimmet, J.M. and J.M. Hare, *Emerging role for bone marrow derived mesenchymal stem cells in myocardial regenerative therapy.* Basic Res Cardiol, 2005. **100**(6): p. 471-81.

30. Ryan, J.M., et al., *Mesenchymal stem cells avoid allogeneic rejection.* J Inflamm (Lond), 2005. **2**: p. 8.

31. Le Blanc, K., et al., *HLA expression and immunologic properties of differentiated and undifferentiated mesenchymal stem cells.* Exp Hematol, 2003. **31**(10): p. 890-6.

32. Di Nicola, M., et al., *Human bone marrow stromal cells suppress T-lymphocyte proliferation induced by cellular or nonspecific mitogenic stimuli.* Blood, 2002. **99**(10): p. 3838-43.

33. Wang, J.S., et al., *The coronary delivery of marrow stromal cells for myocardial regeneration: pathophysiologic and therapeutic implications.* J Thorac Cardiovasc Surg, 2001. **122**(4): p. 699-705.

34. Tomita, S., et al., *Autologous transplantation of bone marrow cells improves damaged heart function.* Circulation, 1999. **100**(19 Suppl): p. II247-56.

35. Barbash, I.M., et al., *Systemic delivery of bone marrow-derived mesenchymal stem cells to the infarcted myocardium: feasibility, cell migration, and body distribution.* Circulation, 2003. **108**(7): p. 863-8.

36. Silva, G.V., et al., *Mesenchymal stem cells differentiate into an endothelial phenotype, enhance vascular density, and improve heart function in a canine chronic ischemia model.* Circulation, 2005. **111**(2): p. 150-6.

37. Dai, W., et al., *Allogeneic mesenchymal stem cell transplantation in postinfarcted rat myocardium: short- and long-term effects.* Circulation, 2005. **112**(2): p. 214-23.

38. Tomita, S., et al., *Improved heart function with myogenesis and angiogenesis after autologous porcine bone marrow stromal cell transplantation.* J Thorac Cardiovasc Surg, 2002. **123**(6): p. 1132-40.

39. Assmus, B., et al., *Transplantation of Progenitor Cells and Regeneration Enhancement in Acute Myocardial Infarction (TOPCARE-AMI).* Circulation, 2002. **106**(24): p. 3009-17.

40. Schachinger, V., et al., *Transplantation of progenitor cells and regeneration enhancement in acute myocardial infarction: final one-year results of the TOPCARE-AMI Trial.* J Am Coll Cardiol, 2004. **44**(8): p. 1690-9.

41. Wollert, K.C., et al., *Intracoronary autologous bone-marrow cell transfer after myocardial infarction: the BOOST randomised controlled clinical trial.* Lancet, 2004. **364**(9429): p. 141-8.

42. Schachinger, V., et al., *Intracoronary bone marrow-derived progenitor cells in acute myocardial infarction.* N Engl J Med, 2006. **355**(12): p. 1210-21.

43. Lunde, K., et al., *Intracoronary injection of mononuclear bone marrow cells in acute myocardial infarction.* N Engl J Med, 2006. **355**(12): p. 1199-209.

44. Janssens, S., et al., *Autologous bone marrow-derived stem-cell transfer in patients with ST-segment elevation myocardial infarction: double-blind, randomised controlled trial.* Lancet, 2006. **367**(9505): p. 113-21.

45. Seeger, F., et al., *Cell isolation procedures matter: A comparison of different isolation protocols of bone marrow mononuclear cells used for cell therapy in patients with acute myocardial infarction.* Circulation, 2006. **114**(18): p. II-51.

46. Assmus, B., et al., *Transcoronary transplantation of progenitor cells after myocardial infarction.* N Engl J Med, 2006. **355**(12): p. 1222-32.

47. Chen, S.L., et al., *Improvement of cardiac function after transplantation of autologous bone marrow mesenchymal stem cells in patients with acute myocardial infarction.* Chin Med J (Engl), 2004. **117**(10): p. 1443-8.

48. Chen, S.L., et al., *Effect on left ventricular function of intracoronary transplantation of autologous bone marrow mesenchymal stem cell in patients with acute myocardial infarction.* Am J Cardiol, 2004. **94**(1): p. 92-5.

49. Zambrano, J., et al., *Abstract 1014: The Impact Of Intravenous Allogeneic Human Mesenchymal Stem Cells (ProvacelTM) On Ejection Fraction In Patients With Myocardial Infarction*. 2007. p. II_202-.

50. Zhang, J., et al., *Functional and bioenergetic consequences of postinfarction left ventricular remodeling in a new porcine model. MRI and 31 P-MRS study.* Circulation, 1996. **94**(5): p. 1089-100.

51. Liu, J., et al., *Mitochondrial ATPase and high-energy phosphates in failing hearts.* Am J Physiol Heart Circ Physiol, 2001. **281**(3): p. H1319-26.

52. Hoang, C.D., et al., *Post-infarction left ventricular remodeling induces changes in creatine kinase mRNA and protein subunit levels in porcine myocardium.* Am J Pathol, 1997. **151**(1): p. 257-64.

53. Murakami, Y., et al., *Myocardial creatine kinase kinetics in hearts with postinfarction left ventricular remodeling.* Am J Physiol, 1999. **276**(3 Pt 2): p. H892-900.

54. Murakami, Y., et al., *Myocardial oxygenation during high work states in hearts with postinfarction remodeling.* Circulation, 1999. **99**(7): p. 942-8.

55. Gourine, A.V., et al., *Interstitial purine metabolites in hearts with LV remodeling.* Am J Physiol Heart Circ Physiol, 2004. **286**(2): p. H677-84.

56. Hu, Q., et al., *Profound bioenergetic abnormalities in peri-infarct myocardial regions.* Am J Physiol Heart Circ Physiol, 2006. **291**(2): p. H648-57.

57. Feygin, J., et al., *Relationships between regional myocardial wall stress and bioenergetics in hearts with left ventricular hypertrophy.* Am J Physiol Heart Circ Physiol, 2008. **294**(5): p. H2313-21.

58. Remondino, A., et al., *Altered expression of proteins of metabolic regulation during remodeling of the left ventricle after myocardial infarction.* J Mol Cell Cardiol, 2000. **32**(11): p. 2025-34.

59. Rosenblatt-Velin, N., et al., *Postinfarction heart failure in rats is associated with upregulation of GLUT-1 and downregulation of genes of fatty acid metabolism.* Cardiovasc Res, 2001. **52**(3): p. 407-16.

60. Traverse, J.H., et al., *Regulation of myocardial blood flow by oxygen consumption is maintained in the failing heart during exercise.* Circ Res, 1999. **84**(4): p. 401-8.

61. Zhang, J., et al., *Myocardial oxygenation and high-energy phosphate levels during KATP channel blockade.* Am J Physiol Heart Circ Physiol, 2003. **285**(4): p. H1420-7.

62. Traverse, J.H., et al., *Effect of K+ATP channel and adenosine receptor blockade during rest and exercise in congestive heart failure.* Circ Res, 2007. **100**(11): p. 1643-9.

63. Rahimtoola, S.H., *A perspective on the three large multicenter randomized clinical trials of coronary bypass surgery for chronic stable angina.* Circulation, 1985. **72**(6 Pt 2): p. V123-35.

64. Rahimtoola, S.H., *The hibernating myocardium.* Am Heart J, 1989. **117**(1): p. 211-21.

65. Vanoverschelde, J.L., et al., *Mechanisms of chronic regional postischemic dysfunction in humans. New insights from the study of noninfarcted collateral-dependent myocardium.* Circulation, 1993. **87**(5): p. 1513-23.

66. Canty, J.M., Jr. and J.A. Fallavollita, *Resting myocardial flow in hibernating myocardium: validating animal models of human pathophysiology.* Am J Physiol, 1999. **277**(1 Pt 2): p. H417-22.

67. Canty, J.M., Jr. and J.A. Fallavollita, *Lessons from experimental models of hibernating myocardium.* Coron Artery Dis, 2001. **12**(5): p. 371-80.

68. Canty, J.M., Jr., et al., *Hibernating myocardium: chronically adapted to ischemia but vulnerable to sudden death.* Circ Res, 2004. **94**(8): p. 1142-9.

69. Fallavollita, J.A. and J.M. Canty, Jr., *Differential 18F-2-deoxyglucose uptake in viable dysfunctional myocardium with normal resting perfusion: evidence for chronic stunning in pigs.* Circulation, 1999. **99**(21): p. 2798-805.

70. Fallavollita, J.A., H. Lim, and J.M. Canty, Jr., *Myocyte apoptosis and reduced SR gene expression precede the transition from chronically stunned to hibernating myocardium.* J Mol Cell Cardiol, 2001. **33**(11): p. 1937-44.

71. Fallavollita, J.A., M. Logue, and J.M. Canty, Jr., *Stability of hibernating myocardium in pigs with a chronic left anterior descending coronary artery stenosis: absence of progressive fibrosis in the setting of stable reductions in flow, function and coronary flow reserve.* J Am Coll Cardiol, 2001. **37**(7): p. 1989-95.

72. Fallavollita, J.A., B.J. Malm, and J.M. Canty, Jr., *Hibernating myocardium retains metabolic and contractile reserve despite regional reductions in flow, function, and oxygen consumption at rest.* Circ Res, 2003. **92**(1): p. 48-55.

73. Fallavollita, J.A., B.J. Perry, and J.M. Canty, Jr., *18F-2-deoxyglucose deposition and regional flow in pigs with chronically dysfunctional myocardium. Evidence for transmural variations in chronic hibernating myocardium.* Circulation, 1997. **95**(7): p. 1900-9.

74. McFalls, E.O., et al., *Activation of p38 MAPK and increased glucose transport in chronic hibernating swine myocardium.* Am J Physiol Heart Circ Physiol, 2004. **287**(3): p. H1328-34.

75. McFalls, E.O., et al., *The energetic state within hibernating myocardium is normal during dobutamine despite inhibition of ATP-dependent potassium channel opening with glibenclamide.* Am J Physiol Heart Circ Physiol, 2007. **293**(5): p. H2945-51.

76. McFalls, E.O., et al., *Mitochondrial adaptations within chronically ischemic swine myocardium.* J Mol Cell Cardiol, 2006. **41**(6): p. 980-8.

77. Zeng, L., et al., *Bioenergetic and functional consequences of bone marrow-derived multipotent progenitor cell transplantation in hearts with postinfarction left ventricular remodeling.* Circulation, 2007. **115**(14): p. 1866-75.

78. Amado, L.C., et al., *Cardiac repair with intramyocardial injection of allogeneic mesenchymal stem cells after myocardial infarction.* Proc Natl Acad Sci U S A, 2005. **102**(32): p. 11474-9.

79. Linke, A., et al., *Stem cells in the dog heart are self-renewing, clonogenic, and multipotent and regenerate infarcted myocardium, improving cardiac function.* Proc Natl Acad Sci U S A, 2005. **102**(25): p. 8966-71.

80. Mangi, A.A., et al., *Mesenchymal stem cells modified with Akt prevent remodeling and restore performance of infarcted hearts.* Nat Med, 2003. **9**(9): p. 1195-201.

81. Noiseux, N., et al., *Mesenchymal stem cells overexpressing Akt dramatically repair infarcted myocardium and improve cardiac function despite infrequent cellular fusion or differentiation.* Mol Ther, 2006. **14**(6): p. 840-50.

82. Gnecchi, M., et al., *Paracrine action accounts for marked protection of ischemic heart by Akt-modified mesenchymal stem cells.* Nat Med, 2005. **11**(4): p. 367-8.

83. Gnecchi, M., et al., *Evidence supporting paracrine hypothesis for Akt-modified mesenchymal stem cell-mediated cardiac protection and functional improvement.* Faseb J, 2006. **20**(6): p. 661-9.

84. Mirotsou, M., et al., *Secreted frizzled related protein 2 (Sfrp2) is the key Akt-mesenchymal stem cell-released paracrine factor mediating myocardial survival and repair.* Proc Natl Acad Sci U S A, 2007. **104**(5): p. 1643-8.

85. Wang, X., et al., *Bioenergetic and functional consequences of stem cell-based VEGF delivery in pressure-overloaded swine hearts.* Am J Physiol Heart Circ Physiol, 2006. **290**(4): p. H1393-405.

86. Perin, E.C. and J. Lopez, *Methods of stem cell delivery in cardiac diseases.* Nat Clin Pract Cardiovasc Med, 2006. **3 Suppl 1**: p. S110-3.

87. Vulliet, P.R., et al., *Intra-coronary arterial injection of mesenchymal stromal cells and microinfarction in dogs.* Lancet, 2004. **363**(9411): p. 783-4.

88. Zeng, L., et al., *Multipotent adult progenitor cells from swine bone marrow.* Stem Cells, 2006. **24**(11): p. 2355-66.

89. Zhang, J. and K.M. McDonald, *Bioenergetic consequences of left ventricular remodeling.* Circulation, 1995. **92**(4): p. 1011-9.

90. Zhang, J., et al., *Bioenergetic abnormalities associated with severe left ventricular hypertrophy.* J Clin Invest, 1993. **92**(2): p. 993-1003.

91. Ye, Y., et al., *High-energy phosphate metabolism and creatine kinase in failing hearts: a new porcine model.* Circulation, 2001. **103**(11): p. 1570-6.

92. Chen, W., et al., *In vitro and in vivo studies of 1H NMR visibility to detect deoxyhemoglobin and deoxymyoglobin signals in myocardium.* Magn Reson Med, 1999. **42**(1): p. 1-5.

93. Wang, X., et al., *The role of the sca-1+/CD31- cardiac progenitor cell population in postinfarction left ventricular remodeling.* Stem Cells, 2006. **24**(7): p. 1779-88.

94. Feygin, J., et al., *Functional and bioenergetic modulations in the infarct border zone following autologous mesenchymal stem cell transplantation.* Am J Physiol Heart Circ Physiol, 2007. **293**(3): p. H1772-80.

95. Guccione, J.M., et al., *Mechanism underlying mechanical dysfunction in the border zone of left ventricular aneurysm: a finite element model study.* Ann Thorac Surg, 2001. **71**(2): p. 654-62.

96. Bearzi, C., et al., *Human cardiac stem cells.* Proc Natl Acad Sci U S A, 2007. **104**(35): p. 14068-73.

97. Rota, M., et al., *Local activation or implantation of cardiac progenitor cells rescues scarred infarcted myocardium improving cardiac function.* Circ Res, 2008. **103**(1): p. 107-16.

98. Urbanek, K., et al., *Cardiac stem cells possess growth factor-receptor systems that after activation regenerate the infarcted myocardium, improving ventricular function and long-term survival.* Circ Res, 2005. **97**(7): p. 663-73.

99. Urbanek, K., et al., *Myocardial regeneration by activation of multipotent cardiac stem cells in ischemic heart failure.* Proc Natl Acad Sci U S A, 2005. **102**(24): p. 8692-7.

100. Olivetti, G., et al., *Apoptosis in the failing human heart.* N Engl J Med, 1997. **336**(16): p. 1131-41.

101. Higuchi, M., R.J. Proske, and E.T. Yeh, *Inhibition of mitochondrial respiratory chain complex I by TNF results in cytochrome c release, membrane permeability transition, and apoptosis.* Oncogene, 1998. **17**(19): p. 2515-24.

102. Tillmanns, J., et al., *Formation of large coronary arteries by cardiac progenitor cells.* Proc Natl Acad Sci U S A, 2008. **105**(5): p. 1668-73.

103. Tang, Y.L., et al., *Autologous mesenchymal stem cell transplantation induce VEGF and neovascularization in ischemic myocardium.* Regul Pept, 2004. **117**(1): p. 3-10.

104. Meyer, G.P., et al., *Intracoronary bone marrow cell transfer after myocardial infarction: eighteen months' follow-up data from the randomized, controlled BOOST (BOne marrOw transfer to enhance ST-elevation infarct regeneration) trial.* Circulation, 2006. **113**(10): p. 1287-94.

105. Iso, Y., et al., *Multipotent human stromal cells improve cardiac function after myocardial infarction in mice without long-term engraftment.* Biochem Biophys Res Commun, 2007. **354**(3): p. 700-6.

106. Tusher, V.G., R. Tibshirani, and G. Chu, *Significance analysis of microarrays applied to the ionizing radiation response.* Proc Natl Acad Sci U S A, 2001. **98**(9): p. 5116-21.

107. Tsai, S., et al., *Annotation of the Affymetrix porcine genome microarray.* Anim Genet, 2006. **37**(4): p. 423-4.

108. Zhang, J., et al., *Relationships between myocardial bioenergetic and left ventricular function in hearts with volume-overload hypertrophy.* Circulation, 1997. **96**(1): p. 334-43.

109. Zhang, J., et al., *Effect of left ventricular hypertrophy secondary to chronic pressure overload on transmural myocardial 2-deoxyglucose uptake. A 31P NMR spectroscopic study.* Circulation, 1995. **92**(5): p. 1274-83.

110. Zhang, J., et al., *Oxygen delivery does not limit cardiac performance during high work states.* Am J Physiol, 1999. **277**(1 Pt 2): p. H50-7.

111. Ten Hove, M., et al., *Mechanisms of creatine depletion in chronically failing rat heart.* J Mol Cell Cardiol, 2005. **38**(2): p. 309-13.

112. Wallis, J., et al., *Supranormal myocardial creatine and phosphocreatine concentrations lead to cardiac hypertrophy and heart failure: insights from creatine transporter-overexpressing transgenic mice.* Circulation, 2005. **112**(20): p. 3131-9.

113. Wang, X., et al., *Stem cells for myocardial repair with use of a transarterial catheter.* Circulation, 2009. **120**(11 Suppl): p. S238-46.

114. Trachtenberg, B.H. and J.M. Hare, *Biomarkers of oxidative stress in heart failure.* Heart Fail Clin, 2009. **5**(4): p. 561-77.

115. Raju, S.V., et al., *Activation of the cardiac ciliary neurotrophic factor receptor reverses left ventricular hypertrophy in leptin-deficient and leptin-resistant obesity.* Proc Natl Acad Sci U S A, 2006. **103**(11): p. 4222-7.

116. Rezende, L.F., et al., *Ciliary neurotrophic factor promotes survival of neonatal rat islets via the BCL-2 anti-apoptotic pathway.* J Endocrinol, 2007. **195**(1): p. 157-65.

117. Black, B.L. and E.N. Olson, *Transcriptional control of muscle development by myocyte enhancer factor-2 (MEF2) proteins.* Annu Rev Cell Dev Biol, 1998. **14**: p. 167-96.

118. Naya, F.J., et al., *Mitochondrial deficiency and cardiac sudden death in mice lacking the MEF2A transcription factor.* Nat Med, 2002. **8**(11): p. 1303-9.

119. Heusch, G., *Hibernating myocardium.* Physiol Rev, 1998. **78**(4): p. 1055-85.

120. Heusch, G., R. Schulz, and S.H. Rahimtoola, *Myocardial hibernation: a delicate balance.* Am J Physiol Heart Circ Physiol, 2005. **288**(3): p. H984-99.

121. Canty, J.M., Jr. and J.A. Fallavollita, *Hibernating myocardium represents a primary downregulation of regional myocardial oxygen consumption distal to a critical coronary stenosis.* Basic Res Cardiol, 1995. **90**(1): p. 5-8.

122. Elsasser, A., et al., *Severe energy deprivation of human hibernating myocardium as possible common pathomechanism of contractile dysfunction, structural degeneration and cell death.* J Am Coll Cardiol, 2002. **39**(7): p. 1189-98.

123. Hu, Q., et al., *Reductions in mitochondrial O(2) consumption and preservation of high-energy phosphate levels after simulated ischemia in chronic hibernating myocardium.* Am J Physiol Heart Circ Physiol, 2009. **297**(1): p. H223-32.

124. Wiggers, H., et al., *Energy stores and metabolites in chronic reversibly and irreversibly dysfunctional myocardium in humans.* J Am Coll Cardiol, 2001. **37**(1): p. 100-8.

125. Tian, R. and J.S. Ingwall, *Energetic basis for reduced contractile reserve in isolated rat hearts.* Am J Physiol, 1996. **270**(4 Pt 2): p. H1207-16.

126. Zhang, J., et al., *Myocardial bioenergetics during acute hibernation.* Am J Physiol, 1997. **273**(3 Pt 2): p. H1452-63.

127. Martin, C., et al., *Inorganic phosphate content and free energy change of ATP hydrolysis in regional short-term hibernating myocardium.* Cardiovasc Res, 1998. **39**(2): p. 318-26.

128. Axel, L., *Tissue mean transit time from dynamic computed tomography by a simple deconvolution technique.* Invest Radiol, 1983. **18**(1): p. 94-9.

129. Jerosch-Herold, M., N. Wilke, and A.E. Stillman, *Magnetic resonance quantification of the myocardial perfusion reserve with a Fermi function model for constrained deconvolution.* Med Phys, 1998. **25**(1): p. 73-84.

130. Guth, B.D., et al., *Regional myocardial blood flow, function and metabolism using phosphorus-31 nuclear magnetic resonance spectroscopy during ischemia and reperfusion in dogs.* J Am Coll Cardiol, 1987. **10**(3): p. 673-81.

131. Ye, Y., et al., *Myocardial creatine kinase kinetics and isoform expression in hearts with severe LV hypertrophy.* Am J Physiol Heart Circ Physiol, 2001. **281**(1): p. H376-86.

132. Fallavollita, J.A., M. Logue, and J.M. Canty, Jr., *Coronary patency and its relation to contractile reserve in hibernating myocardium.* Cardiovasc Res, 2002. **55**(1): p. 131-40.

133. Nassenstein, K., et al., *How much myocardial damage is necessary to enable detection of focal late gadolinium enhancement at cardiac MR imaging?* Radiology, 2008. **249**(3): p. 829-35.

134. Selvanayagam, J.B., et al., *Resting myocardial blood flow is impaired in hibernating myocardium: a magnetic resonance study of quantitative perfusion assessment.* Circulation, 2005. **112**(21): p. 3289-96.

135. Wilke, N., et al., *Regional myocardial blood volume and flow: first-pass MR imaging with polylysine-Gd-DTPA.* J Magn Reson Imaging, 1995. **5**(2): p. 227-37.

136. Li, W. and X. Yu, *Quantification of myocardial strain at early systole in mouse heart: restoration of undeformed tagging grid with single-point HARP*. J Magn Reson Imaging, 2010. **32**(3): p. 608-14.

137. Zhou, R., et al., *Assessment of global and regional myocardial function in the mouse using cine and tagged MRI.* Magn Reson Med, 2003. **49**(4): p. 760-4.

138. Page, B., et al., *Persistent regional downregulation in mitochondrial enzymes and upregulation of stress proteins in swine with chronic hibernating myocardium.* Circ Res, 2008. **102**(1): p. 103-12.

139. Schulz, R., et al., *Development of short-term myocardial hibernation. Its limitation by the severity of ischemia and inotropic stimulation.* Circulation, 1993. **88**(2): p. 684-95.

140. Zhang, J., et al., *Effects of dobutamine on myocardial blood flow, contractile function, and bioenergetic responses distal to coronary stenosis: implications with regard to dobutamine stress testing.* Am Heart J, 1995. **129**(2): p. 330-42.

141. Grover, G.J. and K.D. Garlid, *ATP-Sensitive potassium channels: a review of their cardioprotective pharmacology*. J Mol Cell Cardiol, 2000. **32**(4): p. 677-95.

142. Nelson, M.T. and J.M. Quayle, *Physiological roles and properties of potassium channels in arterial smooth muscle.* Am J Physiol, 1995. **268**(4 Pt 1): p. C799-822.

143. Noma, A., *ATP-regulated K+ channels in cardiac muscle.* Nature, 1983. **305**(5930): p. 147-8.

144. Standen, N.B., et al., *Hyperpolarizing vasodilators activate ATP-sensitive K+ channels in arterial smooth muscle.* Science, 1989. **245**(4914): p. 177-80.

145. Duncker, D.J. and R.J. Bache, *Regulation of coronary blood flow during exercise.* Physiol Rev, 2008. **88**(3): p. 1009-86.

146. Quayle, J.M., M.T. Nelson, and N.B. Standen, *ATP-sensitive and inwardly rectifying potassium channels in smooth muscle.* Physiol Rev, 1997. **77**(4): p. 1165-232.

147. Duncker, D.J., et al., *Role of K+ATP channels in coronary vasodilation during exercise.* Circulation, 1993. **88**(3): p. 1245-53.

148. Duncker, D.J., et al., *Endogenous adenosine mediates coronary vasodilation during exercise after K(ATP)+ channel blockade.* J Clin Invest, 1995. **95**(1): p. 285-95.

149. Imamura, Y., et al., *Glibenclamide decreases basal coronary blood flow in anesthetized dogs.* Am J Physiol, 1992. **263**(2 Pt 2): p. H399-404.

150. Samaha, F.F., et al., *ATP-sensitive potassium channel is essential to maintain basal coronary vascular tone in vivo.* Am J Physiol, 1992. **262**(5 Pt 1): p. C1220-7.

151. Yamada, M., *Mitochondrial ATP-sensitive K+ channels, protectors of the heart.* J Physiol, 2010. **588**(Pt 2): p. 283-6.

152. Chen, Y., et al., *Selective blockade of mitochondrial K(ATP) channels does not impair myocardial oxygen consumption.* Am J Physiol Heart Circ Physiol, 2001. **281**(2): p. H738-44.

153. Bache, R.J., et al., *Role of adenosine in coronary vasodilation during exercise.* Circ Res, 1988. **62**(4): p. 846-53.

154. Feigl, E.O., *Berne's adenosine hypothesis of coronary blood flow control.* Am J Physiol Heart Circ Physiol, 2004. **287**(5): p. H1891-4.

155. Gong, G., et al., *Oxidative capacity in failing hearts.* Am J Physiol Heart Circ Physiol, 2003. **285**(2): p. H541-8.

156. Gwirtz, P.A., *Construction and evaluation of a coronary catheter for chronic implantation in dogs.* J Appl Physiol, 1986. **60**(2): p. 720-6.

157. Pantely, G.A., et al., *Regeneration of myocardial phosphocreatine in pigs despite continued moderate ischemia.* Circ Res, 1990. **67**(6): p. 1481-93.

158. Robitaille, P.M., et al., *Transmural high energy phosphate distribution and response to alterations in workload in the normal canine myocardium as studied with spatially localized 31P NMR spectroscopy.* Magn Reson Med, 1990. **16**(1): p. 91-116.

159. Chen, W., et al., *Determination of deoxymyoglobin changes during graded myocardial ischemia: an in vivo 1H NMR spectroscopy study.* Magn Reson Med, 1997. **38**(2): p. 193-7.

160. Hendrich, K., et al., *Phase-modulated rotating frame spectroscopic localization using an adiabatic plane-rotation pulse and single surface coil.* J Magn Reson, 1991. **92**: p. 258-275.

161. Robitaille, P.M., et al., *Spectroscopic imaging and spatial localization using adiabatic pulses and applications to detect transmural metabolite distribution in the canine heart.* Magn Reson Med, 1989. **10**(1): p. 14-37.

162. Neubauer, S., *The failing heart--an engine out of fuel.* N Engl J Med, 2007. **356**(11): p. 1140-51.